Department of Geomatics Engineering

Error Analysis and Stochastic Modeling of MEMS based Inertial Sensors for Land Vehicle Navigation Applications

(URL: http://www.geomatics.ucalgary.ca/links/GradTheses.html)

by

Minha Park

April, 2004

UNIVERSITY OF
CALGARY

THE UNIVERSITY OF CALGARY

Error Analysis and Stochastic Modeling of MEMS based Inertial Sensors for Land

Vehicle Navigation Applications

by

Minha Park

A THESIS

SUBMITTED TO THE FACULTY OF GRADUATE STUDIES

IN PARTIAL FULFILLMENT OF THE REQUIREMENTS

FOR THE DEGREE OF MASTER OF SCIENCE

DEPARTMENT OF GEOMATICS ENGINEERING

CALGARY, ALBERTA

April, 2004

Abstract

Although GPS measurements are the essential information for currently developed land vehicle navigation systems (LVNS), the situation when GPS signals are unavailable or unreliable due to signal blockages must be compensated to provide continuous navigation solutions. In order to overcome the unavailability or unreliability problem in satellite based navigation systems and also to be cost effective, Micro Electro Mechanical Systems (MEMS) based inertial sensor technology has pushed the development of low-cost integrated navigation systems for land vehicle navigation and guidance applications. In spite of low inherent cost, small size, low power consumption, and solid reliability of MEMS based inertial sensors, the errors in the observations from the MEMS-based sensors must be appropriately treated in order to turn the observations into useful data for vehicle position determination. The error analysis would be conducted in the time domain specifying the stochastic variation as well as error sources of systematic nature.

This thesis will address the above issues and present algorithms to identify and model the error sources in MEMS-based inertial sensors. A Kalman filter will be described and applied to analyze the performance of a minimum configured GPS/IMU system for vehicle navigation applications. The performance of the testing system has been assessed via a comparison to Precise Point Position (PPP) reference data. The testing results indicate the effectiveness of the discussed error analysis and modeling method.

Acknowledgements

I wish to express my sincere gratitude to my supervisor, Dr. Yang Gao for his continued supports and understanding. He encouraged me to challenge new ideas and guided me through all aspects of this thesis. He provided the valuable advices, opportunities and assistance that greatly enhanced all the researches during my graduate studies.

I would like to thank some of my colleagues, especially James (Jau-Hsiung) Wang, who participated in field testing with his data acquisition program. Kongzhe Chen is also thanked for providing PPP solution for the performance analysis of field testing. Especially, I would like to acknowledge Eun-Hwan Shin for his willingness to discuss and to give precious advices.

And last, I would like to extend my sincere thanks to my lovely wife, Catherine Hee-Jin Kim for her generous understanding and continuous dedication.

Contents

vii

List of Tables

List of Figures

Notation

x	Vector of Unknowns
z	Vector of Observations
P	Covariance of Unknowns
P	Pseudorange Measurement
R	Covariance of Observations
R_X	Autocorrelation Function
ρ_X	Normalized Autocorrelation Function
S_X	Power Spectral Density Function
K_k	Reflection Coefficient
Φ	State Transition Matrix
Φ	Carrier Phase Measurement
F	Dynamic Matrix
Q	Dynamic Noise Matrix
H	Measurement Design Matrix
τ	Time Lag

Acronyms

CGRF	Canadian Geomagnetic Reference Field
DGPS	Differential Global Positioning System
DLL	Delay Lock Loop
DR	Dead Reckoning
DSP	Digital Signal Processing
GLONASS	GLObal Navigation Satellite System
GPS	Global Positioning System
IMU	Inertial Measurement Unit
INS	Inertial Navigation System
LIGA	Lithography, Galvanic (electrodeposition), Abformung (German word meaning molding)
LVNS	Land Vehicle Navigation System
MEMS	Micro Electro Mechanical Systems
NRCan	Natural Resources of Canada
PLL	Phase Lock Loop
PPP	Precise Point Positioning
PPS	Precise Positioning Service
SPS	Standard Positioning Service

Chapter 1

Introduction

1.1 Background and Objective

The rapidly expanding use of the Global Positioning System (GPS) enables commercial navigation devices to be more popular and attainable for the civil users. GPS provides absolute positioning information covering any part of the world during days and nights. From the blackbox-sized military GPS receivers to the chipsets on cellular phones, GPS receiver technology has been significantly enhanced over the past ten years and it will enable more inexpensive and smaller GPS navigation devices to be possible in the near future. While GPS provides bounded errors for the position and the velocity, GPS users

shall experience signal blockage due to such as interference and jamming. As GPS signal is coming from about 20,200 km from the sky, it is relatively weak and is affected by the atmosphere, line of sight and etc. In spite of many successful research activities to handle identified error sources of GPS measurements such as ionosphere modeling, multipath mitigation and differential GPS, the visibility to adequate number of GPS satellites from the recipient is still critical in using GPS alone navigation devices. Under the tree, inside the building, in the tunnel, between the tall buildings, GPS positioning is difficult due to signal blockage and degradation.

Because of their complementary characteristics, Dead Reckoning (DR) method is often considered to be integrated with GPS. Recently, a low cost integrated navigation system for commercial applications such as car/personal navigation, accident record, and human body detection is getting huge attention around the world. DR method is an approach that has been widely used in marine and airborne navigation for decades, which is a relative positioning method capable of deriving position based on three distinct inputs, namely, a set of starting coordinates, the direction of travel, and the velocity of travel. There are many different types of DR sensors available such as Compass, Gyroscope, Inclinometer, Odometer, Accelerometer, Altimeter, etc. Each system provides its own distinguished output and some sensors can be combined such as Inertial Measurement Unit (IMU), which consists of 3-axis accelerometer and 3-axis gyroscope. Attempting to overcome the cost and size constraints of traditional DR sensors, Micro Electro Mechanical Systems (MEMS) based DR sensors have accelerated the development of low cost integrated navigation systems on single board with latest GPS receiver technology. Considerable

applications and researches are now eagerly being carried out on satellite based navigation system aided by MEMS based DR sensors and have drawn great expectations. Among the applications of MEMS technology, MEMS based inertial sensors like MEMS based gyroscopes and MEMS based accelerometers have been adopted and tested as aiding sensors to improve the navigation information continuity in many applications. MEMS based accelerometers and gyroscopes are becoming more attractive to manufacturers of navigation systems because of their small size, low cost, light weight, low power consumption and ruggedness.

For all that DR and GPS have excellent complementary synergy effect since DR sensors are self-contained and provide the high frequency and continuous information, DR sensors are subject to internal error behaviour and their errors tend to increase with time. Despite remarkable advances of MEMS technology in cost and size constraints, MEMS based inertial sensors have inherited the error behaviour of conventional inertial sensors and they are still considered as very poor devices in accuracy which are suffering from a variety of error sources that are slightly different upon the structure of sensor like mechanical sensors. Hence, in order to integrate MEMS based inertial sensors with GPS and provide a continuous and reliable navigation solution, the characteristics of different error sources and the understanding of the stochastic variation of MEMS based inertial sensors are of significant importance for the development of optimal estimation algorithms (Park and Gao, 2002).

Here, the main purposes of this study are the error characterization of MEMS based inertial sensors and the performance analysis of the prototype of a low cost GPS/MEMS based inertial sensor integrated system for land vehicle applications. The fundamental characteristics of MEMS based accelerometers and gyroscopes will be investigated and the stochastic variation of the sensors will be assessed in the time domain analysis. Furthermore, the different stochastic modeling methods will be studied and one of them will be adopted for the performance analysis of the testing system. When the performance of MEMS based inertial sensors is admissible for a certain application such as the land vehicle navigation systems, a continuous integrated navigation system will be available with cheaper and smaller inertial sensors complementing GPS signal interference and jamming in so-called urban canyons.

1.2 Thesis Outline

Chapter Two gives an overview of currently proposed multi-sensor navigation systems. More specifically, satellite based navigation system and dead reckoning navigation system will be described separately in terms of its characteristics and error behaviours related to multi-sensor navigation system performances. The fundamental ideas of MEMS technology will be introduced and some of currently used MEMS based inertial sensors will be discussed.

Chapter Three discusses how to analyze the stochastic variation of a sensor based on the knowledge of probabilistic and statistical aspects. It gives the mathematical background of time domain representation of stochastic processes and then, it discusses how to approximately identify stochastic variation of measurement data as one of the standard discrete stochastic models that will be used in the optimal estimation algorithm.

Chapter Four gives the estimation of deterministic error sources of MEMS based inertial sensors and associated stochastic modeling. The major deterministic error sources (zero-offset bias and 1st order scale factor) have been estimated and the random noises of MEMS based accelerometer/gyroscope have been modeled based on the discussion of different stochastic modeling methods in chapter Three.

Chapter Five holds the performance analysis of stochastic modeling discussed in the previous chapters. After the experiment of static and 2-D kinematic land vehicle navigation, testing results will be analyzed to explain the influences of previous suggested stochastic modeling scheme in the position domain.

Finally, Chapter Six will be the conclusions of the research as well as some recommendations for the future research.

Chapter 2

Multi-Sensor Navigation Systems

For last several decades, much effort has been applied to the development of sensing devices which measure the physical quantities of interest such as acceleration, velocity, position, pressure, weight, force, sound, and etc converting those quantities into electrical signals. Recently, two main technical advances (Digital Signal Processing (DSP) and Micro Mechanics) have accelerated the development of various applications with less cost and space constraints. From the blackbox-sized military navigation systems to the chipsets on cellular phones, recent advances in sensor technology have enormously been applied in the navigation field. This chapter will provide the basic understanding of multi-sensor navigation systems including specific navigation methods and MEMS technology with MEMS based inertial sensors.

2.1 Concepts of Multi-Sensor Navigation Systems

For the determination of navigation states (e.g., position, velocity, attitude, acceleration), different types of sensors can be considered. The compass can determine the direction relative to the local magnetic north, and the odometer in the vehicle provides the change of distance relative to the initial point. From the coin-sized magnetic compass to GPS or Inertial Navigation System (INS), manifold sensors provide their own distinguished outputs for the use of navigation solution. In many applications, more than one sensor are involved so as to not only determine the navigation states at a certain time but also to provide the continuous navigation trajectory. The term, 'multi-sensor navigation systems', is therefore, often used. Such systems are typically operated with multiple sensors referenced to a common platform and synchronized to a common time base (Schwarz, 2001, p. 2). Each sensor contributes its own stream of data and all the data is optimally processed.

For most multi-sensor navigation systems, two main questions are commonly raised, namely

- What kinds of sensors will be chosen?
- How will the output of each sensor be combined to provide optimal solution?

Considering the cost, the space, the availability, and etc, the proper sensors should be chosen and the development of optimal processing algorithm is necessary for multi-sensor navigation systems. Some sensors have complementary aspects to each other and sometimes, redundant sensors are needed to avoid the possible malfunction or unreliable operation of sensors. Also, different data fusion algorithms can be used for different environmental situations. Figure 2.1 shows one example of sophisticated multi-sensor navigation system data fusion algorithms.
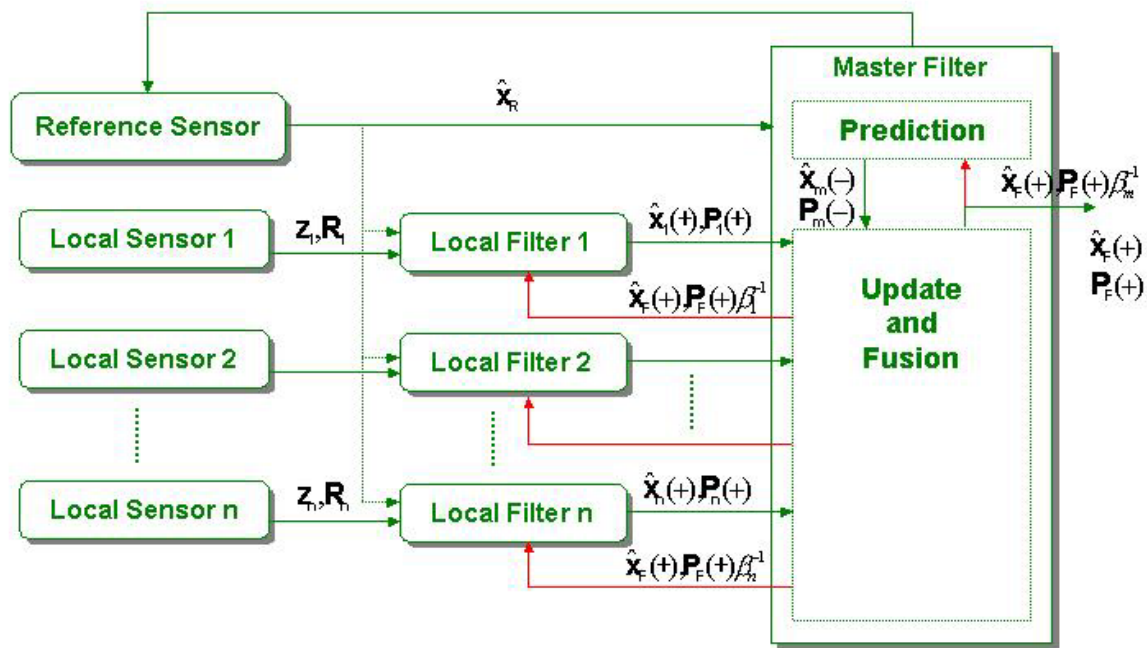
Figure 2.1 Federated Kalman Filter for Multi-Sensor Navigation System (Carlson, 2002)

In the figure,

$\hat{x}_R$ is reference error estimate

z_i is measurement sequence

R_i is measurement error covariance

$\hat{x}_i(+)$ is local error estimate

$P_i(+)$ is local error covariance

$\hat{x}_m(-)$ is optimal error estimate before t_k in master filter

$P_m(-)$ is covariance associated with $\hat{x}_m(-)$

$\hat{x}_F(+)$ is global error estimate

$P_F(+)$ is global error covariance

β_i^{-1} is sharing factor

This example illustrates the federated Kalman filter to a distributed navigation system having 3 local sensors with the associated local filters. There is a reference sensor such as INS whose outputs are employed as a common reference solution by each of three local filters (Carlson, 2002). The federated Kalman filter combines local estimates in the master filter in order to yield the global optimal estimate and then, includes feeding back the information from the master filter to the local filters. This type of architecture requires the full order state vectors in each of local filters, which is a very difficult implementation requirement in applications. For the real implementation procedures, some modifications and changes are necessary in order to make it work properly. All the multi-sensor navigation systems do not have to be complicated like the previous example. Besides, individual sensor investigation should have been performed precisely before putting sensors together. It is a very critical procedure for the reliable and optimal navigation solution to the end. The subsequent sections will briefly describe the two

important navigation methods: Satellite based Navigation method and Dead Reckoning (DR) Navigation method.

2.2 Satellite based Navigation Method

Among the satellites which have been used, and still are used for their different goals, satellite based navigation systems are NNSS TRANSIT (Navy Navigation Satellite System TRANSIT) & NAVSTAR GPS (NAVigation System with Time and Ranging Global Positioning System) by United States, GLONASS (GLObal Navigation Satellite System) by Russia, and proposed GALILEO by European Union near future. In this section, NAVSTAR GPS will be mainly discussed to enhance the understanding of the main issues of the satellite based navigation method. The descriptions of GPS, the GPS observables and the error budgets, and limitations will be given subsequently.

2.2.1 Descriptions of GPS

The NAVSTAR GPS is a satellite-based radio navigation system designed and operated by the U.S. DoD (Department of Defense), providing three-dimensional position, navigation, and time information to the users with a suitable equipment. It became fully operational in 1994 with 21 satellites (plus 3 active spares) on 6 orbital planes in about 20,200 km altitude above the earth's surface with 12 hours orbiting period covering

worldwide. GPS has been designed that at least 4 satellites could be visibly available above the horizon anywhere on the earth, 24 hours a day.
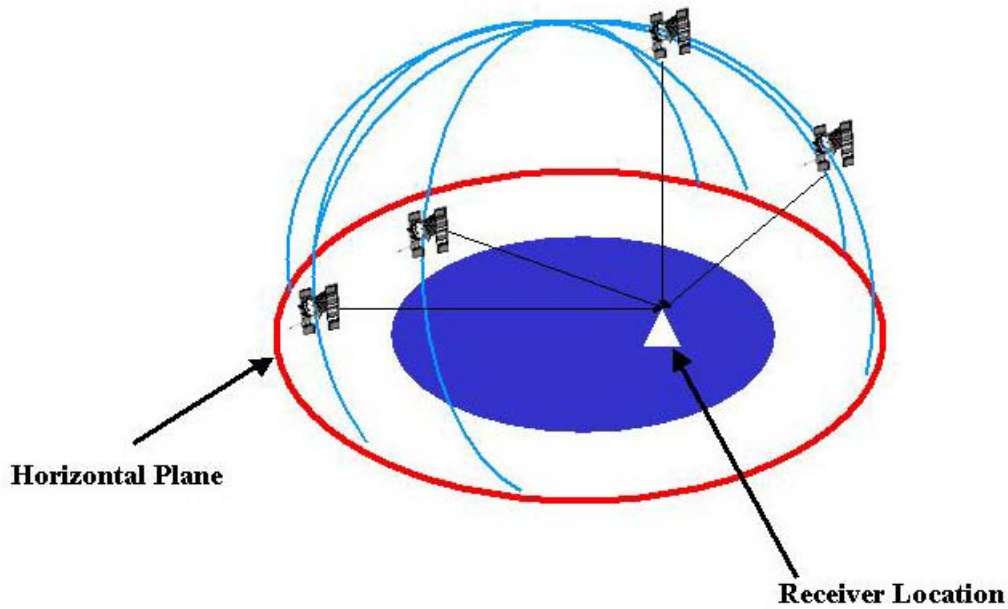
Figure 2.2 GPS Positioning

GPS is primarily a navigation system. The fundamental navigation principle is based on the measurement of so-called *pseudoranges* between the user and at least the four satellites illustrated in Figure 2.2. Starting from the known satellite coordinates in a suitable reference frame (WGS 84), the coordinates of the user antenna can be determined. From the geometrical point of view, three range measurements are sufficient. A fourth observation is necessary because GPS uses the one-way ranging technique, and the receiver clock is not synchronized with the satellite clock. This synchronization error is the reason for the term "pseudorange" (Seeber, 1993, p. 209).

GPS signals are transmitted on two coherent carrier frequencies, L1 (1575.42 MHz) and L2 (1227.60 MHz), which are modulated by various spread spectrum signals. The major carrier, L1, is biphase-modulated by two types of pseudo-random noise codes: one at 1.023 MHz, called the 'C/A-code', and the other at 10.23 MHz, called the 'P-code'. The P-code is intended only for the authorized access because its one-chip wavelength of 30 m provides the most accurate positioning possible. The C/A-code, with its 300 m one-chip wavelength, is used in all cases for initial acquisition and code-signal alignment purposes. Most of civil users have the access to this less accurate C/A-code for positioning. The second carrier signal, L2, contains only P-code modulation, and is intended to give the authorized users the additional capability of actually measuring the ionospheric delays using the two frequencies, the delays being frequency-dependent. In official parlance, the P-code access is reserved for what is called the *Precise Positioning Service* (PPS) mode of operation, whereas everything else is classified as the *Standard Positioning Service* (SPS) (Brown and Hwang, 1997, p. 420). Table 2.1 summarizes some characteristic features of NAVSTAR GPS satellite signals.

Table 2.1 GPS Satellite Signals (Seeber, 1993, p. 217)

Atomic clock (Cs, Rb) Fundamental frequency	10.23 MHz
L1 carrier signal	154×10.23 MHz
L1 frequency	1575.42 MHz
L1 wavelength	19.05 cm
L2 carrier signal	120×10.23 MHz
L2 frequency	1227.60 MHz
L2 wavelength	24.45 cm
P-code frequency (chipping rate)	10.23 MHz (Mbps)
P-code wavelength	29.31 m
P-code period	266 days; 7 days/satellite
C/A-code frequency (chipping rate)	1.023 MHz (Mbps)
C/A-code wavelength	293.1 m
C/A-code period	1 millisecond
Data signal frequency	50 bps
Data signal cycle length	30 seconds

2.2.2 GPS Observables and Error Budgets

As mentioned earlier, at least 4 satellite measurements are acquired to determine the recipient position slaved to the coordinate frame of reference such as WGS 84. Two important observables are generated from GPS raw measurements, which are usually called as pseudorandom code and the carrier signal. These two different observables (code, carrier) are derived or tracked in the separate tracking loops, Delay Lock Loop (DLL) for code tracking loop and Costas Phase Lock Loop (PLL) for carrier tracking loop. A pseudorange from code measurements equals the time shift that is necessary to correlate the incoming code sequence with a code sequence generated in the GPS receiver, multiplied by the velocity of light, and the carrier phase is derived from a phase comparison between the received Doppler shifted carrier signal and the (nominally constant) receiver-generated reference frequency (Seeber, 1993, p. 249). Pseudoranges from code/carrier phase measurements suffer from several error sources and their measurement equations are (Cannon, 2001, p. 106/111)

$$P = \rho + d\rho + c(dt - dT) + d_{ion} + d_{trop} + \varepsilon_P \qquad (2.1)$$

$$\Phi = \rho + d\rho + c(dt - dT) + \lambda N - d_{ion} + d_{trop} + \varepsilon_\Phi \qquad (2.2)$$

where

$\quad P \qquad$ is the pseudorange measurement

$\quad \Phi \qquad$ is the carrier phase measurement

$\quad \rho \qquad$ is the geometric range from the satellite to the receiver

13

$d\rho$ is the orbital errors

dt is the receiver clock offset to GPS time

dT is the satellite clock error

d_{ion} is the ionospheric delay

d_{trop} is the tropospheric delay

ε_P is the pseudorange measurement noise including multipath effect

λ is the GPS carrier wavelength

N is the integer ambiguity

ε_Φ is the carrier phase measurement noise including multipath effect

c is the speed of light

Three major differences between pseudorange measurement and carrier phase measurement are phase advance in ionospheric delay, integer ambiguity, and measurement noise. Contrary to the code measurement, carrier phase measurement has phase advance phenomena resulting in negative sign in equation (2.2). The L1 carrier wavelength is about 19 cm which intends to generate very precise measurements of the phase of the carrier to be made. However, resolving the integer ambiguity is a delicate task which requires quite a long integer convergence time of several tens of minutes or estimated as a float term sometimes. Both of pseudorange and carrier phase measurement noise consist of receiver noise and their own multipath effect. Multipath phenomenon refers to the distortion of a directly received GPS signal by its spurious replica that took an indirect path by the way of reflecting off one or more objects. Clearly, the indirect path taken by the replica or multipath signal will be longer than that taken by the direct

signal. This signifies ranging error that can be quite sizable. As long as the receiver is locked onto the direct signal by virtue of its stronger power, the multipath signal with its erroneous ranging information will only appear to distort the direct signal and perturb its phase to introduce a small ranging error. If the multipath signal is stronger than the direct signal, particularly when the latter is completely obstructed, the multipath error can well be far more significant (Brown and Hwang, 1997, p. 428).

The most common method to minimize the errors of SPS GPS measurements is the Differential GPS (DGPS). With known coordinates of one receiver station, position of the second receiver station can be accurately determined by canceling the common error parts experienced by both stations shown in equation (2.1) and (2.2). Since DGPS method is requiring two receiver stations such as a reference and a rover receiver, the solution is dependent on the separation length of baseline between them. DGPS does not lessen multipath effect and increase the noise level by a factor of $\sqrt{2}$. Table 2.2 summarizes SPS GPS error budgets.

Table 2.2 SPS GPS Error Budgets (Cannon, 2001, p.131)

Error Sources	Typical Values
Satellite error (1σ)	
Orbit & clock error	2.3 m
Propagation errors	
Ionosphere	7 m
Troposphere	0.2 m
Received errors	
Code multipath	1.5 m
Code noise	0.6 m
Carrier multipath	1 ~ 50 mm
Carrier noise	0.2 ~ 2 mm
Total	~ 11.6 m

2.2.3 Limitations of GPS

While GPS provides bounded errors for position and velocity, GPS users experience signal blockage; interference or jamming. As GPS signal is coming from about 22,000 km from the sky, it is relatively weak and affected by the atmosphere, line of sight and etc. In spite of many successful research activities to handle identified error sources such as ionosphere modeling, multipath mitigation and DGPS, the visibility to adequate number of GPS satellites from the recipient is still critical in using GPS alone navigation devices. Under the tree, inside the building, in the tunnel, and between the tall buildings, GPS positioning becomes difficult due to the signal blockage and degradation. Limitations of GPS enforce one to integrate GPS with other navigation sensors to provide the continuous navigation solution.

2.3 Dead Reckoning (DR) Navigation Method

Dead Reckoning (DR) navigation is one of the traditional navigation methods that has been widely used in marine and long range flight applications, which is a relative positioning method capable of deriving position based on three distinct inputs, namely, a set of starting coordinates, the direction of travel, and the velocity of travel. With the known initial coordinates in navigation frame, a set of sensors provides its own navigation outputs in body frame and sensor outputs are processed in the computation

algorithm to provide the new coordinates in navigation frame. DR navigation method is self-contained and it does not require the external signals or inputs. There are many different types of DR sensors available: Compass, Gyroscope, Inclinometer, Odometer, Accelerometer, Altimeter, etc. Each system has distinct output and some sensors can be combined. Two-dimensional DR navigation described in Farrell and Barth (1998, p.5) will be illustrated and explained to help understand DR navigation method. In Figure 2.3, only two coordinate frames are involved; body-frame and navigation-frame.
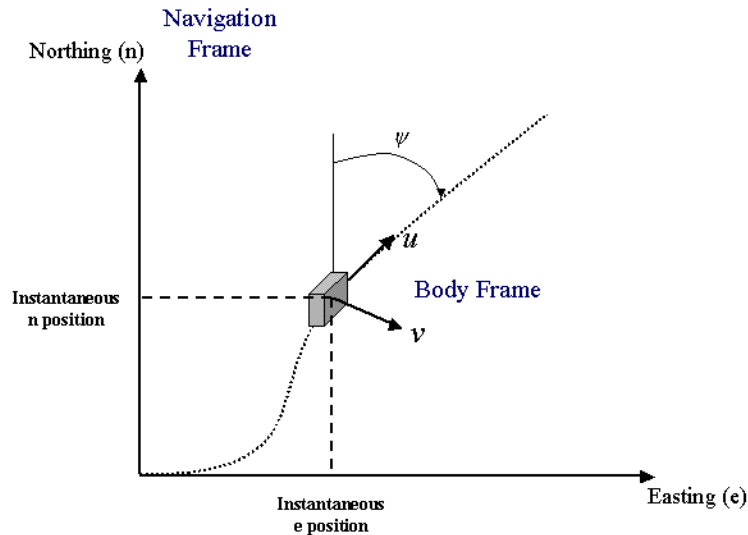
Figure 2.3 Ideal two-dimensional DR Navigation (Farrell and Barth, 1998)

In a modern approach to dead reckoning, body-frame velocity and heading are measured electronically. Instantaneous navigation-frame velocities are computed at a high rate based on the measured heading and the body-frame velocity. The navigation-frame velocities are then integrated to determine the navigation-frame positions. The differential equations describing the ideal mechanization of this approach are

17

$$
\begin{bmatrix} \dot{n}(t) \\ \dot{e}(t) \end{bmatrix} = \begin{bmatrix} \cos(\psi(t)) & -\sin(\psi(t)) \\ \sin(\psi(t)) & \cos(\psi(t)) \end{bmatrix} \begin{bmatrix} u(t) \\ v(t) \end{bmatrix}
\qquad (2.3)
$$

where

(n, e) are the north and the east position in navigation-frame

(u, v) are the components of vehicle velocity in body-frame

ψ is the angle between navigation north axis and body u axis

$R_b^n = \begin{bmatrix} \cos(\psi(t)) & -\sin(\psi(t)) \\ \sin(\psi(t)) & \cos(\psi(t)) \end{bmatrix}$ is the transformation matrix between body and navigation frame

It should be noted that the vehicle position accuracy is dependent on the accuracy of the initial position estimates even in the ideal case. Also, since involved sensors and actual computations are not perfectly accurate, equation (2.3) should be changed into the equations including various system errors as follows:

$$
\begin{bmatrix} \dot{\tilde{n}}(t) \\ \dot{\tilde{e}}(t) \end{bmatrix} = \begin{bmatrix} \cos(\tilde{\psi}(t)) & -\sin(\tilde{\psi}(t)) \\ \sin(\tilde{\psi}(t)) & \cos(\tilde{\psi}(t)) \end{bmatrix} \begin{bmatrix} \tilde{u}(t) \\ \tilde{v}(t) \end{bmatrix}
\qquad (2.4)
$$

where

$\tilde{\psi} = \psi + \delta\psi$,

$\tilde{v} = v + \delta v$,

$\tilde{u} = (1 + \delta s)u + \delta u$

$\delta\psi, \delta v, \delta u$ are the bias terms and δs is the scale-factor error

Assuming $\tilde{v} = 0$ and the lateral velocity is not measured, $\delta v = -v$ and equation (2.4) is then reduced to

$$\begin{bmatrix} \dot{n}(t) \\ \dot{e}(t) \end{bmatrix} = \begin{bmatrix} \cos(\psi(t) + \delta\psi(t)) & -\sin(\psi(t) + \delta\psi(t)) \\ \sin(\psi(t) + \delta\psi(t)) & \cos(\psi(t) + \delta\psi(t)) \end{bmatrix} \begin{bmatrix} (1 + \delta s)u(t) + \delta u(t) \\ v(t) + \delta v(t) \end{bmatrix} \qquad (2.5)$$

Figure 2.4 describes the actual case with some system errors.
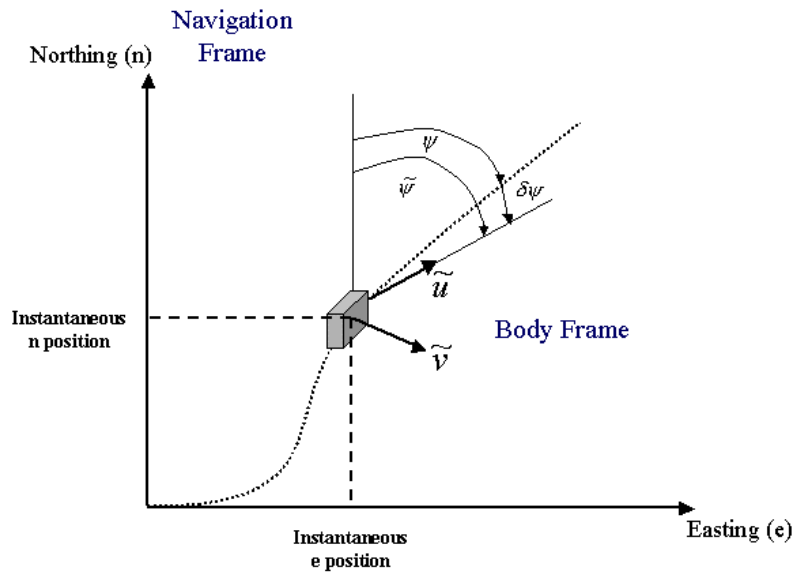
Figure 2.4 Actual two-dimensional DR Navigation (Farrell and Barth, 1998)

Linear analysis of the actual system about the ideal system is carried out by subtracting the actual system from the ideal system and linearizing it with the introduction of error variables. Using Taylor's Theorem, linear error differential equations are obtained as

$$
\begin{bmatrix} \delta \dot{n} \\ \delta \dot{e} \end{bmatrix} = \begin{bmatrix} 1 & 0 \\ 0 & 1 \end{bmatrix} \begin{bmatrix} \delta n \\ \delta e \end{bmatrix} + \begin{bmatrix} -u\sin(\psi(t)) & u\cos(\psi(t)) & \cos(\psi(t)) & -\sin(\psi(t)) \\ u\cos(\psi(t)) & u\sin(\psi(t)) & \sin(\psi(t)) & \cos(\psi(t)) \end{bmatrix} \begin{bmatrix} \delta \psi \\ \delta s \\ \delta u \\ \delta v \end{bmatrix} \quad (2.6)
$$

where $\delta n = n - \hat{n}$ and $\delta e = e - \hat{e}$.

Equation (2.6) is the simplified two-dimensional DR navigation error equation and is very useful for system analysis. In real situation, much more complicated navigation equations are used in three-dimensional rotating coordinate frame such as Earth-Fixed Earth-Centered (EFEC) reference frame. Also, if the velocity of vehicle is obtained by integration of measured accelerations, earth gravity forces should be properly modeled.

There are some of important characteristics to be noticed in the above example. First, initial position errors $(\delta n, \delta e)$ affect all the subsequent positions as a constant offset. That means, one is expected to start with good initial estimated coordinates for the good estimated coordinates in future times. Secondly, the heading bias and scale-factor error of forward velocity is a function of velocity u. Thirdly, the result of error equations depends on the system error modeling. If any of sensor's error is not modeled properly or the unmodeled error affects the system performance, the system would be unreliable and the results would be inaccurate. The size and the nature of the sensor errors are not easy

to characterize, are time variable, and can be affected by events outside the sensor itself (Farrell and Barth, 1998, p. 7). DR navigation method is substantially subject to internal error behaviours and its errors tend to increase with time. The errors that normally arise in calculated navigation states are instrumental errors, computational errors, alignment errors and environment errors. Then, it is of significant importance to characterize error sources and develop precise stochastic modeling of the sensors.

2.4 MEMS Technology

Recent advances in Micro Electro Mechanical Systems (MEMS) based DR sensors are quite significant and are promising the smaller and cheaper systems. MEMS is the integration of mechanical elements, sensors, actuators, and electronics on a common silicon substrate through the utilization of microfabrication technology (Huff, 1999), and see Figure 2.5. MEMS technology is expected to revolutionize a variety of industrial field products by combining together silicon-based microelectronics with micromachining technology, hence, being so called as **systems-on-a-chip** (MEMS and Nanotechnology Clearinghouse, 2003).

MEMS enables the development of smart product capabilities of microsensors and microactuators. This technology is extremely diversely designed and manufactured. Because MEMS devices are manufactured using batch fabrication, sophisticated small silicon chip, which can be placed at a relatively low cost (Huff, 1999).
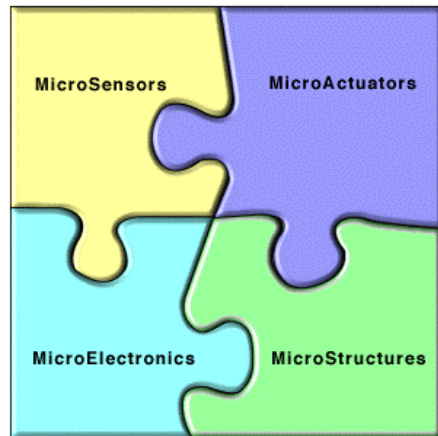
Figure 2.5 Components of MEMS
(http://www.gmu.edu/departments/seor/student_project/syst101_00b/team07/components
.html)

Microelectronics performs the decision making processes like "brain" of systems and microsensors/microacuators are playing roles of "eyes" and "arms" to sense and control the environment. In its most basic form, the sensors gather information from the environment through measuring mechanical, thermal, biological, chemical, optical, and magnetic phenomena (MEMS and Nanotechnology Clearinghouse, 2003). The electronics process the information obtained from the sensors and direct the actuators through some decision making capability to respond by moving, positioning, regulating, pumping, and filtering, thereby, controlling the environment for some desired outcome or purpose.

Since batch fabrication technique is used to manufacture MEMS products, a small silicon chip is possibly produced at a relatively inexpensive cost with the capabilities of functionality, reliability, and sophistication (MEMS and Nanotechnology Clearinghouse,

2003). In the industrial sector, Albany NanoTech (2003) has indicated that "MEMS devices are emerging as product performance differentiators in numerous markets with a projected market growth of over 50% per year. As a breakthrough technology, allowing unparalleled synergy between hitherto unrelated fields of endeavor such as biology and microelectronics, many new MEMS applications will emerge, expanding beyond that which is currently identified or known".

The Silicon has been widely used as engineering materials since it possesses excellent material properties making it an attractive choice for many high-performance mechanical applications. Compared to many other engineering materials, it has much higher strength-to weight ration which is allowing very high bandwidth mechanical devices to be realized. However, MEMS technology is not only making things out of silicon. MEMS technology is a new manufacturing technique of making complex electromechanical elements along with electronics on or between silicon layers using batch fabrication techniques like Integrated Circuits (IC) (Albany NanoTech, 2003).

2.5 MEMS based Inertial Sensors

MEMS research on inertial sensors has been focused primarily on accelerometers and gyroscopes. Of the two, the accelerometers were developed first. Today, MEMS accelerometers enjoy a large commercial market and are considered to be one of the most successful micro sensors ever developed. MEMS gyroscopes, on the other hand, are a relatively new technology. Commercialization of low-grade devices has begun while

intensive research is still being carried out in the laboratories on high-grade devices. A couple of examples of MEMS based accelerometers and gyroscopes available in the market are shown in Figure 2.6.
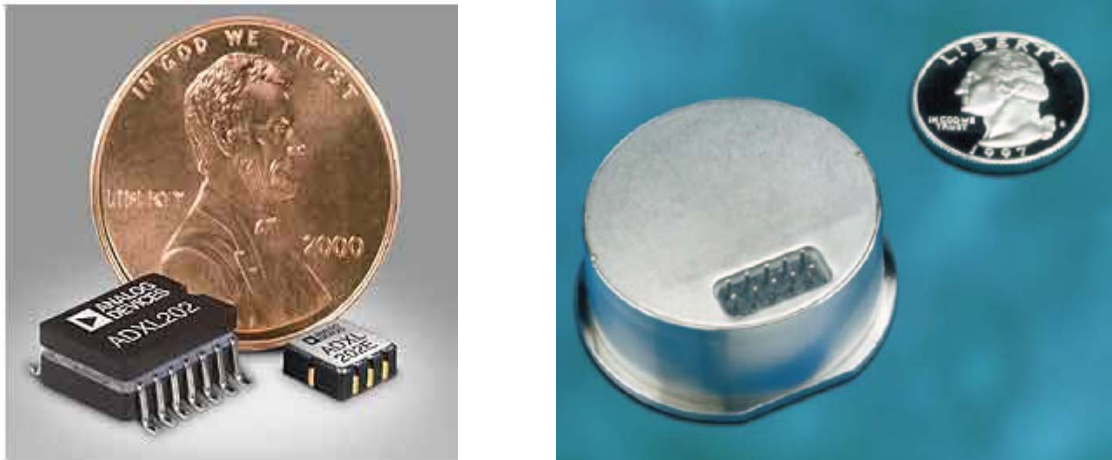
Figure 2.6 ADXL 202 Accelerometer and BEI QRS11 Gyrochip (Courtesy of Analog Device and BEI Inc., U.S.A.)

2.5.1 MEMS based Accelerometers

MEMS accelerometers are widely utilized in a variety of developments and their success is significant. MEMS accelerometers are getting more attractive to manufacturers of navigation systems because of their small size, low cost, light weight, low power consumption and ruggedness. Main considerations for MEMS inertial accelerometers are the mass size, sensing of mass movement, restoring forces, and packaging process. Normally, bigger mass is better and small currents require good electronics. Open/Closed loop system is determined by the usage of restoring forces and vacuuming, thermal sensitivity, and electronics integration are essential factors for packaging technology.

Figure 2.7 illustrates the design of a bulk-micromachined and capacitive signal pick-off accelerometer. The seismic mass and the top and bottom electrodes are made from the silicon. The seismic mass is located in the center of two electrodes and is allowed to move freely between top and bottom electrodes. The change of seismic mass location from the center location is proportional to the change of capacitance and then, capacitance change is being sensed and used to measure the amplitude of the force that led to the displacement of the seismic mass (Kraft, 1997, p. 20).
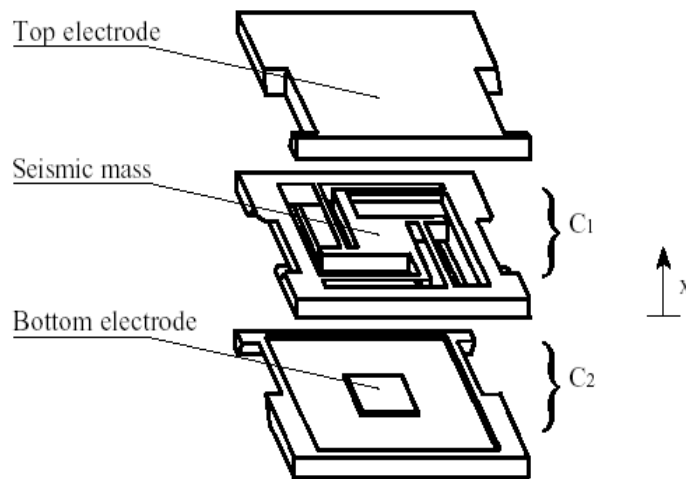
Figure 2.7 Micromachined Accelerometer Design (Kraft, 1997)

MEMS accelerometers can be classified by three categories, which are the position detection of the seismic mass, operation mode, and fabrication process of the sensing elements. The classification descriptions are summarized in the following based on Kraft (1997, p. 12 ~ p.19).

Classification by position detection of the seismic mass

Piesoresistive Signal Pick-off sensors

This method is based upon the piezoresistors that are placed on the supporting beams of the seismic mass. They change their resistance with the deflection of the seismic mass due to the stress induced in the beam.

Capacitive Signal Pick-off sensors

The sensing element typically comprises a seismic mass which can move freely between two fixed electrodes, each forming a capacitor with the seismic mass used as a common center electrode. The differential change in capacitance between the capacitors is proportional to the deflection of the seismic mass from the center position.

Piesoelectric sensing element sensors

This produces an electric charge when subjected to the force caused by the change of the seismic mass.

Resonant element sensors

This type does not detect the position of the seismic mass directly but its influence on an underdamped mechanical structure vibrating at its resonant frequency.

Classification by operation mode

Open loop operation

The deflection of the proof mass provides a measure for the acceleration which is simple design and low in cost.

Closed loop operation

This type uses some form of feedback where an external force is used to compensate the inertia force on the proof mass due to the acceleration, thus keeping the proof mass at zero deflection.

Classification by fabrication process of the sensing elements

Surface micromachining

In surface micromachined sensing elements, the seismic mass is located on the surface of a die, typically it consists of several layers of polysilicon. It is compatible with a standard integrated circuit manufacturing process; it only requires very few additional procedures. Furthermore, with surface micromachining, much smaller sensing elements can be fabricated, thus the interface electronics can be integrated on the same chip. However, the drawback of very small sensing elements is that the seismic mass is very light and it is hard to obtain a good resolution.

Bulk micromachining

In bulk micromachined sensing elements, the seismic mass is inside block, designed as a sandwich of several layers where the proof mass is usually made from single-crystal silicon and the top and the bottom covers either from silicon or Pyrex glass. Because the seismic mass lies within the die, it is well protected and it is possible to choose the damping by varying the ambient pressure of the air or filling the cavity with suitable oil. However, the drawback is that the manufacturing process is not readily compatible with standard integrated circuit (IC) fabrication processes and the size of a typical sensing element is about the size of a die making it difficult to integrate the sensing element with the required interface electronics on a same chip.

LIGA (Lithography, Galvanic, Abformung) Process

LIGA fabrication process is the only process using nickel based seismic mass instead of silicon (Kraft, 1997, p. 14). It has been used to produce the micromachined components allowing three-dimensional structuring capability with high aspect ratios and much greater structural heights which is superior to other micromachining processes. But it involves complicated technical procedures and cannot be used for standard IC manufacturing processes.

2.5.2 MEMS based Gyroscopes

Currently, most of the commercial gyroscopes can be categorized in three groups: rate grade, tactical grade, and navigation grade based on their performance. Different

principles of development of gyroscopes result in a variety of gyroscopes available in the market. MEMS based gyroscopes has been drawn recent attentions to overcome the size, the cost, and the power consumption constraints of the conventional gyroscopes because of their compact size, low-cost, and low power consumption. The majority of MEMS based gyroscopes currently under development operates in a vibratory mode and measures the angular rate instead of the absolute angle. Their operational principle is based on the coupling of mechanical energy between a vibrating motor element and a sensor element through Coriolis acceleration (Tung, 2000). The sensing element is vibrating with constant amplitude controlled by a vibrating motor that maintains the oscillation at constant amplitude. Under the vibration, the sensing element will experience Coriolis acceleration which is proportional to the applied rotation rate and it is measured to provide the information proportional to the angular rotation.

Figure 2.8 illustrates one of MEMS based gyroscopes operating in vibratory mode. It uses a vibrating quartz tuning fork to sense rotation rate and a similar fork in opposite side as a pickup. The piezoelectric drive tines are driven by an oscillator circuit at precise amplitude, causing the tines to move toward and away from one another at a high frequency. This vibration causes the drive fork to become sensitive to angular rate about an axis parallel to its tines, defining the true input axis of the sensor. For vibrating tines, an applied rotation rate causes a sine wave of torque to be produced, resulting from Coriolis acceleration, in turn causing the tines of the pickup fork to move up and down (not toward and away from one another), out of the plane of the fork assembly. The pickup tines thus respond to the oscillating torque by moving in and out of plane, causing

electrical output signals to be produced by the pickup amplifier. Those signals are amplified and converted into a DC signal proportional to the rate by the use of a synchronous switch (demodulator) which responds only to the desired rate signals (BEI Systron Donner Inertial Division. 2003).
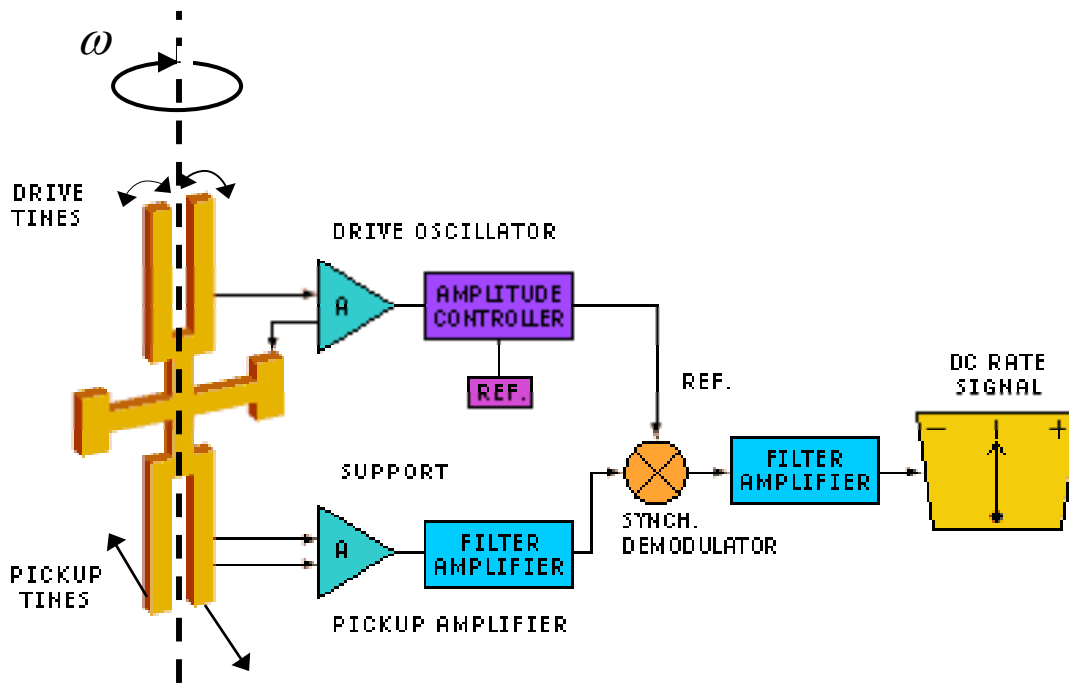
Figure 2.8 MEMS based Quartz Rate Sensor Diagram (Courtesy of BEI Inc., U.S.A.)

Similar to MEMS based accelerometers, either surface or bulk micromachining fabrication can be used for MEMS based gyroscopes (Tung, 2000). In order to achieve a better accuracy for the high-end market, the low-mass problem should be overcome properly. The difficulty in overcoming the 'mass' factor in surface micromachining gyroscopes has led to the recent renewed interest in bulk micromachining. A tremendous progress for the important issues of bulk micromachining fabrication such as high aspect ratio etching, wafer bonding and vacuum packaging enables the bulk micromachining gyroscopes to gain more popularity in recent days.

Chapter 3

Error Analysis of MEMS based Inertial Sensors

This section consists of two main parts, namely, error characterization to identify deterministic error and non-deterministic (stochastic) error sources, and the application of stochastic modeling methods which should be used to characterize the random part of the sensor output. For MEMS based inertial sensors, their deterministic error sources are mainly focused on zero-offset bias and 1st order scale factor. Among special discrete parametric stochastic modeling methods, Autoregressive (AR) model will be described in details for stochastic variation of MEMS based inertial sensors. Modeling inertial sensor errors using AR processes was first introduced and implemented in the reference (Nassar

S. et al., 2003). Further implementation of AR processes for modeling navigation-grade and tactical-grade inertial sensor errors can be found in (Nassar S., 2003).

3.1 Error Models of MEMS based Inertial Sensors

3.1.1 Error Model of MEMS based Accelerometer

The accelerometers that are currently used are mainly classified as either mechanical or solid-state. As mentioned before, all accelerometers are suffering from various error sources which are slightly different upon different types of the accelerometers. Conventional error equation will be first introduced and the error equation will then be simplified according to the tolerance of a specific application such as land vehicle navigation system and MEMS technology.

Conventionally, the measurement in the X-axis provided by accelerometer ($\tilde{a}_x$) can be expressed in terms of the applied acceleration acting along its sensitive axis (a_x) and the accelerations acting along the pendulum and hinge axes, a_y and a_z respectively, by the equation (Titterton and Weston, 1997, p.158):

$$\tilde{a}_x = (1 + S_x)a_x + M_y a_y + M_z a_z + B_f + B_v a_x a_y + n_x \tag{3.1}$$

where

S_x is the scale factor error, usually expressed in polynomial form to include

non-linear effects

M_y, M_z are the cross-axis coupling factors

B_f is the measurement bias or zero offset

B_v is the vibro-pendulous error coefficient

n_x is the random noise

For such an accelerometer, which is dual axes and non-pendulous design, it is reasonable to expect that cross-axis coupling factors and vibro-pendulous error would be insignificant (Allen et al., 1998). Then, the conventional error model can be simplified as below,

$$\widetilde{a}_x = a_x + S_x a_x + B_f + n_x \qquad\qquad (3.2)$$

As indicated by Equation (3.2), the bias and the scale factor are the main concerns for the deterministic error sources. The last term is the stochastic variation of the sensor output. The measurement from Y-axis will be expressed in the same way. In the testing, only 1st order scale factor is considered and equation (3.2) will be modified for the 360° rotation testing which will be described in the Chapter Four.

3.1.2 Error Model of MEMS based Gyroscope

As mentioned in Chapter Two, current commercial gyroscopes utilize different principles of development resulting in various types of gyroscopes with distinct characteristics of each one. Accordingly, assuming the acceleration sensitive errors are negligible, measured angular rate may be modeled for many applications as (Titterton and Weston, 1997, p. 235):

$$\widetilde{\omega}_z = (1 + S_z)\omega_z + M_x\omega_x + M_y\omega_y + B_f + n_z \tag{3.3}$$

where

S_z is the scale factor error which may be expressed as a polynomial in ω_z to represent scale factor non-linearity

M_x, M_y is the cross-axis coupling coefficients

B_f is the measurement bias or zero offset

n_z is the random noise

Using the same assumption in the previous section, equation (3.3) can be simplified mainly concerning zero offset bias and 1st order scale factor as significant contributing deterministic error sources.

$$\widetilde{\omega}_z = \omega_z + S_z\omega_z + B_f + n_z \qquad\qquad (3.4)$$

In equation (3.4), the deterministic and non-deterministic (stochastic) error sources for MEMS based gyroscope are appropriately described, and an estimation and a characterization of those main error sources will be subsequently dealt with in Chapter Four.

3.2 Review of Stochastic Modeling

3.2.1 Stationary Stochastic Processes

Observed quantities in any fields of engineering contain the elements of uncertainty resulting in random characters that we cannot determine theoretically due to various factors. These random characters are usually considered as the random variables which describe the result of a random phenomena. Stochastic (or random) process can be defined to be a collection, or "family" of random variables, which cannot be described fully in terms of a deterministic equation, the value of random variable at any particular time is governed by chance. Thus, each time we perform the "experiment" the value of the quantity that we record at each point of time is determined (at least in part) by some random mechanism (Priestley, 2001, p. 100).

Stationary stochastic process means a certain stochastic process of which probabilistic/statistical properties do not change over time. If a process is stationary up to the 2nd order, the process indicates the same mean and variance at all of different time points and covariance between two different points only depends on the time interval between these two points. This 2nd order stationary stochastic process concept is widely used to deal with random time series in practice. The following mathematical expression and the derivation of the process presume that a process is stationary up to 2nd order.

One way to specify a random process is to describe in detail the conceptual chance experiment giving rise to the process (Brown and Hwang, 1997, p. 75). When the value of the random process cannot be precisely determined, instead a range of possible values can be described with a relative likeliness of each value in probability sense. As it can be seen that many signals with same mean and variance values are quite different, it is very clear that it needs more information than just the mean and the variance to describe random process more precisely. The autocorrelation function (or autocovariance function) for a random process using the second-order probability density function is frequently used to describe random process in time domain. The autocorrelation function for a random discrete process $X(t)$ is defined as

$$R_X(\tau) = E[(X_t - \mu)(X_{t+\tau} - \mu)], \qquad \mu = \text{mean value}, \qquad \tau = 0, \pm 1, \pm 2, \ldots, \qquad (3.5)$$

and the normalized autocorrelation function as,

$$\rho_X(\tau) = R_X(\tau)/R_X(0), \qquad \tau = 0, \pm 1, \pm 2, \ldots\ldots \tag{3.6}$$

Clearly, it tells how well the process is correlated with itself at two different times. If the ergodic hypothesis applies, the autocorrelation function can also be written as

$$R_X(\tau) = \text{a time avarage of } X_t \cdot X_{t+\tau} = \lim_{T \to \infty} \frac{1}{T} \int_0^T X_t \cdot X_{t+\tau}\, dt \tag{3.7}$$

which has the maximum value when the shift $\tau = 0$ and the value decreases as the shift τ increases. $R_X(0)$ is the mean-square value of the process X_t and it is an even function of τ. And also, it is just a mathematical way of saying that $X_{t+\tau}$ becomes completely uncorrelated with X_t for large τ if there are no hidden periodicities in the process.

It has been seen that the autocorrelation function is an important descriptor of a random process and one that is relatively easy to obtain because it depends on only the second-order probability density for the process (Brown and Hwang, 1997, p. 84). Thus, if we are given the form of $R_X(\tau)$, or if we can estimate $R_X(\tau)$ from observational data, then we can use this information to help us to "identify" which of the special models (if any) would fit the process under study (Priestley, 2001, p. 111).

If the autocorrelation function decreases rapidly with τ, the process changes rapidly with time; conversely, a slowly changing process will have an autocorrelation function that decreases slowly with τ. Thus, we would suspect that this important descriptor contains

information about the frequency content of the process; and this is in fact the case (Brown and Hwang, 1997, p. 85). For stationary processes, there is an important relation known as the *Wiener-Khinchine relation;*

$$S_X(j\omega) = \Im[R_X(\tau)] = \int_{-\infty}^{\infty} R_X(\tau)e^{-j\omega\tau}\,d\tau \tag{3.8}$$

where $\Im[\cdot]$ indicates Fourier transform and ω has the usual meaning of (2π)(frequency in hertz). S_X is called the power spectral density function or simply the spectral density function of the process. When we connect the usual spectrum concept like power and spectral, some care is required. In real data, the infinitum can be achieved and is not absolutely integrable. Thus, the integral for the Fourier transform does not converge. Then, truncated version of the original dataset would be used and the Fourier transform of a sample realization of the truncated process will then exist.

The autocorrelation function in the time domain and spectral density function in the frequency domain are the Fourier transform pairs which contain the same basic information about the process, but in different forms,

$$x[n] = \frac{1}{2\pi} \int_{-\pi}^{\pi} X(e^{j\Omega})e^{j\Omega n}\,d\Omega \tag{3.9}$$

where

$$X(e^{j\Omega}) = \sum_{n=-\infty}^{\infty} x[n]\,e^{-j\Omega n} \tag{3.10}$$

Since we can easily transform back and forth between the time and frequency domains, the manner, in which the information is presented, is purely a matter of convenience for the problem at hand in a mathematical sense (Brown and Hwang, 1997, p. 91).

3.2.2 Linear System Modeling

The main purpose of mathematical model of a real physical system is to construct a proper, and tractable representation of system outputs. Since no model is perfect, one attempts to generate models that closely approximate the behaviour of observed quantities. The following linear state equation and sampled data output model are frequently used in navigation field and they give us an useful insight of stochastic modeling in practical application extracted and summarized based on the reference (Maybeck, 1994, p. 145~147). When the most general deterministic linear system model is extended to the stochastic linear system model of

$$\dot{x} = F(t)x(t) + B(t)u(t) + G(t)n_1(t) \qquad (3.11)$$

$$z(t) = H(t)x(t) + n_2(t) \qquad (3.12)$$

which is generated by adding a noise process $n_1(t)$ to the dynamics equation and $n_2(t)$ to the output equation. Using the insights from a probability theory, random parts of above equations, $n_1(t)$ and $n_2(t)$ can be characterized by the joint probability distribution function. That is to say, knowledge of such a joint distribution function or an associated joint density function completely describes the set of random variables. However, the

complete depiction of a joint distribution or density is still generally intractable. Then, try

to express $n_1(t)$ and $n_2(t)$ as the outputs of linear state-described models, called "shaping

filters", driven only by deterministic inputs and white Gaussian noise which is

completely characterized by first two corresponding moments, as shown in Figure 3.1.
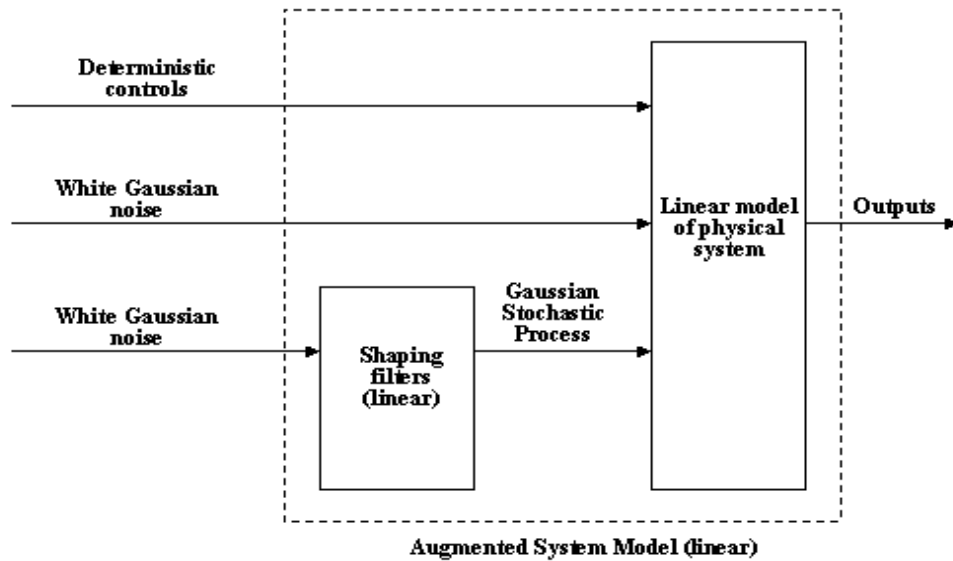
Figure 3.1 Linear System Model (Mayback, 1994)

A linear model of the physical system is driven by deterministic inputs, white Gaussian

noises, and Gauss Markov processes. The white noises are chosen as adequate

representations of wideband noises with essentially constant power density over the

system bandpass. The other Markov processes are time-correlated processes for which a

white model would be inadequate. However, these can be generated by passing white

noise through linear shaping filters (Mayback, 1994, p. 146). Consequently, one can

consider the original system model and the shaping filters as a single "augmented" linear

system, driven only by deterministic inputs and white Gaussian noises. Augmented linear system models are

$$\dot{x} = F(t)x(t) + B(t)u(t) + G(t)w(t) \tag{3.13}$$

$$z(t) = H(t)x(t) + v(t) \tag{3.14}$$

where $x(t)$ is now augmented system state, and $w(t)$ (dynamic driving noise) and $v(t)$ (measurement corrupting noise) are white Gaussian noises, assumed independent of each other and of the initial condition $x(t_0) = x_0$, where x_0 is a Gaussian random variable. These noises are modeling not only the disturbances and noise corruption that affect the system, but also the uncertainty inherent in the mathematical models themselves. Now, the main question is how to generate the shaping filters associated with the certain noise.

3.2.3 Gauss-Markov Processes

In many instances, the use of white Gaussian noise models to describe all noises in a real system may not be adequate. It would be desirable to be able to generate empirical autocorrelation or power spectral density data, and then to develop a mathematical model that would produce an output with duplicate characteristics. If observed data were in fact samples from stationary Gaussian process with a known rational power spectral density (or corresponding known autocorrelation or autocovariance function), then a linear time-invariant system, or *shaping filter*, driven by stationary white Gaussian noise, provides such a model (Maybeck, 1994, p. 180).

If a stationary Gaussian process $X(t)$ is exponentially time-correlated process, it is called a *Gauss-Markov* process. The autocorrelation and spectral functions of this process are the forms,

$$R_X(\tau) = \sigma^2 e^{-\beta|\tau|}$$
(3.15)

$$S_X(j\omega) = \frac{2\sigma^2\beta}{\omega^2 + \beta^2} \quad \left[\text{or} \quad S_X(s) = \frac{2\sigma^2\beta}{-s^2 + \beta^2} \right]$$
(3.16)

and its shaping filter can be depicted by Figure 3.2,
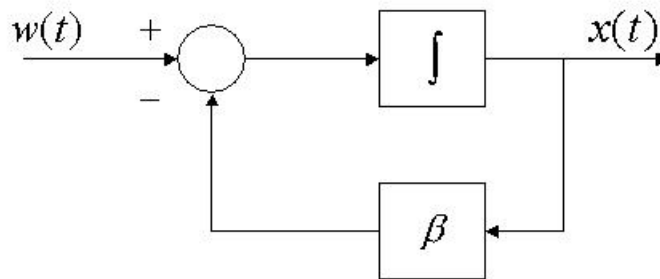
Figure 3.2 Shaping Filter of 1st order Gauss-Markov Process (Mayback, 1994)

The mean-square value and time constant for the process are given by the σ^2 and $1/\beta$ parameters, respectively. The Gauss-Markov process is a very important process in applied work because (i) it seems to fit a large number of physical processes with a reasonable accuracy, and (ii) it has a relatively simple mathematical description (Brown and Hwang, 1997, p. 95). 1st order Gauss-Markov process is very frequently used to describe the signal error behaviours providing an adequate approximation to a wide

variety of empirically observed band-limited (wide or narrow band) noises and it has been reported that 2nd order Gauss-Markov process provides a good model of oscillatory random phenomena, such as vibration, bending, and fuel slosh in aerospace vehicles (Maybeck, 1994, p. 185). In positioning and navigation fields, 1st order Gauss-Markov process has been extensively adopted to describe the sensor noise behaviours due to its simple representation of time-correlated signals. In fact, the estimated autocorrelation sequences and its FFT transforms of the random behaviour of actual sensors have shown quite different features from 1st order Gauss-Markov process. Especially for the inertial sensor noises, it has been shown in Nassar S. et al. (2003) that the autocorrelation function of INS sensor noise is not well represented by a 1st order Gauss-Markov process. Moreover, in (Nassar S., 2003), it has been shown that the accuracy of modeling inertial sensor errors is improved by 15 ~ 35% when using higher order AR models instead of 1st order Gauss-Markov model. The reference by Nassar S. (2003) has given a detailed overview of different modeling methods of AR processes and also provided the static and kinematic testing analysis of navigation and tactical-grade IMUs comparing the proposed higher order AR model results with 1st order Gauss-Markov model results. Considering the very noisy measurements and poor performance of MEMS based inertial sensors in this study, a more precise and appropriate stochastic modeling is recommended agreeing with the above reference. In the following, some of special discrete parameter stochastic models in probability and mathematical statistics theory will be introduced and among them, AR model will be described in details.

3.3 Special Discrete Parametric Models of Stochastic Processes

Considering the very noisy measurements and poor performance of MEMS based inertial sensors, a more precise and appropriate stochastic modeling is desirable. Hence, some of special discrete parameter stochastic models which provide us with a structure for fitting models to practical data will be discussed. These models are widely used in developing the theory of stationary stochastic (or random) processes in probability and mathematical statistics field. Some of important discrete parameter stochastic models are summarized in Table 3.1.

Table 3.1. Special Discrete Parametric Stochastic Models

	Definition	Remarks
White Noise	Purely random process if it consists of a sequence of uncorrelated random variable $$E[X_t] = \mu \, , E[(X_t - \mu)^2] = \sigma^2$$ $$R(s) = \text{cov}\{X_t, X_{t+s}\} = \begin{cases} \sigma^2, s = 0 \\ 0, s \neq 0 \end{cases}$$ $$\rho(s) = \begin{cases} 1, s = 0 \\ 0, s = \pm1, \pm2, \pm3, ... \end{cases}$$	- No memory with all past values up to time (t-1) - Flat power spectrum
AR Model	Autoregressive process of order k(denoted by AR(k)) if it satisfies the difference equation, $$X_t + a_1 X_{t-1} + ... + a_k X_{t-k} = \varepsilon_t$$ where $a_1, a_2, ..., a_k$, are constant coefficients, and $\{\varepsilon_t\}$ is a purely random process	- X_t depends on the combination of it own past and random disturbance - Asymptotically stationary for large t - Also called Markov process

MA Model	Moving average process of order (denoted by MA(l)) if it may be expressed in the form, $X_t = b_0 \varepsilon_t + b_1 \varepsilon_{t-1} + ... + b_l \varepsilon_{t-l}$ where $b_0, b_1, ..., b_l$, are constant coefficients, and $\{\varepsilon_t\}$ is a purely random process	- linear combination of present and past values of $\{\varepsilon_t\}$ process of finite extent - X_t can be computed as weighted average of $(\varepsilon_t, \varepsilon_{t-1}, ..., \varepsilon_{t-l})$
ARMA Model	Mixed autoregressive/moving average process of order (k,l) (denoted by ARMA(k,l)) if it satisfies an equation of the form, $X_t + a_1 X_{t-1} + ... + a_k X_{t-k} = b_0 \varepsilon_t + b_1 \varepsilon_{t-1} + ... + b_l \varepsilon_{t-l}$, where again, $\{\varepsilon_t\}$ is a purely random process and $(a_1, a_2, ..., a_k, b_0, ..., b_l)$ are constant coefficients	- More general model of a large number of "real life" process - Fewer parameters are required compared to pure AR/MA process - ARMA process corresponds to the output obtained by passing white noise through a filter with a rational transfer function
Harmonic Model	"Harmonic process" is defined by, $X_t = \sum_{i=1}^{K} A_i \cos(\omega_i t + \phi_i)$ where $K, \{A_i\}, \{\omega_i\}, (i=1,...,K)$, are constants, and the $\{\phi_i\}, (i=1,...,K)$ are independent random variables, each having a rectangular distribution on the interval $(-\pi, \pi)$	- Related to the numerical technique of harmonic analysis - Describe observational records as sums of sine and cosine waves whose amplitude and frequencies are chosen so as to give the "best fit" to the data - Autocorrelation function consists of a sum of cosine terms, and hence never die out

White noise is the purely random process which actually does not exist. However it is very important and useful mathematical concept to form the basic "building block" used in the construction of both the autoregressive and moving average models. Many of signals which are frequently occurring in practical applications, are described by AR model, MA model, and ARMA model (combination of AR and MA models). Among above discrete parameter stochastic models, AR model is the most widely adopted to

describe random noise output of practical application involving random behaving signals with some of advantages over others, and has been introduced to model the stochastic variation of inertial sensors such as accelerometer and gyroscope lately. The rest of the discussion in this chapter is mostly focused on AR models which will be actually used to characterize stochastic variation of MEMS based inertial sensor unit in Chapter Four.

First, in the autoregressive case, X_t is expressed as a finite linear combination of its own past values and the current value of ε_t, so that the value of ε_t is "drawn into" the process X_t and thus influences all future values, $X_t, X_{t+1}, \ldots\ldots$. In the moving average case, X_t is expressed directly as a linear combination of present and past values of the ε_t process but of finite extent, so that ε_t influences only (l) future values of X_t, namely $X_{t+1}, \ldots\ldots, X_{t+l}$. This feature accounts for the fact that whereas the autocorrelation function of an AR process "dies out gradually", the autocorrelation function of an MA(l) process, as we see, "cuts off" after the point l (Priestley, 2001, p. 136). The autocorrelation function of an AR process which dies out gradually is more suitable of many of the random signals in practical applications. Second, AR model parameters can be estimated in a simpler linear equation compared to MA model. ARMA model has the advantage of representing the same random process with fewer number of parameters than AR model, but it may lead to a set of non-linear equations for parameter determination resulting in much more computation loads.

Considering the linear constant-coefficient difference equation of ARMA model,

$x_t + a_1 x_{t-1} + ... + a_k x_{t-k} = b_0 \varepsilon_t + b_1 \varepsilon_{t-1} + ... + b_l \varepsilon_{t-l}$ can be written as

$$x[t] + \sum_{k=1}^{N} a_k x[t-k] = \sum_{l=0}^{M} b_k \varepsilon[t-l] \qquad (3.17)$$

where N/M is the order of AR/MA sequence.

Applying the z-transform and using the time-shift and the linearity property of the z-transform,

$$X(z) + \sum_{k=1}^{N} a_k z^{-k} X(z) = \sum_{l=0}^{M} b_k z^{-l} E(z) \qquad (3.18)$$

and then,

$$H(z) = \frac{E(z)}{X(z)} = \frac{\sum_{l=0}^{M} b_k z^{-l}}{1 + \sum_{k=1}^{N} a_k z^{-k}} \qquad (3.19)$$

$H(z)$ is normally called as transfer function of the system which completely characterizes the system. Referring to Table 3.1, AR model can be considered as a special case of ARMA model with $M = 0$, its z-transform can be inferred from equation (3.19) as

$$H(z) = \frac{E(z)}{X(z)} = \frac{b_0}{1 + \sum_{k=1}^{N} a_k z^{-k}} \qquad (3.20)$$

Estimation of the AR model parameters b_0 and a_k is the main consideration, respectively. With the standard form of AR model in Table 3.1, ε_t is a purely random process and b_0 will be the variance σ_ε^2 of ε_t. The different estimation methods of parameters a_k have been introduced in literatures and some of them will be described in the subsequent section. Also, if the process is both causal and stable, then all the poles of $H(z)$ must lie inside the unit circle of the z-plane because the Region of Convergence (ROC) is of the form $|z| > r_{max}$, and since the unit circle is included in the ROC, one must have $r_{max} < 1$, where r_{max} equals the largest magnitude of any of the poles of $H(z)$.

More details of AR(1) and AR(2) models are discussed below and these mathematical descriptions will be applied to the analysis of experimental results in subsequent sections.

First order Autoregressive Process (AR(1)) involves "one-step dependence" which is normally expressed in the form,

$$X_t - aX_{t-1} = \varepsilon_t \qquad (3.21)$$

where a is a constant, and $\{\varepsilon_t\}$ is a (stationary) purely random process. It is also called Markov processes because the conditional distribution of X_t depends only on X_{t-1}, i.e.

$$p(X_t \mid X_{t-1}, X_{t-2}, X_{t-3}, \ldots) = p(X_t \mid X_{t-1}) \tag{3.22}$$

In order to keep mathematical derivation of AR(1) model in stationary up to order 2, namely, variance and covariance of $\{X_t\}$ converge to finite values as $t \to \infty$, one assumes that $\mu_\varepsilon = 0$, $|a| < 1$. Upon assumption,

$$E[X_t] = 0, \quad \text{var}(\varepsilon_t) = E[\varepsilon_t^2] = \sigma_\varepsilon^2, \quad \text{cov}(\varepsilon_t, \varepsilon_s) = E[\varepsilon_t \varepsilon_s] = 0, \quad s \neq t \tag{3.23}$$

For sufficiently large t,

$$\sigma_X^2 \sim \sigma_\varepsilon^2 / (1 - a^2), \quad \text{cov}(X_t, X_{t+\tau}) \sim \sigma_\varepsilon^2 \cdot a^\tau / (1 - a^2) \tag{3.24}$$

Therefore, autocorrelation function and its normalized autocorrelation functions can be written as

$$R(\tau) = \sigma_\varepsilon^2 \frac{a^{|\tau|}}{(1 - a^2)}, \qquad \tau = 0, \pm 1, \pm 2, \ldots \tag{3.25}$$

$$\rho(\tau) = R(\tau) / R(0) = a^{|\tau|}, \qquad \tau = 0, \pm 1, \pm 2, \ldots \tag{3.26}$$

Second order Autoregressive Process (AR(2)) equation can be written as,

$$X_t + a_1 X_{t-1} + a_2 X_{t-2} = \varepsilon_t \tag{3.27}$$

where a_1, a_2 are constants, and $\{\varepsilon_t\}$ is a (stationary) purely random process. Using the backward shift operator B,

$$(1 + a_1 B + a_2 B^2) X_t = \varepsilon_t, \text{ or } (1 - \mu_1 B)(1 - \mu_2 B) X_t = \varepsilon_t \tag{3.28}$$

where μ_1, μ_2 ,(assumed distinct) are the roots of the quadratic $f(z) = z^2 + a_1 z + a_2$. Similar to AR(1) model derivation above, one requires that $|\mu_1| < 1, |\mu_2| < 1$ for asymptotically stationarity. Since $\{\varepsilon_t\}$ is an uncorrelated zero-mean sequence, one has,

$E[X_{t-\tau} \varepsilon_t] = 0$, $\tau \geq 1$, $E[X_t \varepsilon_t] = E[\varepsilon_t^2] = \sigma_\varepsilon^2$. With these conditions, one can reach to,

$$\sigma_X^2 = \frac{(1 + a_2)\sigma_\varepsilon^2}{(1 - a_2)(1 - a_1 + a_2)(1 - a_1 + a_2)} \tag{3.29}$$

$$\rho(\tau) = \frac{(1 - \mu_2^2)\mu_1^{\tau+1} - (1 - \mu_1^2)\mu_2^{\tau+1}}{(\mu_1 - \mu_2)(1 + \mu_1 \mu_2)}, \qquad \tau \geq 0 \text{,(For } \tau < 0, \rho(\tau) = \rho(-\tau)) \tag{3.30}$$

Autocorrelation function will behave variously according to the roots of $f(z)$ such as real or complex of AR(2) model. Higher order than 2nd order AR model will follow the equation form indicated in Table 1, corresponding probability properties can be generated similarly to AR(1) or AR(2) models. Considering the problem of fitting these models to the observational data, two separate stages are involved, which are the estimation of the parameters of the model and the determination of the order of the model. These issues are subsequently discussed in the following sections.

3.4 Estimation of Parameters in Autoregressive (AR) Models

The most considered AR model parameter estimation methods are Yule-Walker method, Burg method, and Unconstrained Least-Squares method. For a large amount of the dataset, the results of these three different methods are providing a fairly close estimation of the parameters. However, there are still some of different characteristics of each method to be noticed. Before discussing the estimation methods of AR model, it will be described first that the relationships between the AR model parameters and the autocorrelation sequences relating the AR model parameters to the coefficients in a linear predictor for the process X_t.

3.4.1 Autocorrelation Sequence of AR Model and Levinson-Durbin Algorithm

From the standard form of AR(p) model, the relationship between the parameters and the autocorrelation sequence are described as

$$X_t + a_1 X_{t-1} + ... + a_p X_{t-p} = \varepsilon_t \tag{3.31}$$

$$E[X(t)X(t-\tau)] = -\sum_{k=1}^{P} a_k E[X(t-k)X(t-\tau)] \tag{3.32}$$

Hence,

$$R_X(\tau) = \begin{cases} -\displaystyle\sum_{k=1}^{P} a_k R_X(\tau-k), & \tau > 0 \\[2em] -\displaystyle\sum_{k=1}^{P} a_k R_X(\tau-k) + \sigma_\varepsilon^2 & \tau = 0 \\[2em] R_X(-\tau) & \tau < 0 \end{cases} \tag{3.33}$$

which can be expressed in the matrix form,

$$\mathbf{R}_X \cdot \mathbf{a} = -\mathbf{r}, \tag{3.34}$$

$$\begin{bmatrix} R_X(0) & R_X(1) & \cdots\cdots & R_X(p-1) \\ R_X(1) & R_X(0) & \cdots\cdots & R_X(p-2) \\ \vdots & \vdots & & \vdots \\ R_X(p-1) & R_X(p-2) & \cdots\cdots & R_X(0) \end{bmatrix} \begin{bmatrix} a_1 \\ a_2 \\ \vdots \\ a_p \end{bmatrix} = - \begin{bmatrix} R_X(1) \\ R_X(2) \\ \vdots \\ R_X(p) \end{bmatrix} \tag{3.35}$$

and the mean-square error σ_ε^2 can be determined in equation (3.33) with $\tau = 0$,

$$\sigma_\varepsilon^2 = R_X(0) + \sum_{k=1}^{P} a_k R_X(-k) \tag{3.36}$$

Equations (3.35) and (3.36) are normally combined into a single matrix equation form as

$$\begin{bmatrix} R_X(0) & R_X(1) & \cdots\cdots & R_X(p) \\ R_X(1) & R_X(0) & \cdots\cdots & R_X(p-1) \\ \vdots & \vdots & & \vdots \\ R_X(p) & R_X(p-1) & \cdots\cdots & R_X(0) \end{bmatrix} \begin{bmatrix} 1 \\ a_1 \\ \vdots \\ a_p \end{bmatrix} = \begin{bmatrix} \sigma_\varepsilon^2 \\ 0 \\ \vdots \\ 0 \end{bmatrix} \tag{3.37}$$

The matrix $\mathbf{R}_X$ is the symmetric Toeplitz matrix and it can be efficiently inverted by use of Levinson-Durbin (LD) algorithm instead of inverting $\mathbf{R}_X$ directly to obtain the parameters a_k. LD algorithm is a computationally efficient algorithm for solving the normal equations for the prediction coefficients. LD algorithm recursively processes the symmetric Toeplitz matrix with the first order predictor to the higher order parameters. The procedure is summarized below (Proakis, 1992, p. 224),

Compact normal equations of AR(p) model from equation (3.37) is

$$R_X(\tau) = -\sum_{k=1}^{P} a_p(k) R_X(\tau - k), \qquad \tau = 1,2,......,p \tag{3.38}$$

and the minimum mean-square prediction error(MMSE) is simply

$$E_p = R_X(0) + \sum_{k=0}^{P} a_p(k) R_X(-k), \qquad \tau = 0 \tag{3.39}$$

the augmented normal equations can be expressed as

$$\sum_{k=0}^{P} a_p(k) R_X(\tau - k) = 0, \qquad \tau = 1,2,3,......,p, \qquad a_p(0) = 1 \tag{3.40}$$

beginning with the solution to the first-order predictor obtained by solving equation (3.40),

$$a_1(1) = -\frac{R_X(1)}{R_X(0)} \tag{3.41}$$

and the resulting MMSE is

$$E_1 = R_X(0) + a_1(1)R_X(-1) = R_X(0)[1 - |a_1(1)|^2] \tag{3.42}$$

let $a_1(1) = K_1$ be the first reflection coefficient. Next, a set of equations from (3.37) is used to solve for the coefficients $a_2(1)$ and $a_2(2)$ of the 2nd order predictor and express the solution in terms of 1st order predictor.

$$\begin{aligned} a_2(1)R_X(0) + a_2(2)R_X^*(1) &= -R_X(1) \\ a_2(1)R_X(1) + a_2(2)R_X(0) &= -R_X(2) \end{aligned} \tag{3.43}$$

by using substituting $a_2(1)$ and the result of (3.41),

$$a_2(2) = -\frac{R_X(2) + a_1(1)R_X(1)}{R_X(0)[1 - |a_1(1)|^2]} = -\frac{R_X(2) + a_1(1)R_X(1)}{E_1} \tag{3.44}$$

$$a_2(1) = a_1(1) + a_2(2)a_1^*(1) \tag{3.45}$$

let $a_2(2) = K_2$, the second reflection coefficient. Now, the general expressions of LD algorithm for AR(p) model are summarized below,

$$E_0 = R_X(0) \tag{3.46}$$

$$a_k(k) = K_k = -\frac{R_X(k) + \sum_{j=1}^{k-1} a_{k-1}(j) R_X(k-j)}{E_{k-1}} \tag{3.47}$$

$$a_k(j) = a_{k-1}(j) + K_k a_{k-1}^*(k-j), \qquad j = 1,2,......,k-1, \qquad k = 1,2,......,p \tag{3.48}$$

$$E_k = E_{k-1}[1 - |K_k|^2] \tag{3.49}$$

The key step of LD algorithm is to estimate the reflection coefficient based on the previous coefficient/s. In the linear prediction estimation sense, the LD algorithm described above is based on minimizing the forward prediction error. Equations above are quite efficiently used to estimate AR model parameters for the different methods which will be subsequently described.

3.4.2 Yule-Walker Method for AR Model Parameter Estimation

The Yule-Walker method constructs the equation (3.35) by using the estimates of autocorrelation sequences from the windowed measured data and uses the LD algorithm described above to solve for AR model parameters. That is, Yule-Walker method uses the windowed input data and the minimization of the forward prediction error in the least-squares sense. Since the autocorrelation matrix in equation (3.35) needs to be positive semidefinite, the biased form of the autocorrelation estimate is advisable,

$$\hat{R}_X(\tau) = \frac{1}{N} \sum_{t=1}^{N-|\tau|} (X_t - \overline{X})(X_{t+\tau} - \overline{X}) \tag{3.50}$$

in the practical situation. It always produces a stable AR model. However, Yule-Walker method is not suitable for a short period of data resulting in poor performance of parameter determination because it applies windowing to the data.

3.4.3 Burg Method for AR Model Parameter Estimation

Contrary to Yule-Walker method, the Burg method is not using the estimates of autocorrelation sequences from the input data but it estimates the reflection coefficients by minimizing both of the forward and the backward prediction errors in the least square sense with the constraint that the AR parameters satisfy the Levinson-Durbin recursion.

The Burg method estimation derivation is summarized below (Proakis, 1992, p. 503). Suppose that we are given the data X_t, $t = 0,1,2,\ldots\ldots,N\text{-}1$, and let us consider the forward and backward linear prediction estimates of order p, which are given as

$$\hat{X}_t = -\sum_{k=1}^{P} a_p(k) X_{t-k} \tag{3.51}$$

$$\hat{X}_{t-p} = -\sum_{k=1}^{P} a_p^*(k) X_{t-p+k} \tag{3.52}$$

and the corresponding forward and backward errors are defined as $e_p^f(t) = X_t - \hat{X}_t$ and

$e_p^b(t) = X_{t-p} - \hat{X}_{t-p}$, where $a_p(k)$, $0 \le k \le p-1$ are the prediction coefficients. The least-squares error is

56

$$E_p = \sum_{j=p}^{N-1} [| e_p^f(j) |^2 + | e_p^b(j) |^2] \tag{3.53}$$

This error is to be minimized by selecting the prediction coefficients, subject to the constraint that they satisfy the Levinson-Durbin recursion given by (3.48). When the equation (3.48) is substituted into expressions for $e_p^f(t)$ and $e_p^b(t)$, the result is the pair of order-recursive equations for the forward and backward prediction errors given below,

$$e_0^f(t) = e_0^b(t) = X_t \tag{3.54}$$

$$e_k^f(t) = e_{k-1}^f(t) + K_k e_{k-1}^b(t-1), \qquad k = 1.2.......,p \tag{3.55}$$

$$e_k^b(t) = K_k^* e_{k-1}^f(t) + e_{k-1}^b(t-1), \qquad k = 1.2.......,p \tag{3.56}$$

Now, if we substitute from (3.55) and (3.56) into (3.53) and perform the minimization of least-squares error (E_p) with respect to the reflect coefficient (K_k), we obtain the result,

$$\hat{K}_k = \frac{-\sum_{j=k}^{N-1} e_{k-1}^f(j) e_{k-1}^b(j-1)}{\frac{1}{2} \sum_{j=k}^{N-1} [| e_{k-1}^f(j) |^2 + | e_{k-1}^b(j-1) |^2]}, \qquad k = 1.2.......,p \tag{3.57}$$

The term in the numerator of (3.57) is an estimate of the cross-correlation between the forward and backward prediction errors. With the normalization factors in the denominator of (3.57), it is apparent that $| K_k | < 1$, so that the all-pole model obtained from the data is stable.

The main advantage of Burg method is that it has high resolution for short data records. That is, Burg method is suitable not only for the large data records but also for the short data records. It still provides a stable and computationally efficient model. Burg method, however, is sensitive to the initial phase of a sinusoid for the sinusoidal signals in noise and exhibits spectral line-splitting for high-order models.

3.4.4 Unconstrained Least-Squares Method for AR Model Parameter Estimation

Similar to Burg method, the unconstrained least-squares method minimizes both the forward and backward linear prediction errors to determine AR model parameters but it is not constrained by Levinson-Durbin recursion algorithm. The forward and backward linear prediction errors described in (3,49) can be expressed with the corresponding forward and backward linear prediction estimates,

$$
\begin{aligned}
E_p &= \sum_{j=p}^{N-1}[\,|\,e_p^f(j)\,|^2 + |\,e_p^b(j)\,|^2\,] \\
&= \sum_{j=p}^{N-1}\left[\,|\,X(j)+\sum_{k=1}^{P}a_p(k)X(j-k)\,|^2 + |\,X(j-p)+\sum_{k=1}^{P}a_p^*(k)X(j-p+k)\,|^2\,\right]
\end{aligned}
\tag{3.58}
$$

$$
\sum_{k=1}^{P}a_p(k)R_X(l,k) = -R_X(l,0)\,, \qquad l=1,2,\ldots\ldots,m
\tag{3.59}
$$

The minimizing procedure of unconstrained least-squares method is the same as Burg method. However, instead of using Levinson-Durbin recursion, minimization of E_p with respect to the prediction coefficients yields the set of linear equations and an associated correlation matrix is not Toeplitz. The form of the unconstrained least-squares method

58

described above has also been called the unwindowed data least-squares method. Its performance have been found to be superior to the Burg method, in the sense that the unconstrained least-squares method does not exhibit the same sensitivity to such problems as line-splitting, sinusoidal signal in noise. Computational efficiency is also comparable to the efficiency of the Levinson-Durbin algorithm but with this method, there is no guarantee that the estimated AR parameters yield a stable AR model (Proakis, 1992, p. 508).

3.5 Determination of Order of the Stochastic Models

Even a priori information on the order of an AR Model was given, the optimal order of the AR model is still unknown which needs to be estimated. One of the common ways to determine the order of the AR model is to investigate the residual variance in accordance to different orders. Assuming the true model is of finite order, as the estimated order is getting close to the true model, the residual variance wouldn't reduce significantly. It should be kept in mind that a higher order AR model would increase the state vector of the Kalman Filter error states. As a result, it would increase the computational loads even result in the unstable solutions.

Some of model order selection methods have been reported such as Final Prediction Error (FPE) and Akaike's Information Criterion(AIC) proposed by Akaike (1969,1974), Minimum Description Length(MDL) by Rissanen (1983) and etc. However, the methods

above have been indicated that they do not provide definitive and consistent results (Proakis, 1992, p. 510). Therefore, investigation of the residual variance considering state vector increase of Kalman Filter will be used to select the model order in the testing. This has been also suggested by Nassar S. (2003) for navigation and tactical-grade IMUs.

Chapter 4

Estimation of Deterministic Error Sources and Stochastic Modeling

4.1 Estimation Principles

Based on the study in the previous chapters, the estimation of deterministic error sources and stochastic error characterization of a certain type of MEMS based inertial sensor will be described subsequently in this chapter. In this research, RGA300CA inertial sensor unit shown in Figure 4.1 from Crossbow Corp was used to facilitate the performance tests since the sensor is claimed as the ideal system for a land vehicle. RGA300CA sensor

consists of tri-axial bulk-micromachined capacitive accelerometer and single-axis vibratory rate gyroscope.
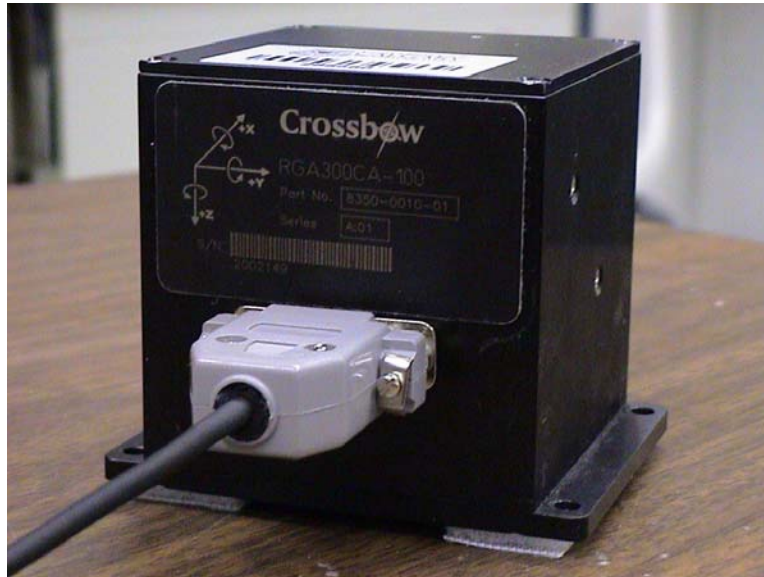

Figure 4.1 RGA300CA (3-Axis Accel. & 1-Axis Gyro)

First, deterministic error sources of RGA300CA are confined to zero-offset bias and 1st order scale factor from this point. The estimation of deterministic error sources of accelerometer and gyroscope will be dealt with separately due to their distinct raw measurements. The basic principle is to compare the actual measurements of accelerometer and gyroscope with a reference dataset and to obtain the desired error sources by one of conventional optimal estimation method (Least Squares). Details are followed in the subsequent subchapters including testing results and analysis.

Once the deterministic error sources are estimated, the stochastic variation can be assessed by compensating the deterministic error sources from raw measurements in

static position for a certain period of time. The stochastic variation of each axis of accelerometer and gyroscope will be described in time domain and characterized by using Autoregressive (AR) model resulting in appropriate order and parameter/s of AR model for each of them. Most of the tests have been performed in the Multi-Sensor Lab at The University of Calgary with the room temperature (about 21°C) maintained. For the sensor unit, 20 Hz datalogging rate and approximate bandwidth of 10 Hz were used with data logging system (GyroView Version 2.4) from Crossbow Corp. and also, the model SM2330SQ version 4.11 motor was used with SMI 1.310 windows S/W from Animatics Corporation. Sensor unit and rotation panel were connected to separate computers with RS-232 port cables; the output of the accelerometer measurements was saved in text file format; both were turned on and off every time with about 30 minutes apart and were warmed up for about 20 minutes before each datalogging. In addition, the local gravity value ($9.8080.\text{m/s}^2$) in the Multi-Sensor Lab at The University of Calgary has been used as the reference gravity value.

4.2 Estimation of MEMS based Accelerometer Deterministic Error Sources

First, RGA300CA has been tested in the rotation panel connected to SmartMotor from Animatics Corp.. A testing table was carefully leveled relative to the local gravity vector. Once an accelerometer was attached to the testing table properly, the accelerometer output was collected at a constant speed of rotation depicted by Figure 4.2. The actual

measurements of X/Y/Z axes of the accelerometer were compared with the reference acceleration determined by the testing table orientation and local gravity value ($9.8080.m/s^2$).

Figure 4.2 Accelerometer Testing Setup

For an accelerometer which is non-pendulous in design, it is reasonable to expect that cross-axis coupling factors and vibro-pendulous error would be insignificant (Allen, J.J. et al., 1998). Therefore, the simplified error model given in equation (3.2) can be used. As mentioned previously, the bias and the scale factor are the main concerns for the deterministic error sources of the sensor, and only 1st order of scale factor is considered in the testing.

Before testing, a small modification is necessary to equation (3.2) in order to fit the 360°

rotation test setup as below:

$$\tilde{a}_x = a_x(\cos\theta) + S_x a_x(\cos\theta) + B_f + n_x \qquad (4.1)$$

$$\theta = \omega(t - t_1), \omega = 360°/(t_2 - t_1) \qquad (4.2)$$

where

ω is angular velocity

t is instantaneous time

t_1 is time at first +1g
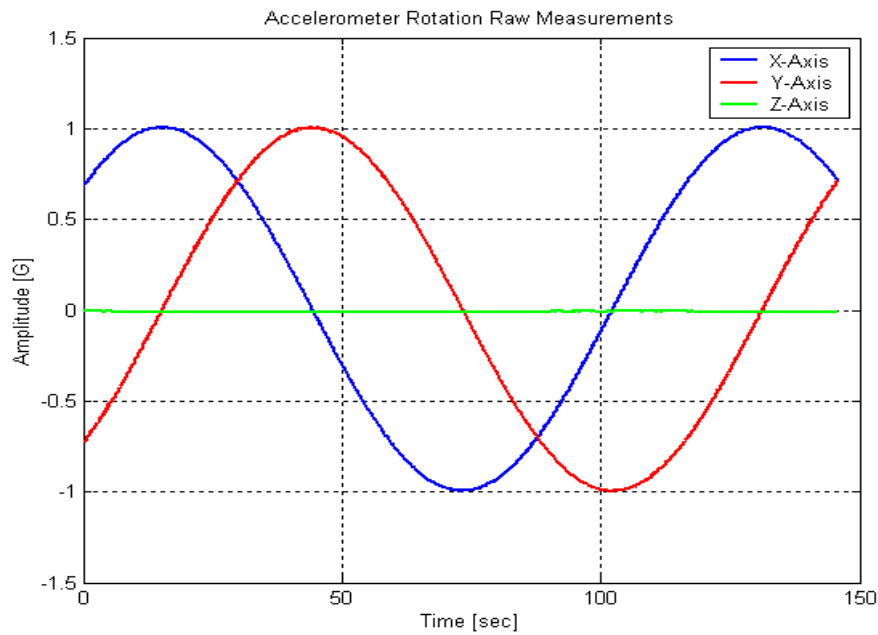
t_2 is time at second +1g

Figure 4.3 RGA300CA Accelerometer Rotation Measurements

65

If the rotation panel can be controlled to provide precise angular velocity, the orientation of acceleration motion can be generated easily. Otherwise, the angular velocity can be estimated by obtaining the time (t_1) at first +1g of an axis, and the time (t_2) at second +1g of an axis using line regression method with the 2nd order polynomial function ($y = ax^2 + bx + c$). Namely, once the coefficients of the second order polynomial function are obtained, the time t_1 and t_2 are determined by $t = -\dfrac{b}{2a}$. Even though there still exist errors in the approximation, the line regression method can be considered much more accurate than any other human measurements of revolution time. Due to the instability of the rotating motor and the initial misalignments, the angular velocity should be calculated for every run (20 times). Similar to the angular velocity calculation, the bias or zero offset (B_f) and the scale factor (S_x) in equation (4.1) can be obtained by using Least Squares method with the rotational measurements and reference gravity value. The results of 20 tests with their mean & standard deviation for 3 axes are shown in Table 4.1, and the bias and the scale factor stability are illustrated in Figure 4.4 and 4.5.

Table 4.1 Bias and Scale Factor Results of Accelerometer

	X-axis		*Y-axis*		*Z-axis*	
	Bias[mg]	*S.F.[%]*	*Bias[mg]*	*S.F.[%]*	*Bias[mg]*	*S.F.[%]*
1	1.1548	-0.0849	0.6447	-0.0807	1.9912	-0.1045
2	2.8427	-0.0852	1.3094	-0.1033	3.2705	-0.1345
3	2.2067	-0.0355	3.8652	-0.1902	1.9736	-0.1370
4	1.7903	-0.0434	4.3118	-0.1551	1.5669	-0.1513
5	1.5776	-0.0306	4.3459	-0.1509	1.4362	-0.1606
6	1.6411	-0.1552	3.7548	-0.1318	1.1185	-0.1466
7	1.3423	-0.1358	3.5154	-0.1504	2.2184	-0.1504
8	1.5614	-0.1068	2.9473	-0.1144	0.5651	-0.0649
9	2.5189	-0.1131	3.2060	-0.1205	0.8855	-0.0846
10	3.8183	-0.1159	3.2152	-0.1254	1.2129	-0.0835

| 11	1.5750	-0.1400	1.1294	-0.1651	3.2332	-0.0602
12	2.4533	-0.1262	1.1018	-0.1506	3.5628	-0.0751
13	3.3925	-0.1293	1.5480	-0.1209	3.1330	-0.0814
14	3.4469	-0.0925	1.9380	-0.1167	2.8823	-0.0851
15	2.4924	-0.0779	2.1209	-0.1322	2.6424	-0.0719
16	4.3743	-0.0651	2.2410	-0.1009	2.2395	-0.0692
17	3.0543	-0.0474	1.9292	-0.1189	1.9984	-0.0648
18	1.9111	-0.0833	1.8029	-0.1116	2.1606	-0.0706
19	2.7809	-0.0978	1.6697	-0.1042	1.8483	-0.0648
20	1.9869	-0.0937	1.8692	-0.1246	1.8634	-0.0629
Mean	2.3961	-0.0930	2.4233	-0.1284	2.0901	-0.0962
St.D.	0.8858	0.0359	1.1304	0.0256	0.8356	0.0357
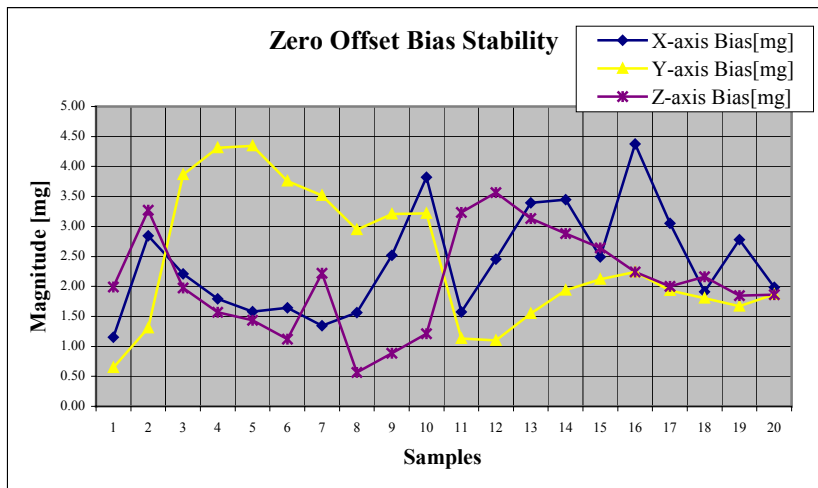
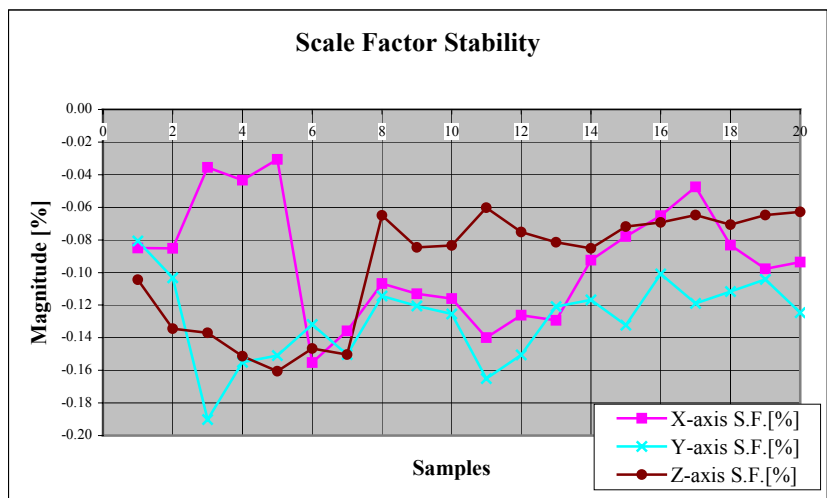Figure 4.4 Zero Offset Bias Stability of Accelerometer

Figure 4.5 Scale Factor Stability of Accelerometer

67

According to the results shown above, among three axes, y-axis has the largest fluctuation of zero-offset bias and the smallest of scale factor but the differences between axes are nominal. In terms of the magnitude, the mean values of zero-offset biases for 3 axes are a few mili-g's which are more typical values compared with the basic information ($<\pm30mg$) from the manufacturer's specifications. Those results can be used as a reference value to compare with values when the sensor unit is horizontally or vertically leveled in the vehicle. In the unleveled case, the mean values of zero-offset biases can be considered as mean zero error and then, they can be compensated from the raw measurements of the accelerometer. Also, the mean values of 1st order scale factor for 3 axes are much more descriptive than the value ($<1\%$) from the manufacturer's specifications. Those numbers will be referenced in performance analysis in chapter Five.

4.3 Estimation of MEMS based Gyroscope Deterministic Error Sources

As discussed in the previous chapter, the deterministic error sources of RGA300CA Yaw rate gyroscope are zero-offset bias and 1st order scale factor. Analogous to the accelerometer case, the simplified form of error equation (3.4) without any modification will be in use to analyze actual gyroscope's Yaw rate measurements. This time, the rotational table has been precisely leveled out horizontally shown in Figure 4.6 and provided the reference angular rate which is supposed to be correspondent to Yaw rate of gyroscope assuming that Earth rotation rate effect is nominal.
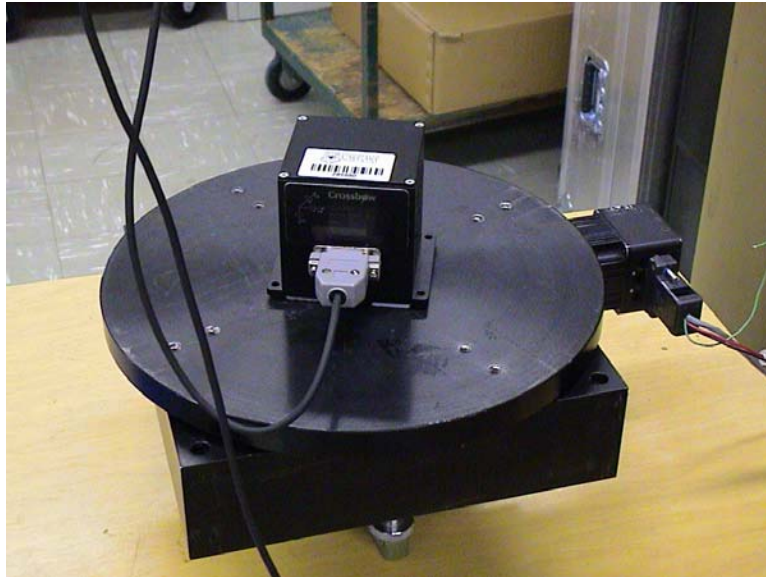
Figure 4.6 Gyroscope Testing Setup

During a typical test schedule, the rotation rate of the rate table is stepped through a series of angular rates starting from zero deg/s recording data at each stage. The rotation speed is kept constant for a set period at each step and the sensor outputs allowed to stabilize, before recording the output signals. The applied angular rate is varied in incremental steps between the maximum and minimum desired rotation rates. At each step, the signals from gyroscope are recorded when the sensor is in equilibrium (Titterton and Weston, 1997, p.205).

In this experiment, the applied rotation rate has been increased from zero deg/s to 80 deg/s and then, decreased until negative 80 deg/s. After that, it resumed to increase from negative 80 deg/s to zero deg/s. For each rotation rate steps (10 deg/s), dwell time consists of stabilization time (about 10 seconds) and sample time (about 10 seconds). 33

subsets of data have been recorded based on the same scheme and combined together to compose a series of measurements. One of the testing results has been illustrated in Figure 4.7.
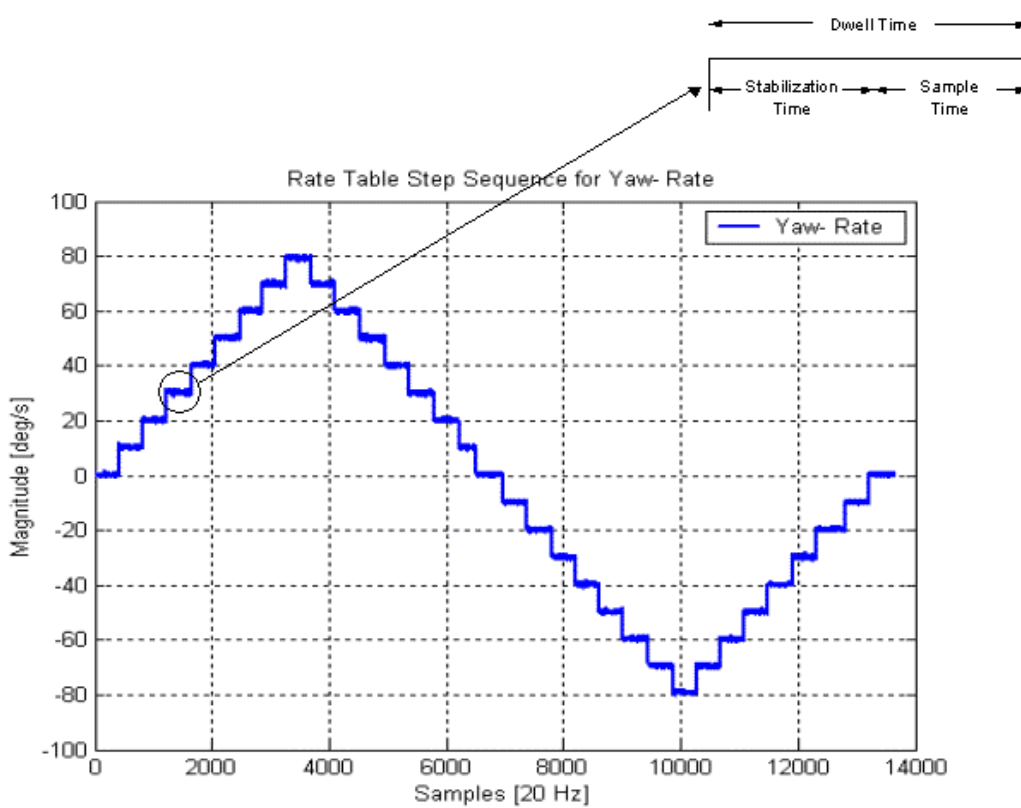

Figure 4.7 Rate Table Step Sequence

Those recorded data has been averaged out to provide a list of measurements resulting in measurement matrix in Least Squares estimation scheme. Accordingly, two parameters (zero-offset bias and 1st order scale factor) could be estimated by simple Least Squares process with 33 measurements. The same test has been performed ten times with approximately 30 minutes interval. The results of 10 tests with their mean & standard deviation for Yaw-rate are shown in Table 4.2 and the bias and the scale factor stability are illustrated in Figure 4.8.

Table 4.2 Bias and Scale Factor Results of Gyroscope

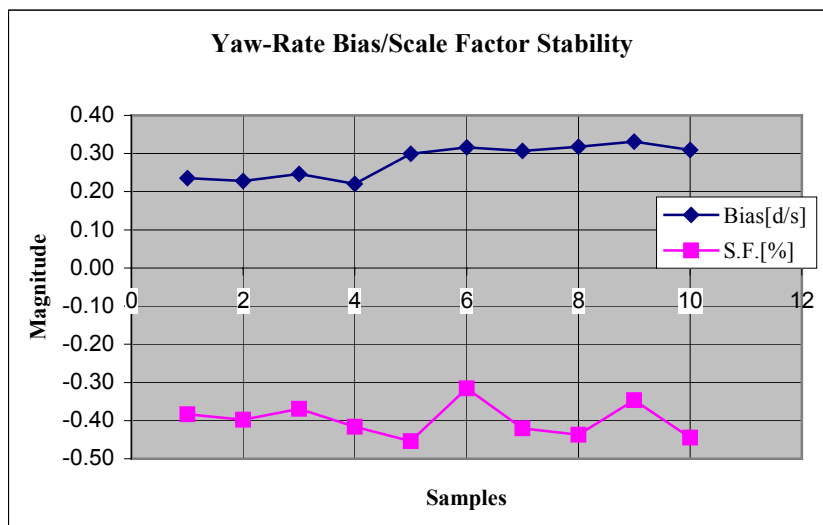|	Yaw-Rate	
	Bias[d/s]	S.F.[%]
1	0.2359	-0.3837
2	0.2284	-0.3977
3	0.2469	-0.3693
4	0.2206	-0.4164
5	0.2990	-0.4538
6	0.3164	-0.3154
7	0.3071	-0.4203
8	0.3180	-0.4367
9	0.3310	-0.3462
10	0.3095	-0.4445
Mean	0.2813	-0.3984
St.D.	0.0407	0.0449

Figure 4.8 Zero-Offset Bias/Scale Factor Stability of Gyro.

The mean and the standard deviation shown in Table 4.2 are more specific values compared with manufacturer's specifications provided with the sensor unit. Relatively, the results of gyroscope have less fluctuation than those of accelerometer in both of zero-offset bias and scale factor. Shorter recording time of each step of rotation rate could be

71

beneficial to the gyroscope's results compared with accelerometer results. As mentioned earlier in accelerometer case, the gyroscope's results shown above can be used as the comparable value when the sensor unit is actually set up for real applications.

4.4 Stochastic Modeling of MEMS based Accelerometer and Gyroscope

Based on the discussion in section 3.4, 3.5, and 3.6 of Chapter Three, the stochastic variation (random noise) of experimental output of accelerometer and gyroscope inside RGA300CA will be analyzed and modeled appropriately. Among the various special discrete parametric models of stochastic processes, Autoregressive (AR) model and purely random process (white noise) will be used. AR model parameters will be estimated by using Burg method. Then, corresponding order of AR model will be approximated by investigating the residual variance in accordance to different orders considering the increase of state vector in Kalman Filter error state.

Before proceeding, one of the important issues in the analysis of characteristics of random process, which is the span of observation time of the experimental data should be considered. This is a fundamental limitation, irrespective of the means of processing the data. The following summarizes a thorough explanation and feasible example to get at least a rough estimate of the amount of experimental data needed for a given required accuracy provided by the reference (Brown and Hwang, 1997, p. 106 ~ p. 108). The time

of the data to be analyzed must, of course, be finite; and as a practical matter, it is preferred not to analyze any more data than is necessary to achieve reasonable results. Remember that since this is a matter of statistical inference, there will always remain some statistical uncertainty in the result. One way to specify the accuracy of the experimentally determined spectrum or autocorrelation function is to say that its variance must be less than a specified value. The variance of an experimentally determined autocorrelation satisfies the inequality

$$Var\, V_X(\tau) \le \frac{4}{T} \int_0^\infty R_X^2(\tau) d\tau \qquad (4.3)$$

where it is assumed that a single sample realization of the process is being analyzed, and

T is time length of the experimental record

$R_X(\tau)$ is autocorrelation function of the Gaussian process under consideration

$V_X(\tau)$ is time average of $X_T(t)X_T(t+\tau)$ where $X_T(t)$ is the finite-length sample of $X(t)$ [i.e., $V_X(\tau)$ is the experimentally determined autocorrelation function based on a finite record length]

$$V_X(\tau) = [\text{time avg. of } X_T(t)X_T(t+\tau)] = \frac{1}{T-\tau} \int_0^{T-\tau} X_T(t)X_T(t+\tau)\, dt \qquad (4.4)$$

Also, $V_X(\tau)$ is admitted as an unbiased estimator of $R_X(\tau)$ and it would appear to be a well-behaved estimator of $R_X(\tau)$. When it is assumed that $X(t)$ is the 1st order Gauss-Markov process with an autocorrelation function

$$R_X(\tau) = \sigma^2 e^{-\beta|\tau|} \tag{4.5}$$

Substituting the assumed Gauss-Markov autocorrelation function into Equation (4.3), then it yields

$$Var[V_X(\tau)] \leq \frac{2\sigma^4}{\beta T} \tag{4.6}$$

Furthermore, when the estimated time constant $(1/\beta)$ of 1 sec and the accuracy of 10 percent are needed for its autocorrelation function,

$$\frac{Var[V_X(\tau)]}{\sigma^4} \leq \frac{2}{\beta T}$$

$$T = \frac{1}{(0.1)^2} \cdot \frac{2}{\beta} = 200 \text{ sec} \tag{4.7}$$

Note that 10 percent accuracy is really not an especially demanding requirement, but yet the data required is 200 times the time constant of the process.

Once the rough idea of the time span of experimental data was obtained, the accelerometer's output was analyzed first. For the stochastic modeling, the static measurements of RGA300CA system for about 11 hours were collected 10 times with a minimum 2 hours interval and 20 minutes warm-up period.

Figure 4.9 shows one sample dataset of accelerometer that have been repeated for about 11 hours in well-leveled static mode. It is clear that the temperature variation of the sensor unit affects the sensor measurements significantly. It is well indicated in many literatures that the temperature is the main concern of sensor output stability. Therefore, relatively stable parts of the original accelerometer measurements were only used and the trends of them were removed as shown in Figure 4.10.
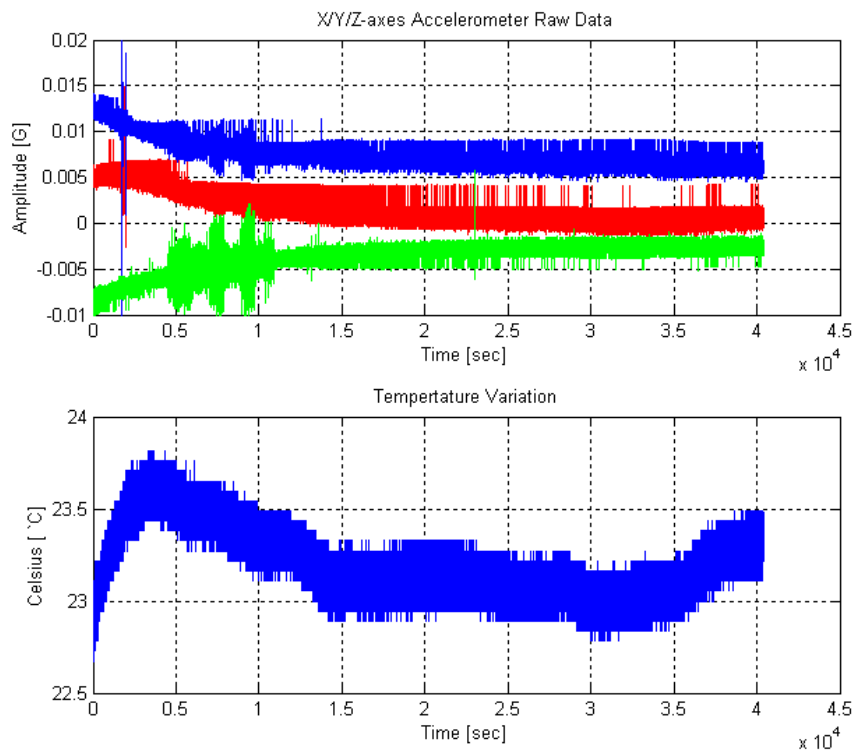

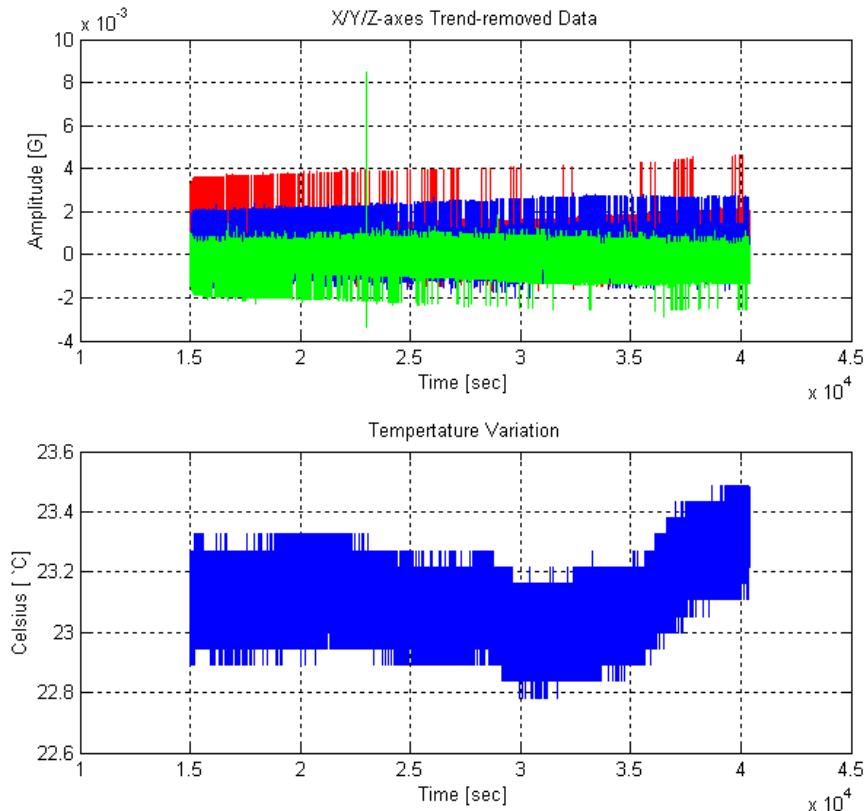Figure 4.9 RGA300CA Accelerometer Static Measurements

Figure 4.10 Trend-Removed Stable Part of Accelerometer Output

Using the experimental data shown above, the autocorrelation sequences for 3 axes were generated and they have shown the significant different features compared with the conventional autocorrelation features of 1st order Gauss Markov process which has been widely used in navigation field. The following two Figures 4.11 and 4.12 indicate how different theoretical autocorrelation function of 1st order Gauss Markov process and empirically estimated autocorrelation functions are.
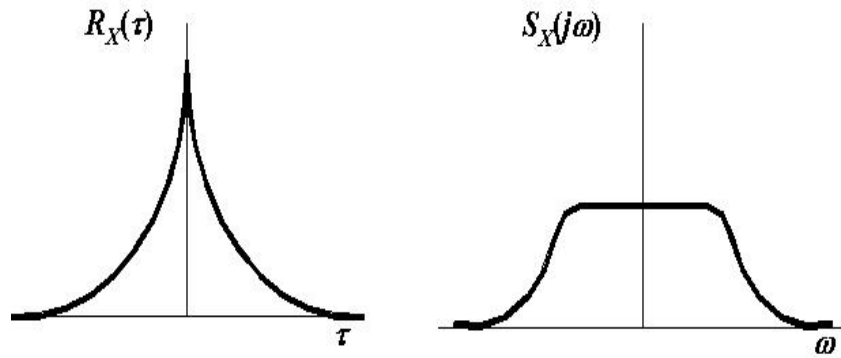
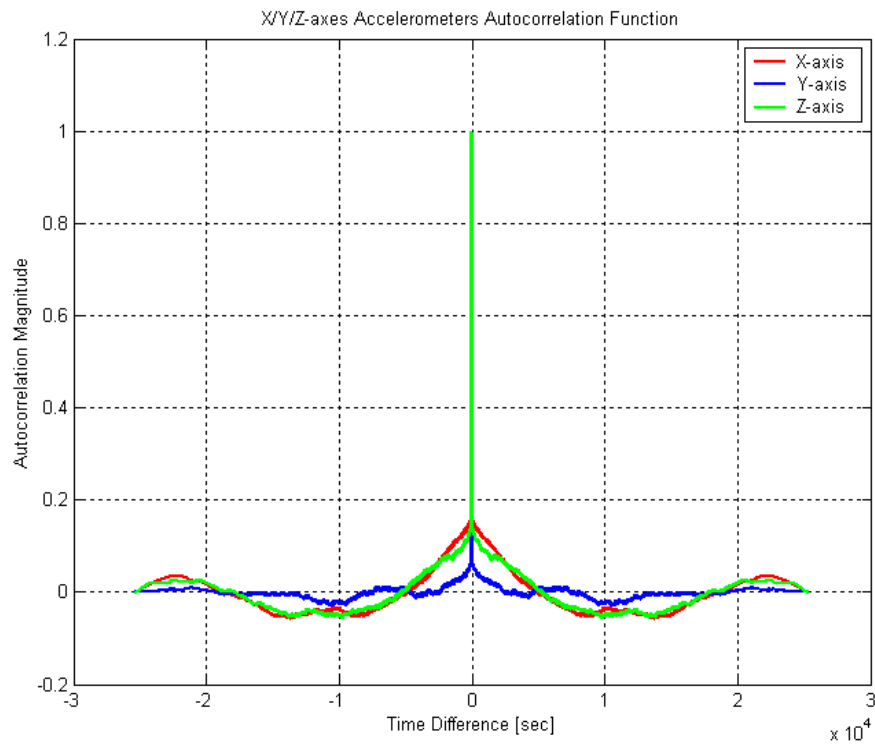Figure 4.11 Autocorrelation and Its FFT Transform of 1st Order Gauss Markov Process

Figure 4.12 Empirically Estimated Autocorrelation Functions of 3 Axes of Accelerometer

It is the biggest motivation to model the stochastic variation in the different way rather than conventional 1st order Gauss Markov process. Figure 4.12 shows the results of one of the sample datasets. As 1st order Gauss Markov modeling is quite well known, only

AR modeling procedure will be described. As described earlier, there are two main steps involved in AR modeling, namely, parameter estimation and order determination. Once the three parameter estimation methods in the previous section were performed to estimate the parameters using the sample dataset (about 8 hours with a sampling rate of 20Hz), they have provided very close results from one to the other. Therefore, in spite of some distinct characteristics, any methods could be used in this experiment. In the testing, the Burg method has been applied. To assess the proper determination of the order for AR model, the estimated residual variance σ_ε^2 in accordance to different orders was chosen to be analyzed. In order to avoid abrupt increase in the error states of the Kalman filter due to the increase of the order of the AR model, an appropriate order ought to be determined when the variance plot starts to be leveled out in Figure 4.13.
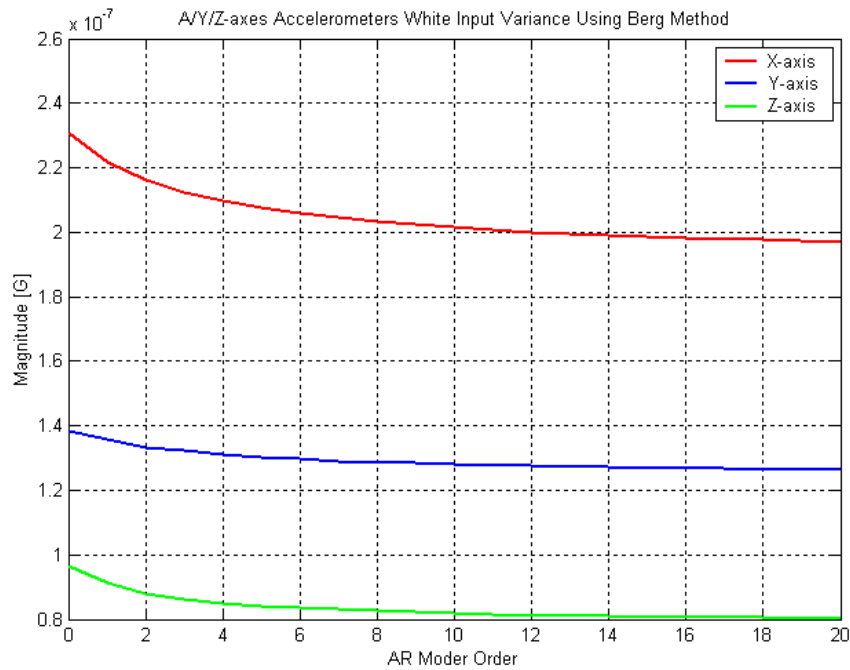

Figure 4.13 White Noise Variance Plot with Different Orders of AR model for Accelerometer

Based on the results shown in Figure 4.13, 4th order AR model has been chosen and its parameters were estimated by the Burg method.

For the stochastic variation of the gyroscope (yaw angle rate only), the analogous routine has been performed. First step was to investigate the raw measurements of sensor output and to try to remove the trend to get close to zero mean of dataset. And then, the empirically estimated autocorrelation sequence was generated to view how correlated each measurement is to one another as the time gap increases. Same as the accelerometer case, 20Hz dataset were used and the time gap is increased by 0.05 second.

Different from accelerometer output, the gyroscope output has shown that it was little affected by variation of sensor temperature in Figure 4.14. Accordingly, it was not necessary to window some part of raw measurements like accelerometer's case. For stochastic analysis of the gyroscope, the whole data of about 11 hours datasets have been used. The empirically estimated autocorrelation function of gyroscope output has shown a strikingly result which is impulse amplitude when the time difference is zero and the rest of them are pretty close to zero in Figure 4.15. It indicates that the stochastic variation of gyroscope output would behave like a purely random process (white noise). 10 sets of static dataset have presented very similar results. Also, its FFT transform pair (Spectral Density Function) has shown an empirical representation of white noise assumption for the spectral amplitude of white noise to be spread out for all frequencies sketched in Figure 4.16.
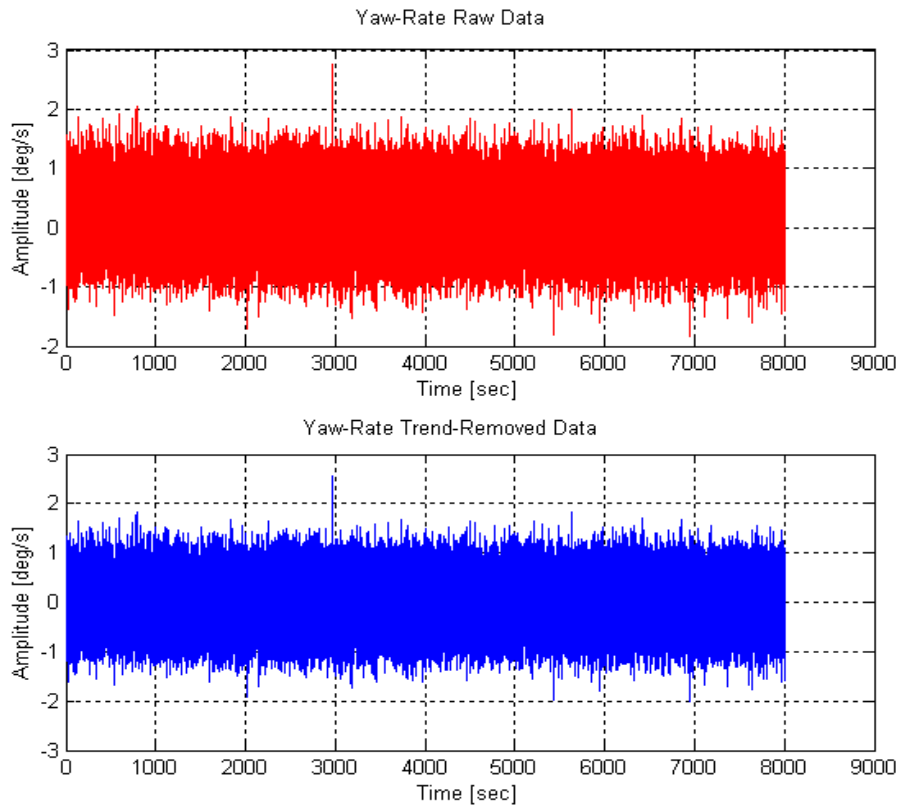
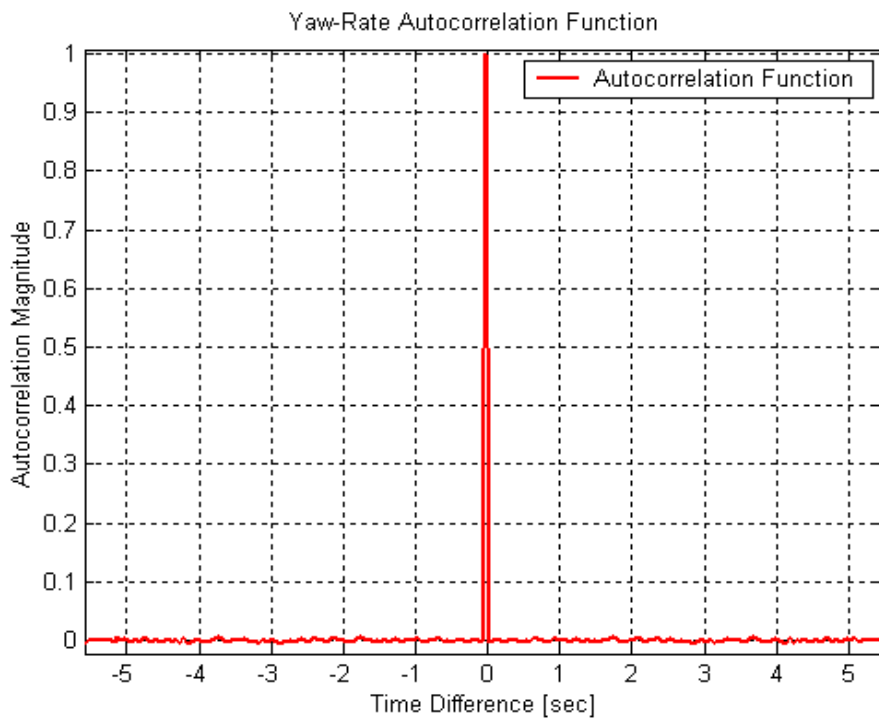Figure 4.14 Raw and Trend-Removed Data of Gyroscope Output

Figure 4.15 Empirically Estimated Autocorrelation Function of Gyroscope Output

80
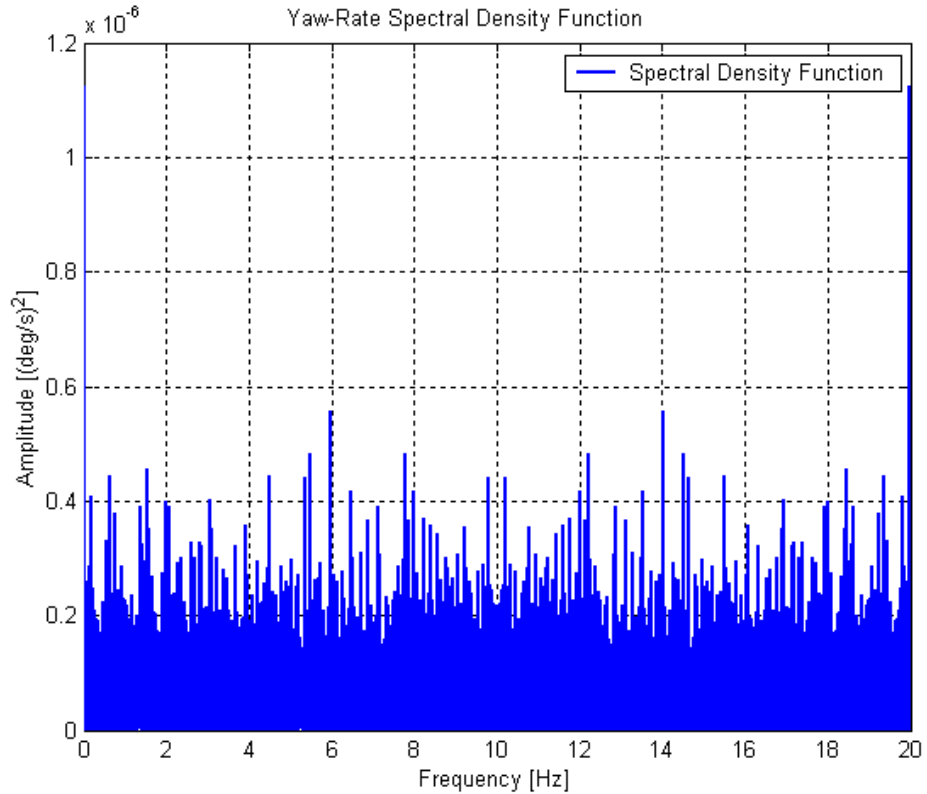
Figure 4.16 Empirically Estimated Spectral Density Function of Gyroscope Output

The empirically estimated autocorrelation function and its FFT transform (spectral density function) in Figure 4.15 and 4.16 have represented that the stochastic variation of the gyroscope could be modeled as purely random process (white noise) even though the white noise is only the mathematical abstraction, not the real process. In addition, as the estimated residual variance σ_ε^2 in accordance to different orders for the determination of the proper AR model parameter estimation has been sketched in 4.17, the residual variance has not significantly decreased in any point and has provided very close values from zero order to 20th order situation. It is another useful indication that gyroscope output could be modeled as purely random process (white noise) with the mean square value ($\sigma_\varepsilon^2 = 0.19293$ deg/s).
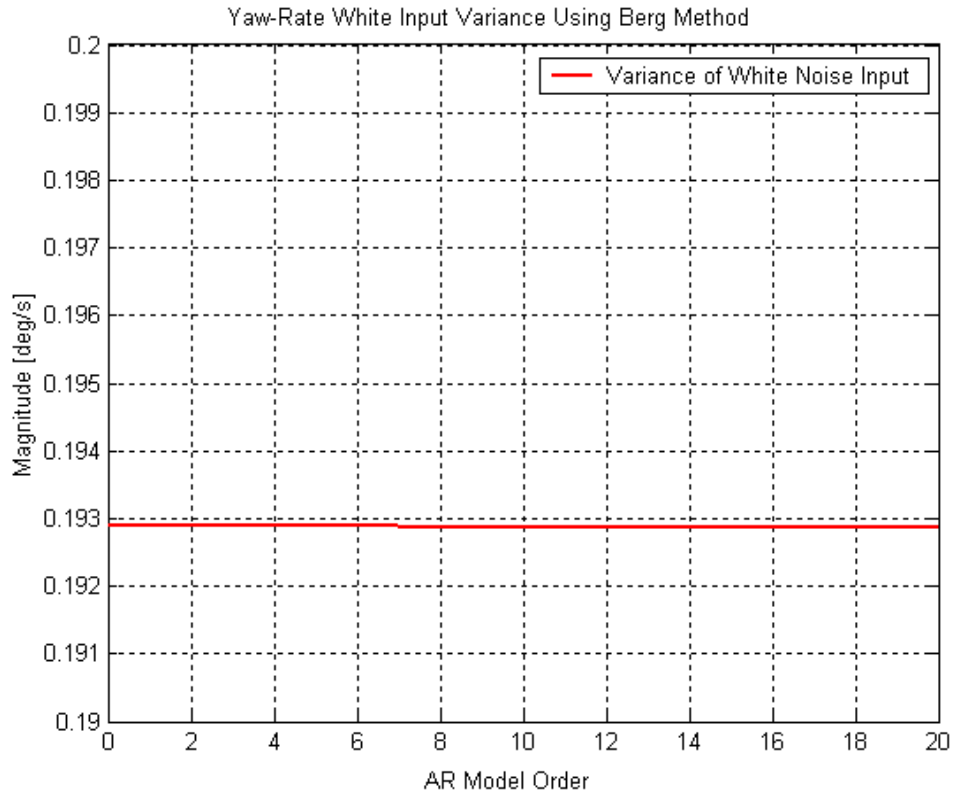
Figure 4.17 White Noise Variance Plot with Different Orders of AR model for Gyroscope Output

In sum, the two main parts of error analysis of MEMS based Inertial Unit (RGA300CA) have been described. First, the main deterministic error sources (zero-offset bias and 1st order scale factor) for both accelerometer and gyroscope of GRA300CA have been estimated and the results in Table 4.1 and Table 4.2 will be referenced in the performance test in the next chapter. Secondly, the random parts of the original measurements of accelerometer and gyroscope of RGA300CA have been analyzed mainly in the time domain and modeled by 4th order AR model for the stochastic variations of X/Y/Z axes of accelerometer and purely random process for the stochastic variation of the gyroscope. Then, their results will be very essential input information in Kalman filter formulation in static testing and also kinematic testing which implements MEMS based inertial sensors

82

and a low-cost GPS receiver integrated system in the performance analysis in Chapter

Five.

Chapter 5

Performance Analysis

This chapter presents the performance analysis of the static and kinematic testings for the MEMS based inertial sensor (RGA300CA) with the methods suggested in the previous chapters. For the static testing, one channel (X-axis) of 3-axis accelerometer will be demonstrated and analyzed to provide the comparable results between 1st order Gauss Markov and 4th order Autoregressive stochastic modeling methods. For the kinematic tests, the same schemes of stochastic modeling will be applied to Kalman filter implementation. On October 21, 2003, a kinematic test was conducted using a MEMS based inertial sensor (RGA300CA), a low-cost GPS receiver module (Leadtek GPS-9543), a digital compass (Honeywell HMR-3300), and a high precision dual-frequency GPS receiver (Javad Legacy GPS receiver). The testing took place at one of the parking

lots in the University of Calgary. The reference trajectory was generated using Precise Point Positioning (PPP) S/W developed by Dr.Gao' research group in Geomatics engineering department in the University of Calgary (Gao, 2003).

5.1 Static Testing and Results

The main purpose of the static testing is to test the implementation of Kalman filter in a static mode with position updates with different accuracy to see the influence of the stochastic modeling by 4th order AR model over the conventional 1st order Gauss Markov process modeling. Considering the fact that this type of MEMS inertial sensor can be used with GPS, the position information from GPS is assumed to be available to update.

Accordingly, the corresponding Kalman filter state-space representation mathematics with 4th order AR model for one channel of accelerometer can be described as follows,

$$\dot{\hat{p}} = \hat{v}$$
$$\dot{\hat{v}} = \hat{\alpha} \tag{5.1}$$

$$(\dot{p} + \delta\dot{p}) = (v + \delta v)$$
$$(\dot{v} + \delta\dot{v}) = (\alpha + \delta\alpha) \tag{5.2}$$

where $[p, v, \alpha] = $ [position,velocity,acceleration]. Then, the error state dynamic matrix (F) is formed as in equation (5.3) and the transition matrix (Φ) can be approximated shown as below,

$$
\begin{bmatrix} \delta \dot{p} \\ \delta \dot{v} \\ \delta \dot{\alpha} \end{bmatrix} = \begin{bmatrix} 0 & 1 & 0 \\ 0 & 0 & 1 \\ 0 & 0 & 0 \end{bmatrix} \begin{bmatrix} \delta p \\ \delta v \\ \delta \alpha \end{bmatrix} \tag{5.3}
$$

$$
\text{F}
$$

$$
\Phi = I + F \Delta t \tag{5.4}
$$

$$
\begin{bmatrix} \delta p_k \\ \delta v_k \\ \delta \alpha_k \end{bmatrix} = \begin{bmatrix} 1 & \Delta t & 0 \\ 0 & 1 & \Delta t \\ 0 & 0 & 1 \end{bmatrix} \begin{bmatrix} \delta p_{k-1} \\ \delta v_{k-1} \\ \delta \alpha_{k-1} \end{bmatrix} \tag{5.5}
$$

Now, the error state model including 6 states, 1 for position, 1 for velocity, 4 for 4th order AR model for X-axis accelerometer bias leads to the matrix equation (Brown and Hwang, 1997, p. 207) as,

$$
x_k = \Phi x_{k-1} + Bw(k) \tag{5.6}
$$

$$
\begin{bmatrix} \delta p_k \\ \delta v_k \\ \delta \alpha_k \\ \delta \alpha_{k-1} \\ \delta \alpha_{k-2} \\ \delta \alpha_{k-3} \end{bmatrix} = \begin{bmatrix} 1 & \Delta t & 0 & 0 & 0 & 0 \\ 0 & 1 & \Delta t & 0 & 0 & 0 \\ 0 & 0 & -a_1 & -a_2 & -a_3 & -a_4 \\ 0 & 0 & 1 & 0 & 0 & 0 \\ 0 & 0 & 0 & 1 & 0 & 0 \\ 0 & 0 & 0 & 0 & 1 & 0 \end{bmatrix} \begin{bmatrix} \delta p_{k-1} \\ \delta v_{k-1} \\ \delta \alpha_{k-1} \\ \delta \alpha_{k-2} \\ \delta \alpha_{k-3} \\ \delta \alpha_{k-4} \end{bmatrix} + \begin{bmatrix} 0 \\ 0 \\ 1 \\ 0 \\ 0 \\ 0 \end{bmatrix} w(k) \tag{5.7}
$$

$$Q = E[ww^T] \tag{5.8}$$

The parameter estimation results in the previous chapter have been used to construct the state transition matrix and the covariance matrix (Q) associated with w_k. A 20Hz sampling rate is also used. And the measurement equation in matrix form is,

$$z_k = Hx_k + v_k \tag{5.9}$$

$$z_k = \begin{bmatrix} 1 & 0 & 0 & 0 & 0 & 0 \end{bmatrix} \begin{bmatrix} \delta p_k \\ \delta v_k \\ \delta \alpha_k \\ \alpha_{k-1} \\ \alpha_{k-2} \\ \alpha_{k-3} \end{bmatrix} + v_k \tag{5.10}$$

$$R = E[vv^T] \tag{5.11}$$

As mentioned earlier, it is assumed that GPS positioning information is available to update at certain accuracy. In the testing, four different position-updating accuracies (R matrix) have been simulated to obtain the relative performance of stochastic modeling in the position domain corresponding to different updating accuracies. Also, updating intervals have been simulated in two ways. The first one is the sampling rate update which means that there is no predicted interval. The second one is the case with update period and prediction period simulating any possible GPS outages. For both cases, the

position estimation errors of 1st order Gauss Markov process and 4th order AR model are demonstrated using the same scale.

In from Figure 5.1 to Figure 5.4, the sampling rate (20Hz) updating results are sketched approximately for 7 hours static data with different updating accuracies. As indicated in Table 5.1, 4th order AR model results have shown very similar improvement (about 30%) over 1st order GM process model in four different updating accuracies. The scale of Root Mean Square (RMS) value of the position estimation errors was dependent on the updating accuracies which have been simulated in the testing.
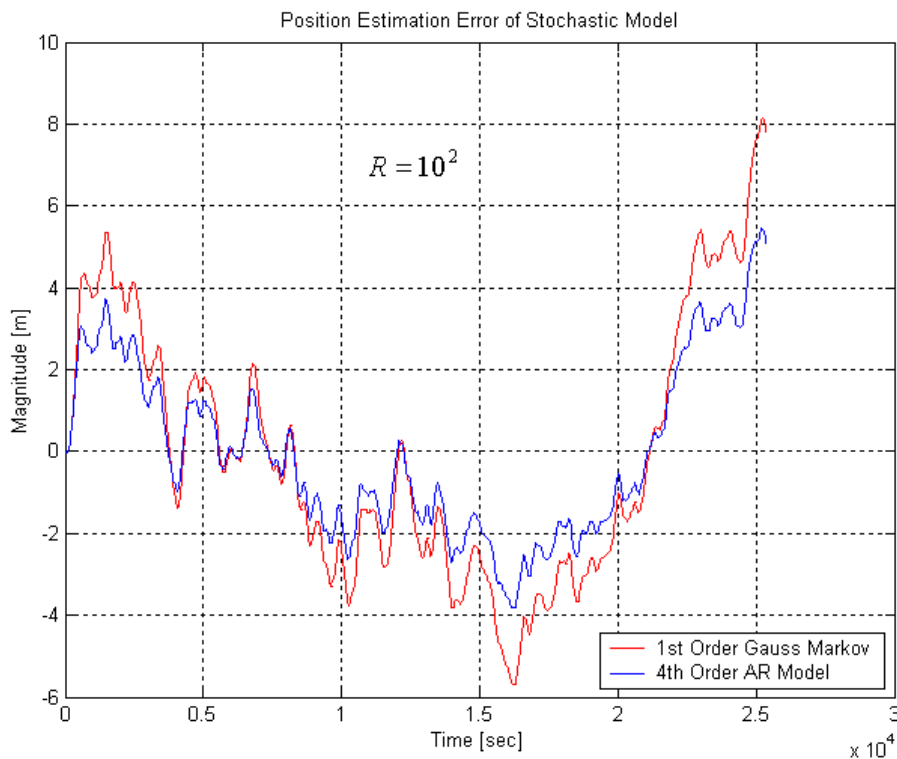

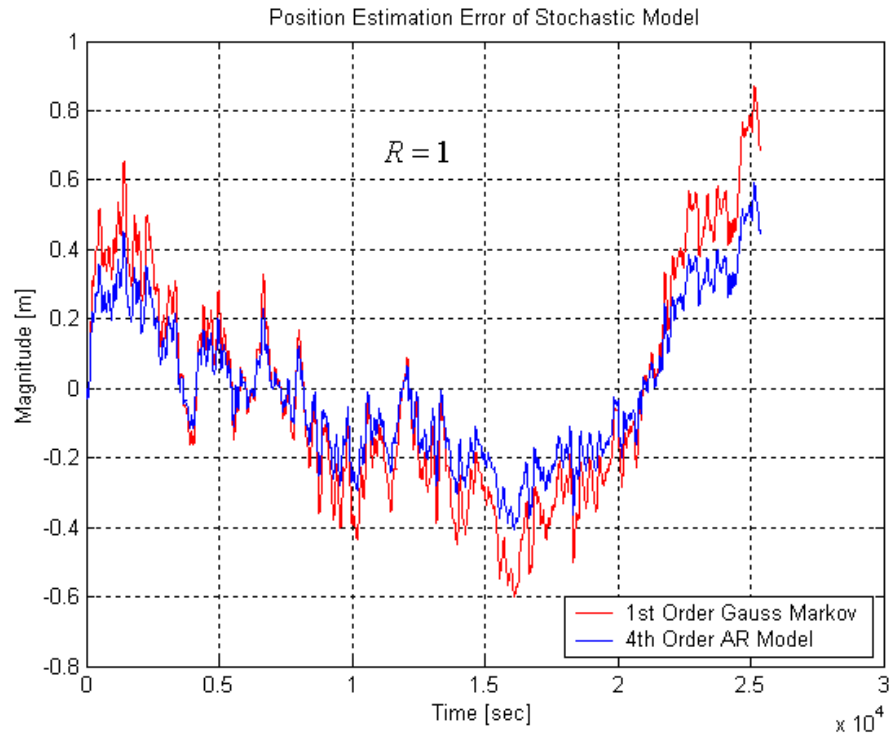Figure 5.1 Position Estimation Error (Sampling Rate Updates [20Hz], R=10^2)

Figure 5.2 Position Estimation Error (Sampling Rate Updates [20Hz], R=1)
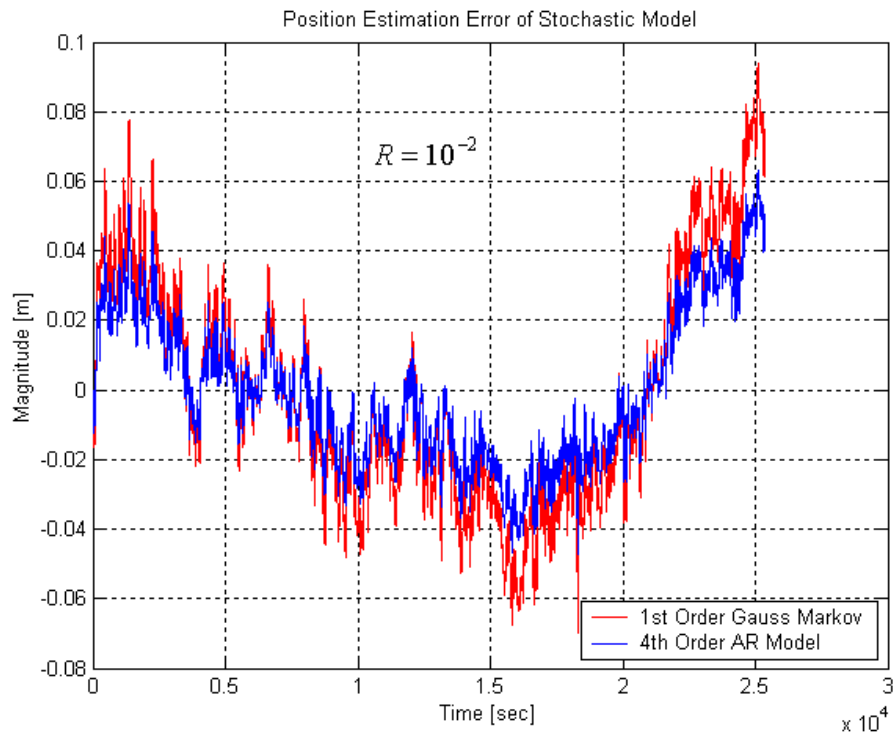
Figure 5.3 Position Estimation Error (Sampling Rate Updates [20Hz], R=10^{-2})
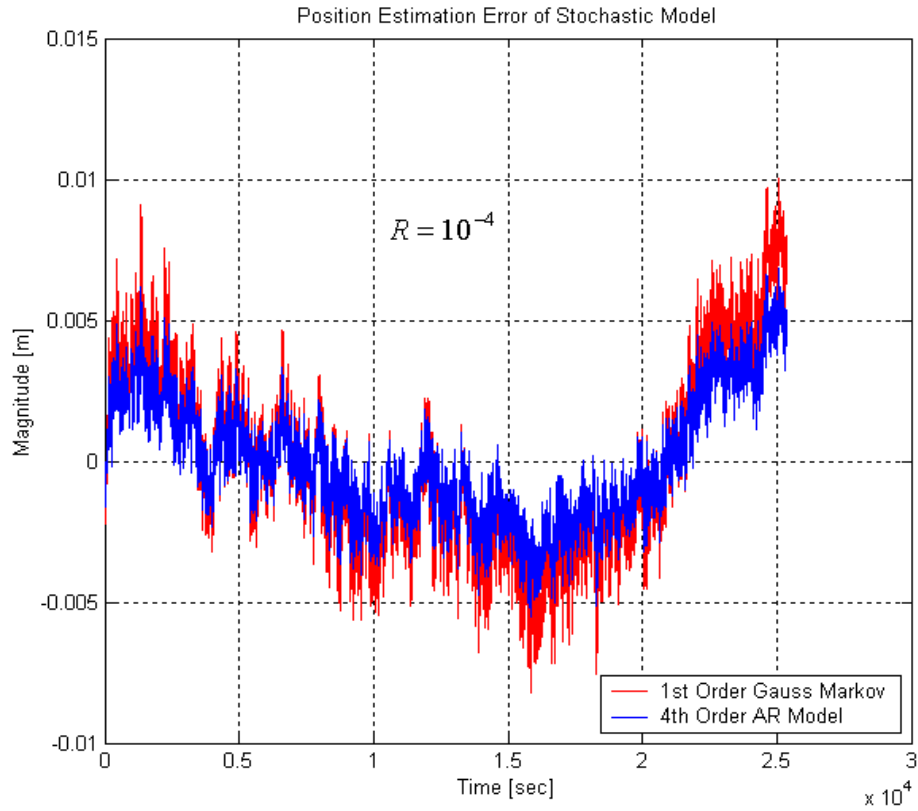
Figure 5.4 Position Estimation Error (Sampling Rate Updates [20Hz], R=10^{-4})

Table 5.1 Statistics of Position Estimation Error (Sampling Rate Updates [20Hz])

	Mean[m]	St.D[m]	RMS[m]	% Improv.
When R=10^2,				
1st G.M. model	-0.0567	3.1563	3.15680924	
4th AR model	-0.0293	2.1212	2.12140235	32.80
When R=1,				
1st G.M. model	-0.0014	0.3259	0.325903007	
4th AR model	-0.00077835	0.2181	0.218101389	33.08
When R=10^{-2},				
1st G.M. model	-0.48108E-04	0.0332	0.033200035	
4th AR model	-0.26045E-04	0.0222	0.022200015	33.13
When R=10^{-4},				
1st G.M. model	-1.4642E-06	0.0034	0.0034	
4th AR model	-7.99E-07	0.0023	0.0023	32.35

90

The Kalman filter error states have been estimated with position update/prediction intervals. The position estimation errors using 30-second update/prediction period with different updating accuracies have been sketched in from Figure 5.5 to Figure 5.8 and their statistics are presented in Table 5.2. Being different from sampling rate update case, the improvement rate in the 30-second update/prediction case has been gradually decreased, as updating accuracies have gotten better. Furthermore, the improvement by precise stochastic modeling tends to be lessened for the magnitude of position estimation error itself when the prediction period is increased into 60 seconds or 120 seconds described in Figure 5.9, Figure 5.10 and Table 5.3.

Figure 5.5 Position Estimation Error (30sec. Update/30sec. Prediction, R=10^2)
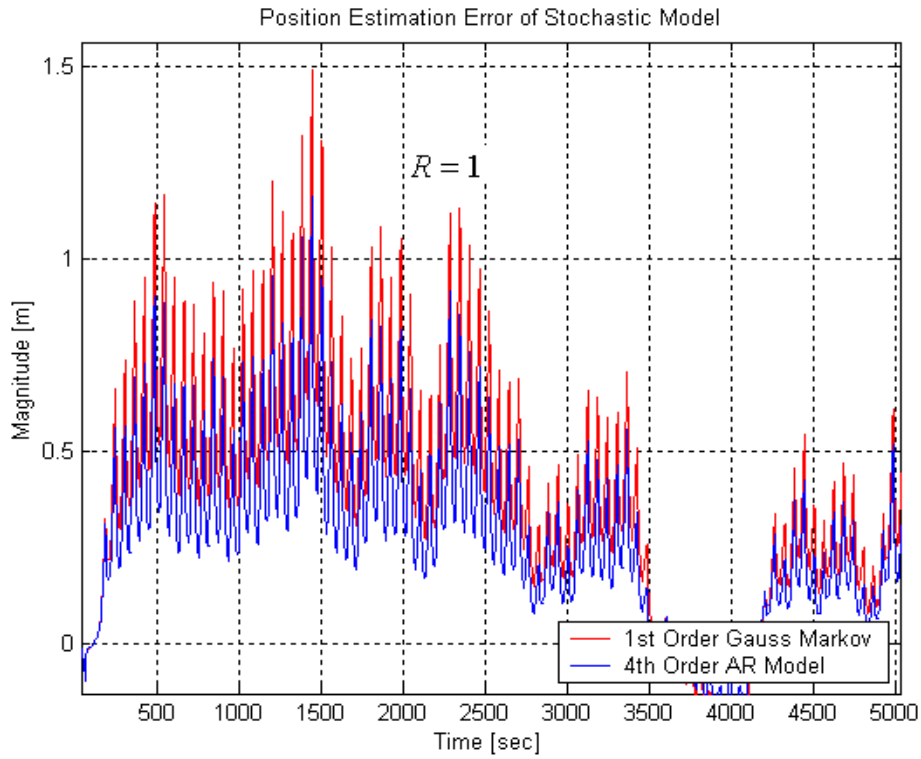
Figure 5.6 Position Estimation Error (30sec. Update/30sec. Prediction, R=1)

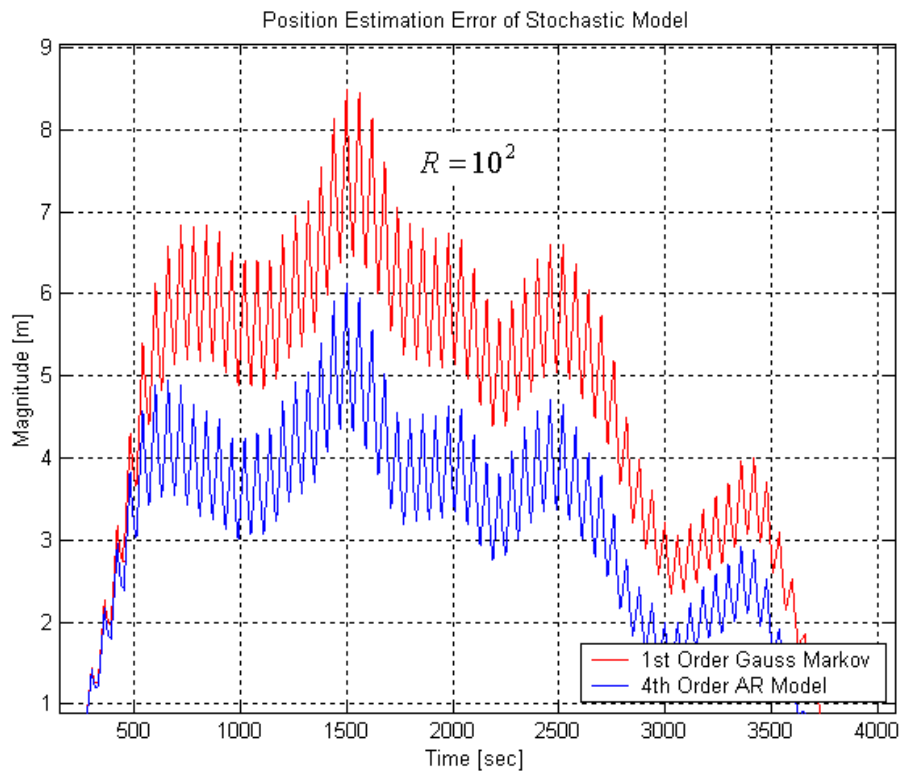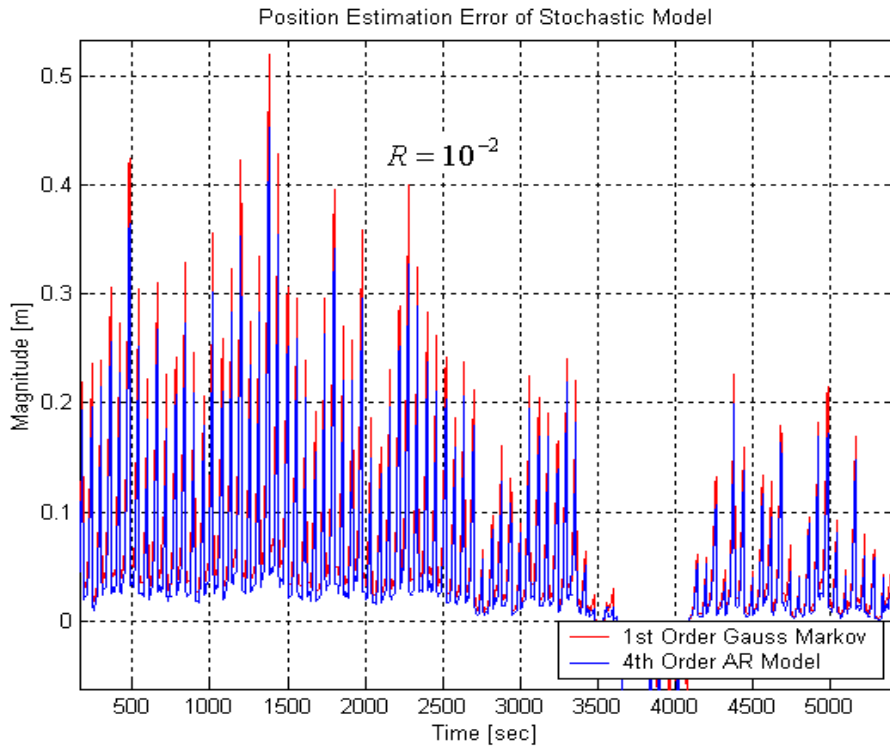Figure 5.7 Position Estimation Error (30sec. Update/30sec. Prediction, R=10^{-2})
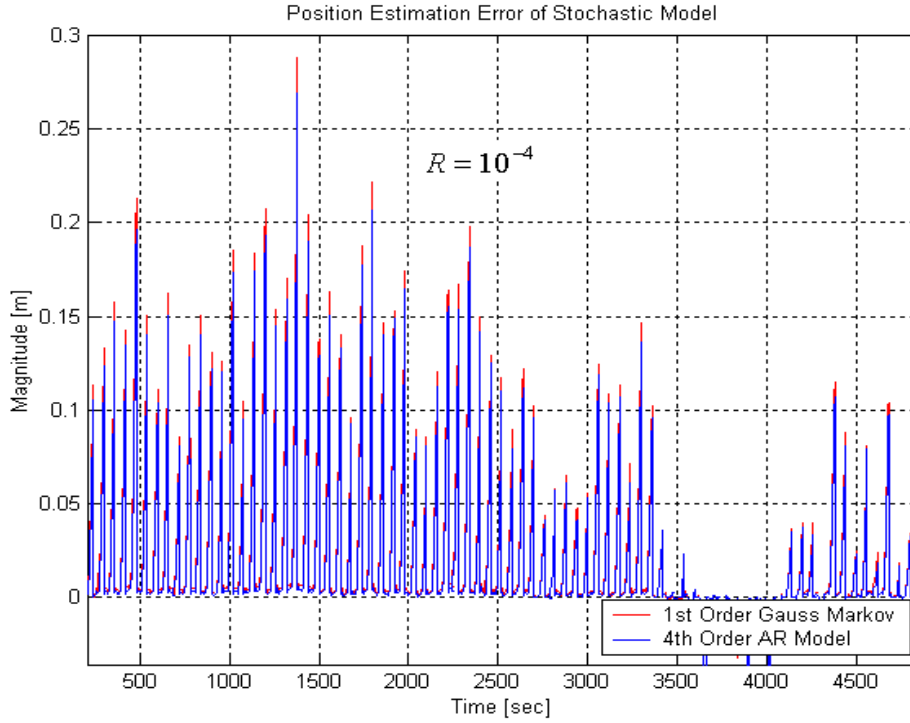
Figure 5.8 Position Estimation Error (30sec. Update/30sec. Prediction, R=10^{-4})

Table 5.2 Statistics of Position Estimation Error (30sec. Update/30sec. Prediction)

	Mean[m]	St.D[m]	RMS[m]	% Improv.
When R=10^2,				
1st G.M. model	-0.0987	4.4690	4.470089785	
4th AR model	-0.0510	3.0227	3.023130214	32.37
When R=1,				
1st G.M. model	-0.0024	0.5071	0.507105679	
4th AR model	-0.0012	0.3575	0.357502014	29.50
When R=10^{-2},				
1st G.M. model	1.4060E-04	0.1018	0.101800097	
4th AR model	2.0972E-04	0.0820	0.0820	19.45
When R=10^{-4},				
1st G.M. model	8.9102E-05	0.0440	0.0440	
4th AR model	4.9343E-05	0.0408	0.0408	7.27

Figure 5.9 Position Estimation Errors (R=10^{-2} [m], 60 sec Up/60 sec Pr)

Figure 5.10 Position Estimation Errors (R=10^{-2} [m], 120 sec Up/120 sec Pr)

Table 5.3 Statistics of Position Estimation Error (R=10^{-2} [m])

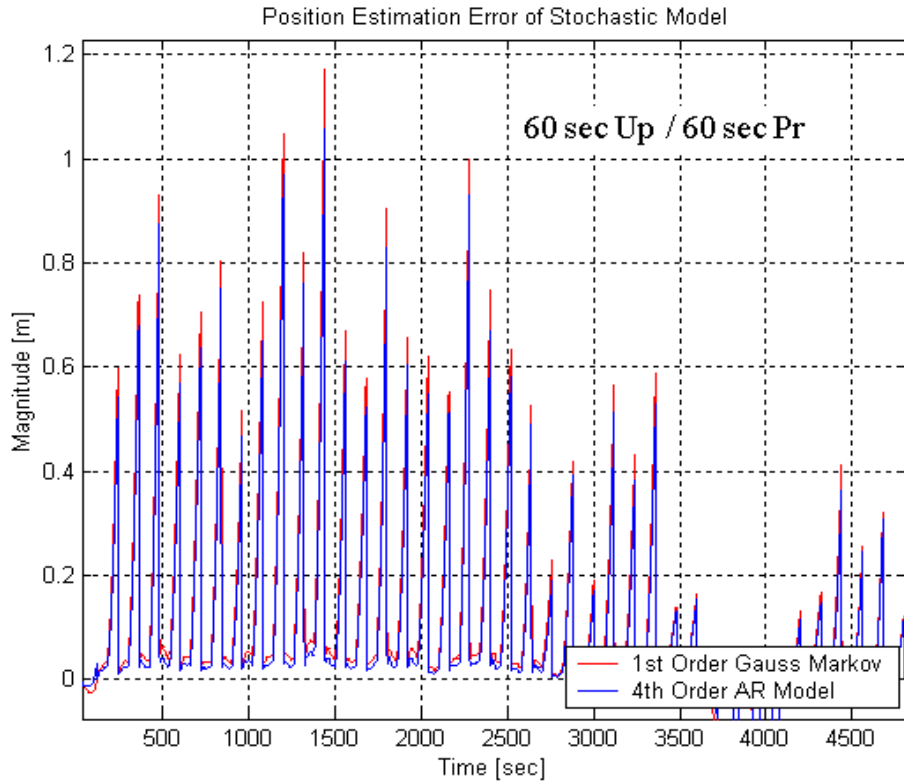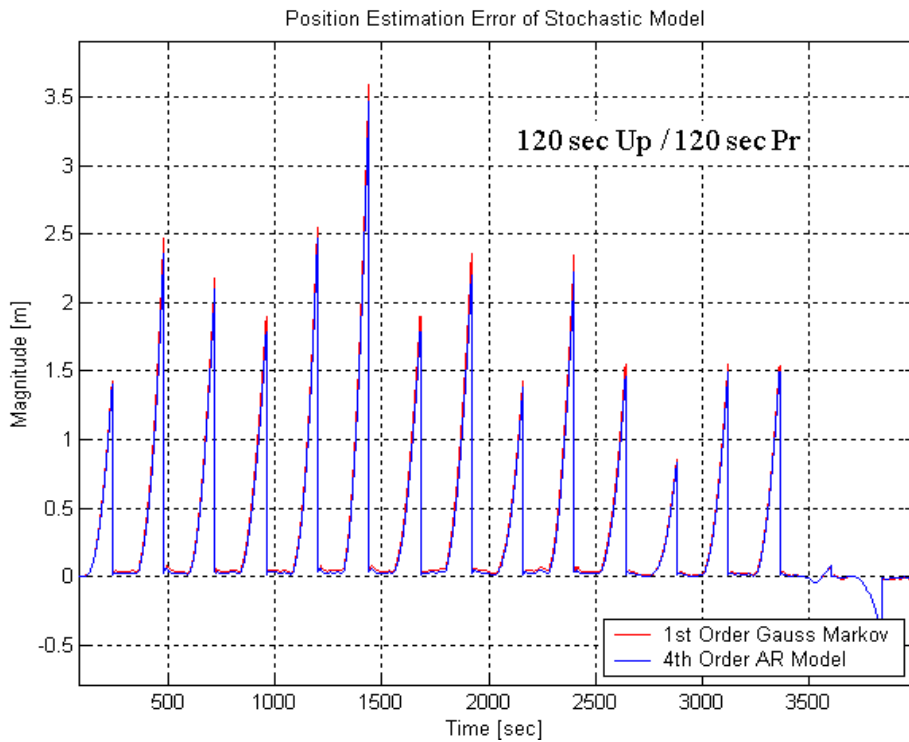|	Mean[m]	St.D[m]	RMS[m]	% Improv.
When 10sec Up/10sec Pr				
1st G.M. model	-7.7661E-05	0.0523	0.052300058	
4th AR model	-3.9530E-05	0.0371	0.037100021	29.06
When 30sec Up/30sec Pr				
1st G.M. model	1.4060E-04	0.1018	0.101800097	
4th AR model	2.0972E-04	0.0820	0.0820	19.45
When 60sec Up/60sec Pr				
1st G.M. model	2.5760E-04	0.2199	0.219900151	
4th AR model	2.3117E-04	0.1961	0.196100136	10.82
When 120sec Up/120sec Pr				
1st G.M. model	-0.0046	0.6282	0.628216842	
4th AR model	-0.0039	0.5913	0.591312861	5.87

Consequently, the results of the Kalman filter implementation of X-axis of the accelerometer in static mode presents that 4th order AR model has performed better than 1st order Gauss-Markov model in both of continuous update and update/prediction cases. In addition, the rate of the improvement by AR model over Gauss-Markov model tends to decrease as updating information accuracy increases and prediction period increases. It is because Kalman filter gain is more dependent on the measurement updating information accuracy and then, the precise stochastic modeling of the system has less contribution to the final position estimates when the prediction period gets longer due to GPS signal outrage.

5.2 Kinematic Testing and Results

5.2.1 Kinematic Testing System Configuration

The kinematic testing was conducted to qualify the performance of the integrated system of MEMS based inertial sensor (RGA300CA) and the low-cost GPS receiver module (Leadtek GPS-9543) utilizing different stochastic modeling schemes (4th order AR model and 1st order Gauss-Markov model). It is a simplified navigation testing with the assumptions that the testing area is 2-dimensional, flat (nominal roll/pitch) and nonaccelerating (short testing duration). Also, the initial misalignment is assumed to be negligible.

For the initial position and heading information, a dual frequency GPS receiver (Javad Legacy GPS receiver) and a digital compass (Honeywell HMR-3300) have been used and the measurements from the high precision Javad Legacy GPS receiver were also processed to generate the reference trajectory.

Two GPS antennas (Javad Legacy and Leadtek GPS 9531) were mounted on the roof of the testing van and the testing system was held tight inside the vehicle shown in Figure 5.11 and Figure 5.12. Two laptop computers were needed to record the reference GPS measurements and integrated system with different acquisition S/W separately.

Figure 5.11 Kinematic Testing System

Figure 5.12 Testing Van

Table 5.4 summarizes the basic specifications of each sensor in the testing system. Those specifications are referenced and also compared with the results of static multi-position testing, especially for RGA300CA.

Table 5.4 System Specifications (Courtesy of Crossbow, Leaktek, Honeywell Inc.)

Specifications	
	RGA300CA
Angular Rate	
Range: Yaw (°/sec)	±100
Bias: Yaw (°/sec)	<±2.0
Scale Factor Accuracy (%)	<1
Non-Linearity (%FS)	<0.3
Resolution (°/sec)	<0.025
Bandwidth (Hz)	>25
Random Walk (°/hr$^{1/2}$)	<2.25
Acceleration	
Range: X/Y/Z (g)	±2
Bias: X/Y/Z (mg)	<±30
Scale Factor Accuracy (%)	<1
Non-Linearity (%FS)	<1
Resolution (mg)	<1.0
Bandwidth (Hz)	>50
Random Walk (m/s/hr$^{1/2}$)	<0.15
	GPS-9543
Main Chip	SiRF star II
Tracking Channel	12
L1 Frequency (MHz)	1575.42 C/A code
Position Accuracy (m)	10, 2D
Input Massage	NMEA/SiRF Binary
Output Massage	SiRF Binary + NMEA-0183
Time Mark	Output 1pps
	HMR3300
Heading Accuracy	1°
Resolution	0.1°
Repeatability	0.5°

5.2.2 Mathematical Error Model

Kalman filter mathematical derivation for 2-dimensional testing using X/Y accelerometer and yaw rate measurements along with GPS position updates is followed below based on the discussion in the reference (Farrell, J.A. and Barth, M., 1998, p.8~9).

$$
\begin{bmatrix} \dot{n} \\ \dot{e} \\ \dot{v}_n \\ \dot{v}_e \\ \dot{\psi} \end{bmatrix} = \begin{bmatrix} v_n \\ v_e \\ \cos(\psi)\alpha_u - \sin(\psi)\alpha_v \\ \sin(\psi)\alpha_u + \cos(\psi)\alpha_v \\ \omega_r \end{bmatrix} = \begin{bmatrix} v_n \\ v_e \\ \alpha_n \\ \alpha_e \\ \omega_r \end{bmatrix}
\tag{5.12}
$$

where $[\alpha_u, \alpha_v]$ are the measured accelerations in the body frame, ω_r is the measured yaw rate in the body frame, and

$$
\begin{bmatrix} \alpha_n \\ \alpha_e \end{bmatrix} = \begin{bmatrix} \cos(\psi) & -\sin(\psi) \\ \sin(\psi) & \cos(\psi) \end{bmatrix} \begin{bmatrix} \alpha_u \\ \alpha_v \end{bmatrix}
\tag{5.13}
$$

When bias errors are modeled in each of the sensors,

$$
\tilde{\alpha}_u = \alpha_u + \delta\alpha_u
\tag{5.14}
$$

$$
\tilde{\alpha}_v = \alpha_v + \delta\alpha_v
\tag{5.15}
$$

$$
\tilde{\omega}_r = \omega_r + \delta\omega_r
\tag{5.16}
$$

the actual mechanization system is modeled as

$$
\begin{bmatrix} \dot{\hat{n}} \\ \dot{\hat{e}} \\ \dot{\hat{v}}_n \\ \dot{\hat{v}}_e \\ \dot{\hat{\psi}} \end{bmatrix} = \begin{bmatrix} \hat{v}_n \\ \hat{v}_e \\ \cos(\hat{\psi})\tilde{\alpha}_u - \sin(\hat{\psi})\tilde{\alpha}_v \\ \sin(\hat{\psi})\tilde{\alpha}_u + \cos(\hat{\psi})\tilde{\alpha}_v \\ \tilde{\omega}_r \end{bmatrix}
\tag{5.17}
$$

Linearization about the trajectory results in the following set of equations,

$$
\begin{bmatrix} \delta\dot{n} \\ \delta\dot{e} \\ \delta\dot{v}_n \\ \delta\dot{v}_e \\ \delta\dot{\psi} \end{bmatrix} = \begin{bmatrix} 0 & 0 & 1 & 0 & 0 \\ 0 & 0 & 0 & 1 & 0 \\ 0 & 0 & 0 & 0 & -\alpha_e \\ 0 & 0 & 0 & 0 & \alpha_n \\ 0 & 0 & 0 & 0 & 0 \end{bmatrix} \begin{bmatrix} \delta n \\ \delta e \\ \delta v_n \\ \delta v_e \\ \delta\psi \end{bmatrix} + \begin{bmatrix} 0 & 0 & 0 \\ 0 & 0 & 0 \\ \cos(\psi) & -\sin(\psi) & 0 \\ \sin(\psi) & \cos(\psi) & 0 \\ 0 & 0 & 1 \end{bmatrix} \begin{bmatrix} \delta\alpha_u \\ \delta\alpha_v \\ \delta\omega_r \end{bmatrix}
\tag{5.18}
$$

including bias errors in error states, error state dynamic matrix (F) is formed as in equation (5.18) and the transition matrix (Φ) can be approximated shown as below,

$$
\begin{bmatrix} \delta\dot{n} \\ \delta\dot{e} \\ \delta\dot{v}_n \\ \delta\dot{v}_e \\ \delta\dot{\psi} \\ \delta\dot{\alpha}_u \\ \delta\dot{\alpha}_v \\ \delta\dot{\omega}_r \end{bmatrix} = \underbrace{\begin{bmatrix} 0 & 0 & 1 & 0 & 0 & 0 & 0 & 0 \\ 0 & 0 & 0 & 1 & 0 & 0 & 0 & 0 \\ 0 & 0 & 0 & 0 & -\alpha_e & \cos(\psi) & -\sin(\psi) & 0 \\ 0 & 0 & 0 & 0 & \alpha_n & \sin(\psi) & \cos(\psi) & 0 \\ 0 & 0 & 0 & 0 & 0 & 0 & 0 & 1 \\ 0 & 0 & 0 & 0 & 0 & 0 & 0 & 0 \\ 0 & 0 & 0 & 0 & 0 & 0 & 0 & 0 \\ 0 & 0 & 0 & 0 & 0 & 0 & 0 & 0 \end{bmatrix}}_{F} \begin{bmatrix} \delta n \\ \delta e \\ \delta v_n \\ \delta v_e \\ \delta\psi \\ \delta\alpha_u \\ \delta\alpha_v \\ \delta\omega_r \end{bmatrix}
\tag{5.19}
$$

100

$$\Phi_{INS} = I + F\Delta t \tag{5.20}$$

$$
\begin{bmatrix} \delta n_k \\ \delta e_k \\ \delta v_{nk} \\ \delta v_{ek} \\ \delta \psi_k \\ \delta \alpha_{uk} \\ \delta \alpha_{vk} \\ \delta \omega_{rk} \end{bmatrix}
=
\begin{bmatrix}
1 & 0 & \Delta t & 0 & 0 & 0 & 0 & 0 \\
0 & 1 & 0 & \Delta t & 0 & 0 & 0 & 0 \\
0 & 0 & 1 & 0 & -\alpha_e \Delta t & \cos(\psi)\Delta t & -\sin(\psi)\Delta t & 0 \\
0 & 0 & 0 & 1 & \alpha_n \Delta t & \sin(\psi)\Delta t & \cos(\psi)\Delta t & 0 \\
0 & 0 & 0 & 0 & 1 & 0 & 0 & \Delta t \\
0 & 0 & 0 & 0 & 0 & 1 & 0 & 0 \\
0 & 0 & 0 & 0 & 0 & 0 & 1 & 0 \\
0 & 0 & 0 & 0 & 0 & 0 & 0 & 1
\end{bmatrix}
\begin{bmatrix} \delta n_{k-1} \\ \delta e_{k-1} \\ \delta v_{nk-1} \\ \delta v_{ek-1} \\ \delta \psi_{k-1} \\ \delta \alpha_{uk-1} \\ \delta \alpha_{vk-1} \\ \delta \omega_{rk-1} \end{bmatrix} \tag{5.21}
$$

Now, the error state model including 14 states, 2 for position, 2 for velocity, 1 for misalignment, 8 for 4th order AR model of X/Y-axis of accelerometer biases and 1 for white noise for yaw rate bias lead to the matrix equation is

$$
\begin{bmatrix} \delta n_k \\ \delta e_k \\ \delta v_{nk} \\ \delta v_{ek} \\ \delta \psi_k \\ \delta \alpha_{uk} \\ \delta \alpha_{uk-1} \\ \delta \alpha_{uk-2} \\ \delta \alpha_{uk-3} \\ \delta \alpha_{vk} \\ \delta \alpha_{vk-1} \\ \delta \alpha_{vk-2} \\ \delta \alpha_{vk-3} \\ \delta \omega_{rk} \end{bmatrix}
=
\left[\begin{array}{ccccc|ccccccccc}
1 & 0 & \Delta t & 0 & 0 & 0 & 0 & 0 & 0 & 0 & 0 & 0 & 0 & 0 \\
0 & 1 & 0 & \Delta t & 0 & 0 & 0 & 0 & 0 & 0 & 0 & 0 & 0 & 0 \\
0 & 0 & 1 & 0 & -\alpha_e \Delta t & \cos(\psi)\Delta t & 0 & 0 & 0 & -\sin(\psi)\Delta t & 0 & 0 & 0 & 0 \\
0 & 0 & 0 & 1 & \alpha_n \Delta t & \sin(\psi)\Delta t & 0 & 0 & 0 & \cos(\psi)\Delta t & 0 & 0 & 0 & 0 \\
0 & 0 & 0 & 0 & 1 & 0 & 0 & 0 & 0 & 0 & 0 & 0 & 0 & \Delta t \\ \hline
0 & 0 & 0 & 0 & 0 & -a_{u1} & -a_{u2} & -a_{u3} & -a_{u4} & 0 & 0 & 0 & 0 & 0 \\
0 & 0 & 0 & 0 & 0 & 1 & 0 & 0 & 0 & 0 & 0 & 0 & 0 & 0 \\
0 & 0 & 0 & 0 & 0 & 0 & 1 & 0 & 0 & 0 & 0 & 0 & 0 & 0 \\
0 & 0 & 0 & 0 & 0 & 0 & 0 & 1 & 0 & 0 & 0 & 0 & 0 & 0 \\
0 & 0 & 0 & 0 & 0 & 0 & 0 & 0 & 0 & -a_{v1} & -a_{v2} & -a_{v3} & -a_{v4} & 0 \\
0 & 0 & 0 & 0 & 0 & 0 & 0 & 0 & 0 & 1 & 0 & 0 & 0 & 0 \\
0 & 0 & 0 & 0 & 0 & 0 & 0 & 0 & 0 & 0 & 1 & 0 & 0 & 0 \\
0 & 0 & 0 & 0 & 0 & 0 & 0 & 0 & 0 & 0 & 0 & 1 & 0 & 0 \\
0 & 0 & 0 & 0 & 0 & 0 & 0 & 0 & 0 & 0 & 0 & 0 & 0 & 0
\end{array}\right]
\begin{bmatrix} \delta n_{k-1} \\ \delta e_{k-1} \\ \delta v_{nk-1} \\ \delta v_{ek-1} \\ \delta \psi_{k-1} \\ \delta \alpha_{uk-1} \\ \delta \alpha_{uk-2} \\ \delta \alpha_{uk-3} \\ \delta \alpha_{uk-4} \\ \delta \alpha_{vk-1} \\ \delta \alpha_{vk-2} \\ \delta \alpha_{vk-3} \\ \delta \alpha_{vk-4} \\ \delta \omega_{rk-1} \end{bmatrix}
+
\begin{bmatrix} 0 \\ 0 \\ 0 \\ 0 \\ 0 \\ w_{uk} \\ 0 \\ 0 \\ 0 \\ w_{vk} \\ 0 \\ 0 \\ 0 \\ w_{\omega k} \end{bmatrix}
$$

$$(5.22)$$

$$Q = E[\mathbf{w}\mathbf{w}^{\mathrm{T}}] \tag{5.23}$$

$$\begin{bmatrix} z_n \\ z_e \end{bmatrix} = \begin{bmatrix} 1\ 0\ 0\ 0\ 0\ 0\ 0\ 0\ 0\ 0\ 0\ 0\ 0\ 0 \\ 0\ 1\ 0\ 0\ 0\ 0\ 0\ 0\ 0\ 0\ 0\ 0\ 0\ 0 \end{bmatrix} \begin{bmatrix} \delta n_k \\ \delta e_k \\ \delta v_{nk} \\ \delta v_{ek} \\ \delta \psi_k \\ \delta \alpha_{uk} \\ \delta \alpha_{uk-1} \\ \delta \alpha_{uk-2} \\ \delta \alpha_{uk-3} \\ \delta \alpha_{vk} \\ \delta \alpha_{vk-1} \\ \delta \alpha_{vk-2} \\ \delta \alpha_{vk-3} \\ \delta \omega_{rk} \end{bmatrix} + v_k \tag{5.24}$$

$$R = E[\mathbf{v}\mathbf{v}^{\mathrm{T}}] \tag{5.25}$$

Again, the parameter estimation results in the previous chapter have been used to construct the state transition matrix and the covariance matrix (Q) associated with w_k and R matrix has been constructed by using RMS values of GPS trajectory accuracy compared with PPP solutions.

5.2.3 Testing Dataset and Data Processing

The testing dataset is composed of 3 different system files and 1 reference GPS file. The system files are using the same computer time. Their logging formats are

Table 5.5 Testing System Dataset Logging Formats

GPS									
time_index	(int)GPS_Time	Lat	Lon	GPS_heading	GPSVn	GPSVe	HDOP	SN	SNR_total
Compass									
time_index	Compass_heading	Compass_pitch	Compass_roll						
RGA300CA									
time_index	RGA_Roll		RGA_pitch	RGA_Yaw	RGA_Ax	RGA_Ay	RGA_Az	RGA_Temp	

For the field testing, the system has included about 20 minutes warming-up period, compass calibration period, static motion period, and kinematic motion period. After warming period, a digital compass was calibrated using 360° rotation circle motion each time and then, at least 5 minutes static collection was made. It has been done this way because on/off zero-offset bias should have been examined before actual kinematic data processing. Total kinematic testing duration was limited to 10 minutes and the same testing routine was conducted 10 times.

For the initial heading, the term, magnetic north, refers to the position of the earth's magnetic pole and it differs from a geodetic north. The angle between magnetic north and the geodetic north direction is called magnetic declination. As the magnetic declination does not remain constant in time, it needs to be referred to a recent geographic lookup table or geodetic services available in order to add or subtract the proper declination angle to correct for the geodetic north. Fortunately, Natural Resources of Canada (NRCan) provides a recent estimation of the declination based on Canadian Geomagnetic Reference Field (CGRF) which is a model of the magnetic field over the Canadian region.

As a result, 17.183° E declination angle was obtained through the University of Calgary campus and then, it was added to the initial heading from HMR3300 magnetic compass.

The initial position was provided through Precise Point Positioning (PPP) process of Javad Legacy GPS receiver measurements, which has sub-meter accuracy. PPP solution also generates the reference trajectory to qualify the performance of the integrated system. The data processing associated with kinematic testing is illustrated in Figure 5.13.
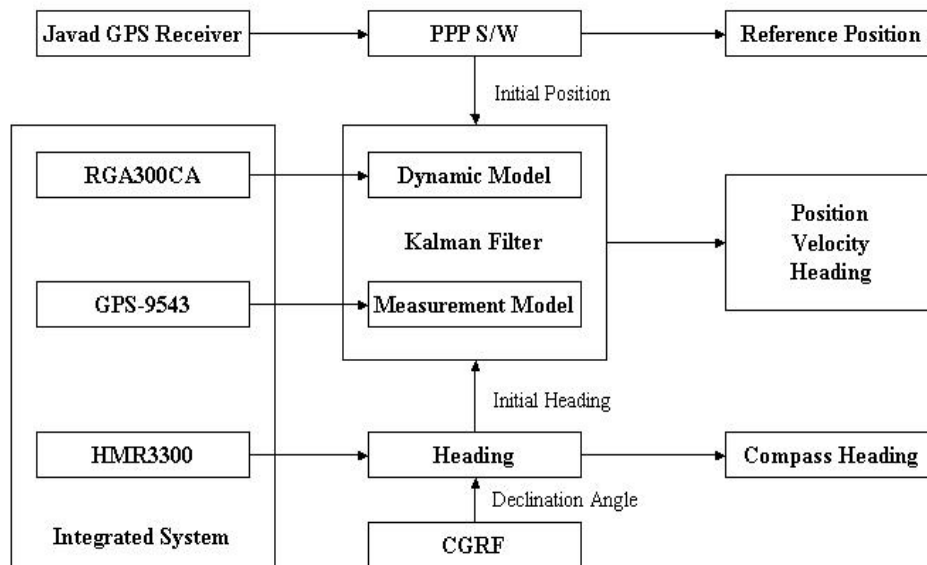
Figure 5.13 Data Processing Flow

The trajectory generated by the integrated system has been compared with reference trajectory using GPS time synchronization. The same data processing has been conducted for two different stochastic modeling schemes.

5.2.4 Testing Results and Analysis

The kinematic testing has been conducted in one of the parking lots in University of Calgary which is relatively flat and an open area to fulfill the testing assumptions described previously. The vehicle was driven at the speed of 10 to 30 km/hr with 6 major turns. Around the corners, the speed was reduced and then, was accelerated along the straight path comparatively. The same driving testing was repeated 10 times with the same routine of data collection in the same area. One of the raw measurements of accelerometer and gyroscope is sketched in Figure 5.14.
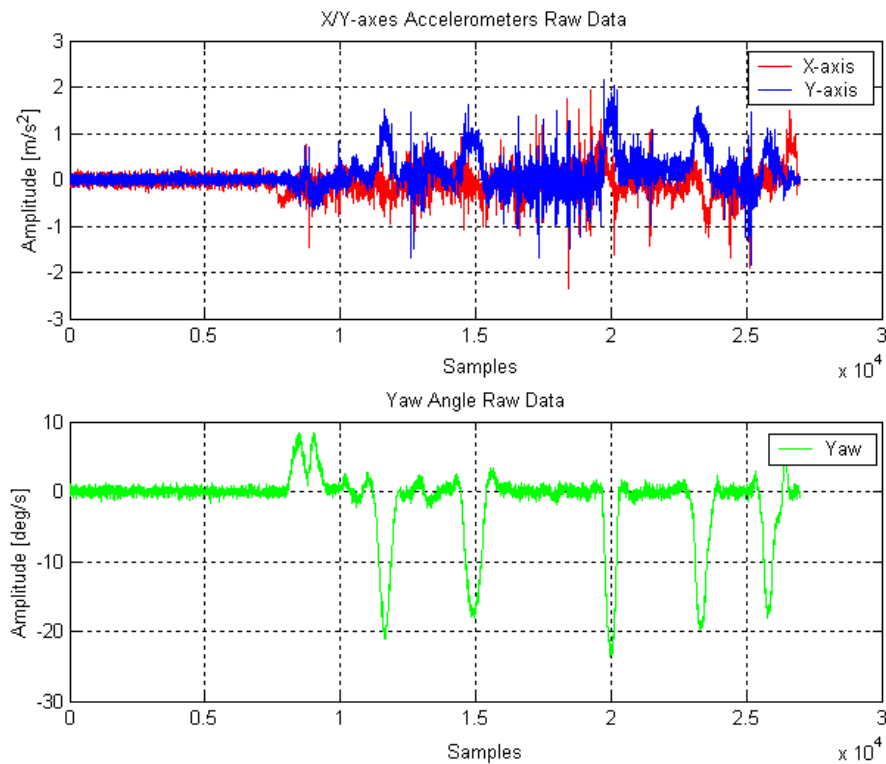

Figure 5.14 Kinematic Testing Raw Measurements

As illustrated and also described previously, the actual collection of dataset consists of two parts, namely, static mode and kinematic mode after warming up and compass calibration periods. About 5 minutes, the static mode dataset was referenced with zero-offset bias estimation described in Chapter Four. With an initial position from PPP processing of GPS measurements and initial heading corrected by CGRF, Kalman filter error estimation has been processed composed of dynamic model using measurements of X/Y axes of accelerometer, Yaw rate gyroscope of RGA300CA and measurement model using measurements of GPS-9543 module. The trajectories of the integrated system using 4th order AR model and 1st order GM model were generated with the 1-sec updates first and were compared with PPP solution trajectory and GPS-9543 solution trajectory. After that, the system trajectories were generated with 5-sec, 10-sec, 20-sec, 30-sec, 60-sec update intervals. Some of them are illustrated in from Figure 5.15 to Figure 5.18.
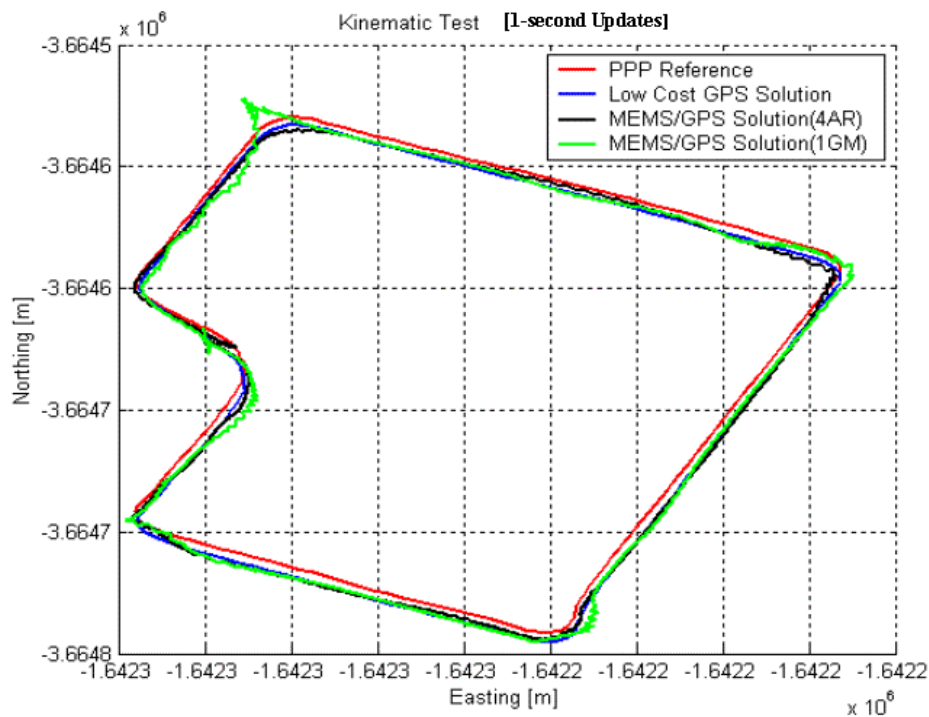

Figure 5.15 Kinematic Testing Trajectory Plots (1-sec Updates)
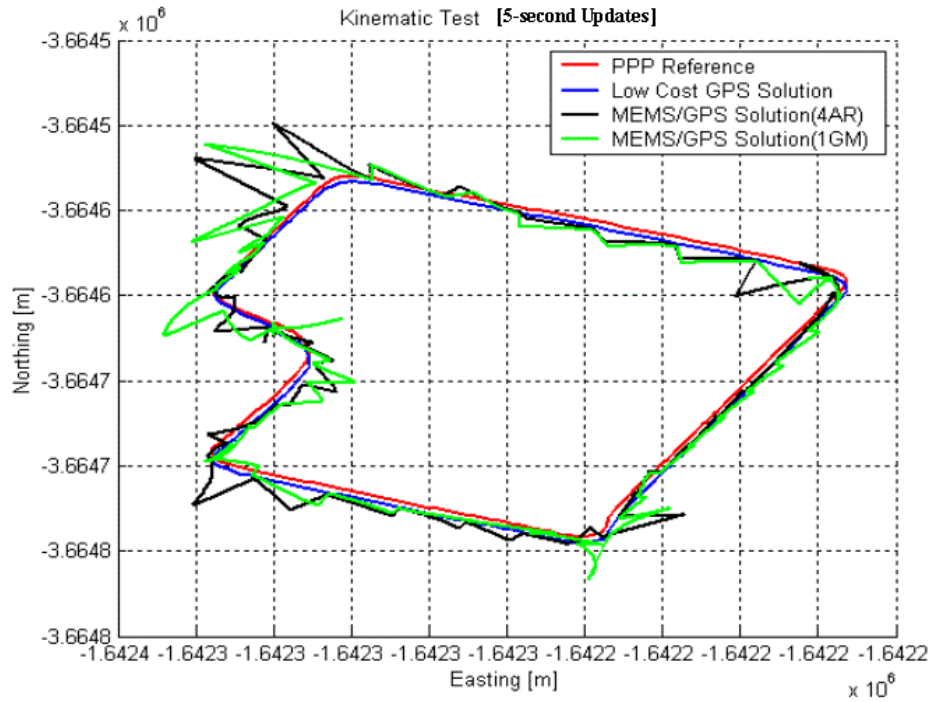
Figure 5.16 Kinematic Testing Trajectory Plots (5-sec Updates)
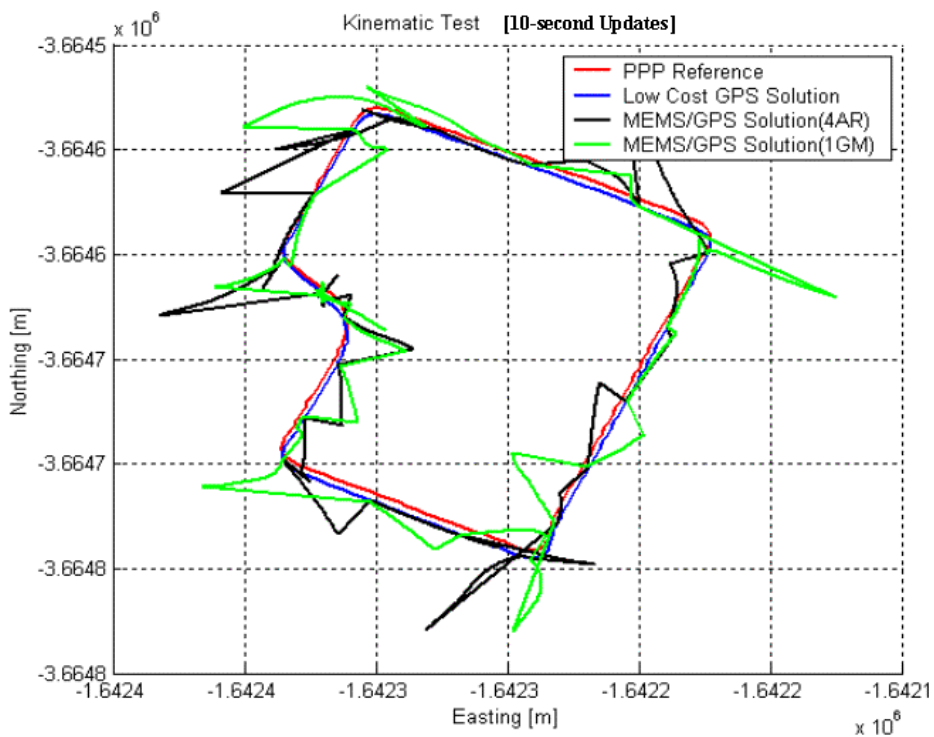

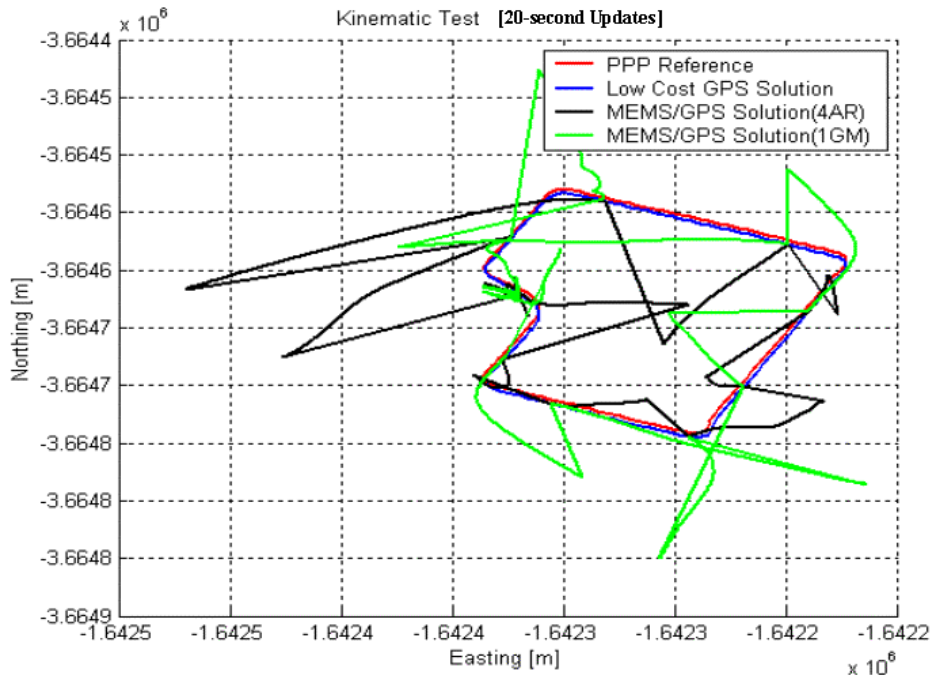Figure 5.17 Kinematic Testing Trajectory Plots (10-sec Updates)

Figure 5.18 Kinematic Testing Trajectory Plots (20-sec Updates)

In the 1-sec update case, the system trajectories by both 4th AR model and 1st order GM model processes have indicated slightly better performance than GPS-9543 solution. In the 5-sec, 10-sec, 20-sec update cases, the system solutions are showing that the position errors have increased between updates. The biggest position errors have often occurred in the corner sections. It is because the Yaw rate error plays a bigger role than the acceleration error in position generation. While previous four figures illustrate the horizontal position trajectory, the following two figures show northing and easting position errors of different updating cases compared with PPP solution. It is noticed that the solutions of 4th order AR model and 1st order GM model are varying as the updating intervals have increased.
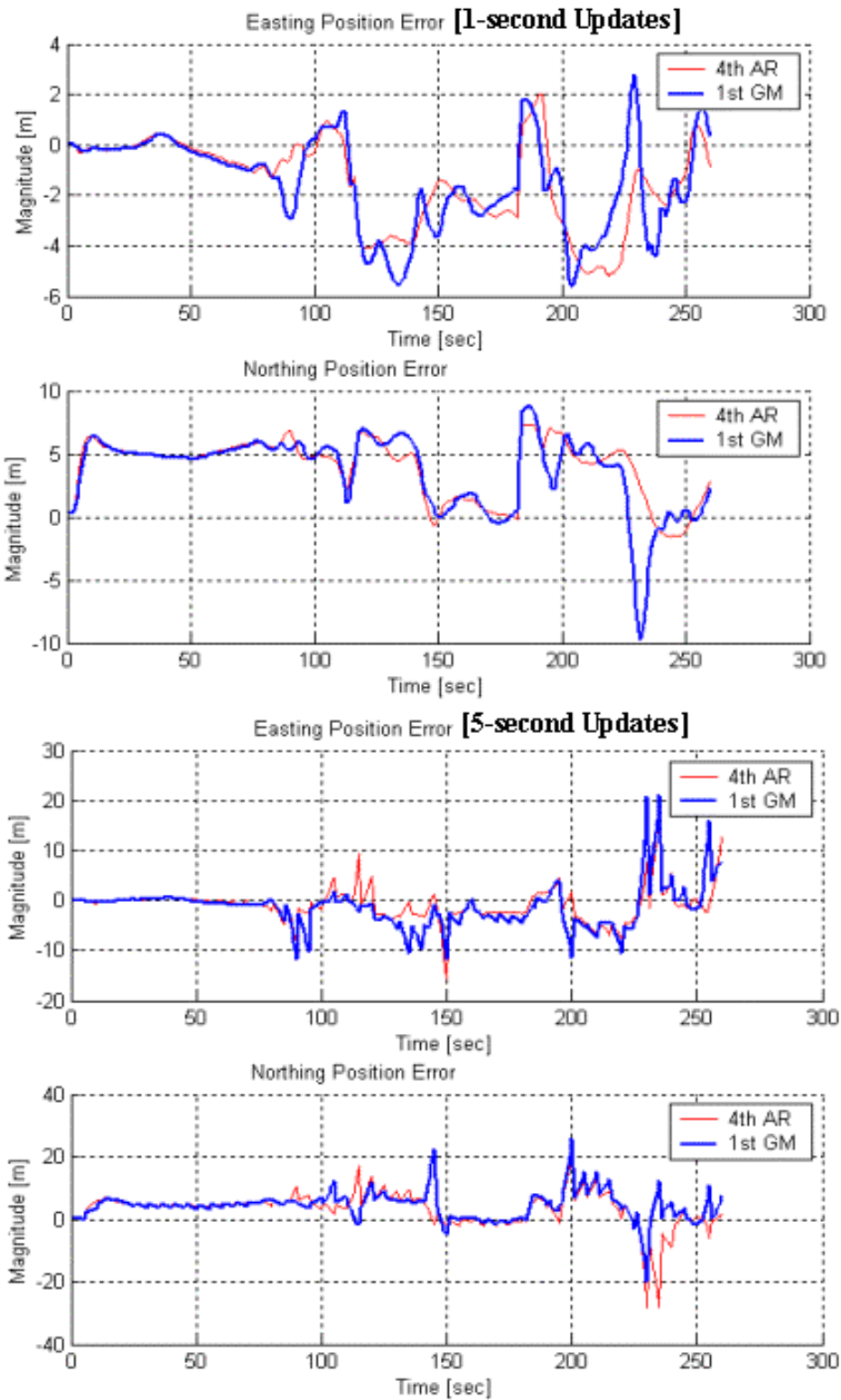
108

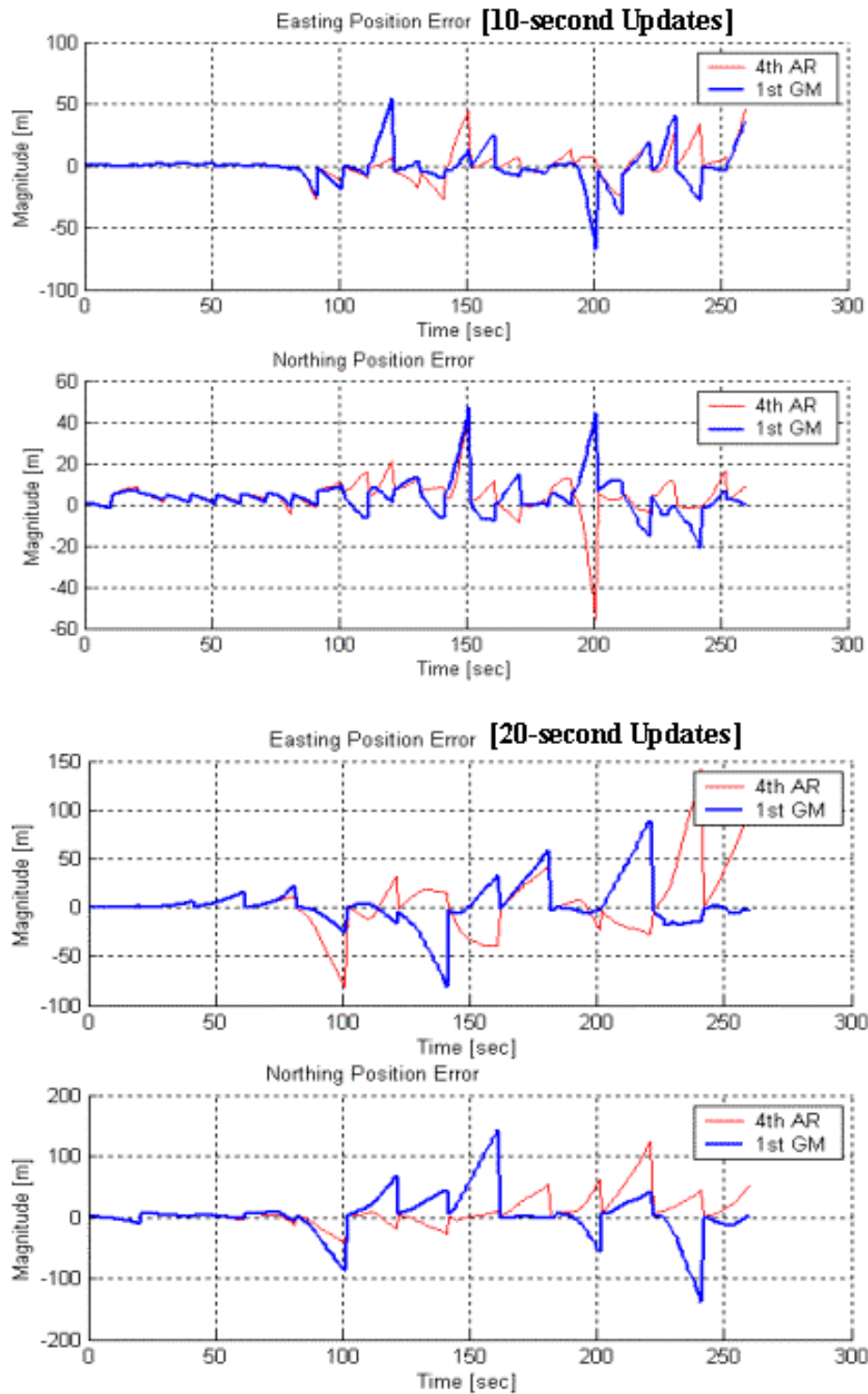Figure 5.19 Kinematic Testing Position Error Plots (1/5 sec Updates)

Figure 5.20 Kinematic Testing Position Error Plots (10/20 sec Updates)

It is clear that the position error in each channel tends to increase without GPS position updates and settle down with updates. Also, the kinematic mode position error is much bigger than the static mode position error in all update interval cases. In the 10-sec update case, the maximum position error has reached to about 60 meters and even worse, 100 meter position error has been shown in the 20 sec update case. The numerical result of position errors of kinematic testing is summarized in Table 5.6.

Table 5.6 Kinematic Position Errors

Position Errors			
	X RMS	**Y RMS**	**Hrioz. RMS**
1-sec Update			
4th AR Model	2.2643	4.5664	5.0970
1st GM Model	2.3521	4.7023	5.2578
5-sec Update			
4th AR Model	3.4984	6.5326	7.4104
1st GM Model	4.5062	6.3012	7.7466
10-sec Update			
4th AR Model	10.9184	9.5629	14.5142
1st GM Model	13.6273	9.3777	16.5422
20-sec Update			
4th AR Model	31.0981	25.9061	40.4749
1st GM Model	22.6127	36.6627	43.0754
30-sec Update			
4th AR Model	21.2120	76.1587	79.0575
1st GM Model	60.9515	53.1926	80.8983
60-sec Update			
4th AR Model	111.8538	165.9589	200.1340
1st GM Model	276.4774	149.9599	314.5278

Unit : [meters]

Based on the position error plots and numerical values, the estimation with 4th order AR model has produced better results than the estimation with 1st order GM model in kinematic testing. However, the improvement is relatively smaller than the one in static testing. It can be explained that more unmodeled deterministic error sources are involved in the kinematic environments.

The kinematic testing described here has made very important assumptions mentioned earlier. Therefore, the results with those assumptions and data processing method presented above, should be understood very carefully.

Chapter 6

Conclusions and Recommendations

6.1 Conclusions

The main objectives of this research are to investigate the error behaviours of MEMS based inertial sensors and the performance analysis of the prototype of a low-cost GPS/MEMS based inertial sensor integrated system for land vehicle applications. The major motivation is that GPS signal is not always available to the users and GPS based solutions are degraded due to poor geometry, and multipath effect even though GPS based navigation system is becoming smaller and inexpensive to be more popular and attainable for civil users and have been immensely adopted for land vehicle applications.

Complementing the disadvantages of the GPS based navigation system, MEMS based inertial sensors have pushed the development of the inexpensive and smaller integrated system to provide the reliable and continuous navigation solutions for land vehicle applications. However, in spite of low inherent cost, small size, low power consumption, and solid reliability of MEMS based inertial sensors, MEMS based inertial sensors are still considered as very poor devices in accuracy. Consequently, this study has emphasized the error characterization and performance analysis of MEMS based inertial sensors trying to turn the raw measurements of the sensors into reliable and useful data in optimal data processing for vehicle position determination.

The research led to the basic principle of multi-sensor navigation system, MEMS technology and MEMS based inertial sensors, error analysis of MEMS based inertial sensors, error estimation, and performance analysis. The major contributions of this research are:

- Identification of different types of error sources of MEMS based inertial sensors

- Estimation of major deterministic error sources (zero-offset bias and 1st order scale factor) and stochastic modeling of random noise using special standard parametric stochastic models

- Performance analysis of MEMS based inertial sensors compared to Autoregressive (AR) model and Gauss Markov (GM) model in static and kinematic environments

Through Kalman Filter implementation in static testing and kinematic testing, the results from the 1st order Gauss Markov process and the proposed 4th order AR model have been compared with different interval updates and with prediction. The 4th order AR model has resulted in a better performance in both cases in this experiment. In static testing, the position estimation errors of 1st order GM process and 4th order AR model were compared according to different updating intervals and different updating information accuracies. Overall, AR model results have shown a better performance over 1st order GM process agreeing with the results in the reference (Nassar S. et al., 2003). As indicated in Table 5.1, Table 5.2 and Table 5.3, the rate of improvement by AR model over GM model tend to decrease as updating accuracy increases and prediction period increases. The kinematic testing has been performed in the 2-dimentional, and relatively flat environment assuming nominal Earth rotation rate effect and negligible initial misalignment of the system. Also, it should be noticed that the initial heading from HMR3300 digital magnetic compass was corrected by the recent estimation of the magnetic declination based on CGRF. As illustrated in Table 5.6, the improvement in kinematic testing by AR model is relatively smaller than the one in static testing, which can be explained that the unmodeled error sources are involved in the kinematic environments with a series of assumptions.

In order to adopt low-cost sensors in the integrated navigation system with satisfactory performance, the precise calibration of the deterministic error sources and the proper stochastic modeling of the noise behaviour of different sensors are recommended. Several stochastic models have been discussed in this research and they can be used to help

115

develop optimal algorithms for the integration of MEMS based inertial sensors with other enabling systems such as GPS.

6.2 Recommendations

As illustrated in the performance analysis, the quality performance of MEMS based inertial sensors is not quite acceptable to aid GPS system for land vehicle application for longer period of GPS signal outrage. As MEMS technology enhances fast and more MEMS based navigation sensors are available in the market, it is recommended to test and qualify more and better performance sensors to develop GPS/MEMS based inertial sensor integrated navigation system for continuous navigation solutions.

Based on different structure principles of MEMS based inertial sensors, it is recommended to identify the various deterministic error sources of the sensors and quantify them for optimal data processing algorithm and performance analysis.

Along with the identification and quantification of the deterministic error sources of sensors, stochastic error analysis should also be emphasized. Stochastic analysis of sensor random noise was mainly discussed in time domain in this research. For the better understanding of the sensor system and enhancement of optimal algorithm, the stochastic modeling is to be further investigated in the frequency domain. Depending on the nature of sensors, environments, and implementation procedures, different types of stochastic

modeling schemes could be considered and further investigated to identify the most suitable modeling method for a certain application.

In the performance analysis, the limited and simplified Kalman filter was implemented using a low-cost GPS chipset and MEMS based inertial sensors of 3-axis accelerometer and 1-axis gyroscope in this research. Using different types of GPS receivers and various grade MEMS based IMU's consisting of 3-axis accelerometer and 3-axis gyroscope, Kalman filter estimation of 3-D kinematic motion will be implemented and the various issues of Kalman filter implementation will be also studied for further research.

References

Albany Nanotech (2003). Technology Focus.

http://www.albanynanotech.org/technology/MIL/index.cfm

Allen, J.J. et al. (1998). Integrated Micro-Electro Mechanical Sensor Development for Inertial Application. Sandia National Laboratories, Albuquerque, NM, U.S.A.

BEI Systron Donner Inertial Division (2003). An Introduction to Quartz Inertial Technology. http://www.systron.com/tech.asp.

Brown, R.G. and Hwang, P.Y.C. (1997). *Introduction to Random Signals and Applied Kalman Filtering*. John Wiley & Sons, Inc, U.S.A.

Cannon, M.E. (2001). *Satellite Positioning: Lecture Notes ENGO 561*. Dept. of Geomatics Eng., The University of Calgary, Calgary, Canada.

Carlson, N.A. (2002). Federated Filter for Distributed Navigation and Tracking Applications. In *Proceedings on ION 58th Annual Meeting/CIGTF 21st Guidance Test Symposium*, Albuquerque, NM, U.S.A.

Chen, C.-T. (1999). *Linear System Theory and Design*. Oxford University Press.

Farrell, J.A. and Barth, M. (1998). *The Global Positioning System & Inertial Navigation*. McGraw-Hill Companies, Inc. U.S.A.

Gao, Y. (2003). P^3 Manual. Dept. of Geomatics Eng., the University of Calgary, Calgary, Canada.

Gardner, J.W., Varadan, V.K., Awadelkarim, O.O. (2001). *Microsensors MEMS and Smart Devices*. John Wiley & Sons, Ltd.

Gelb, A., Kasper Jr., J. F., Nash Jr., R. A., Price, C. F., and Sutherland Jr., A. A. (1974). *Applied Optimal Estimation*. The M.I.T. Press.

Huff, M.A.(1999). Position Paper: MEMS Manufacturing, The MEMS Exchange. Reston, Virginia, U.S.A.

Kealy, A., Tsakiri, M., Stewart, M. (1999). Land Navigation in the Urban Canyon – A Kalman Filter Solution using Integrated GPS, GLONASS and Dead Reckoning. In *Proceedings of ION GPS*, Nashville, TN.

Kealy, A., Young, S.S., Leahy, F., Cross, P. (2001). Improving the Performance of Satellite Navigation System for Land Mobile Applications Through the Integration of MEMS Inertial Sensors. In *Proceedings of ION GPS*, Salt Lake City, UT.

Kraft, M. (1997). *Closed Loop Digital Accelerometer Employing Oversampling Conversion*. School of Engineering, Coventry University, UK.

Lemaire, C., Sulouff, B. (1999). Surface Micromachined Sensors for Vehicle Navigation Systems. Analog Devices, Inc.

Maybeck P.S. (1994). *Stochastic Models, Estimation, Control Volume 1*. Mathematics In Science and Engineering, Ohio, U.S.A.

MEMS and Nanotechnology Clearinghouse (2003). What is MEMS technology?
http://www.memsnet.org/mems/what-is.html.

MEMS and Nanotechnology Clearinghouse (2003). Fabricating MEMS
http://www.memsnet.org/mems/fabrication.html.

Nassar S. (2003). *Improving the Inertial Navigation System (INS) Error Model for INS and INS/DGPS Applications*. Dept. of Geomatics Eng., the University of Calgary, Calgary, Canada.

Nassar S., Schwarz K.P., Noureldin A. and El-Sheimy N. (2003). Modeling Inertial Sensor Errors Using Autoregressive (AR) Models. In *Proceedings of ION NTM*, Anaheim, CA.

Park, M. and Gao, Y. (2002) Error Analysis of Low-Cost MEMS based Accelerometers for Land Vehicle Navigation, In *Proceedings of ION GPS*, Portland, OR.

Priestley M.B. (2001). *Spectral Analysis and Time Series*. Academic Press, London, UK.

Proakis J.G., Rader, C.M., Ling, F., and Nikias, C.L. (1992). *Advanced Digital Signal Processing*. Macmillan Publishing Company, New York, U.S.A.

Salychev, O.S., (1998). *Inertial Systems in Navigation and Geophysics*, Bauman MSTU Press, Moscow.

Salychev, O.S., Voronov, V.V., Cannon, M. E., Nayak, N., and Lachapelle, G. (2000). Low cost INS/GPS integration: Concepts and Testing. In *Proceedings of ION NTM*, Anaheim, CA.

Schwarz, K.P. and Wei, M. (2001). *INS/GPS Integration for Geodetic Applications: Lecture Notes ENGO 623*. Dept. of Geomatics Eng., The University of Calgary, Calgary, Canada.

Seeber, G. (1993). *Satellite Geodesy*. Walter de Gruyter, Berlin, Germany.

Shin, E.-H. (2001). *Accuracy Improvement of Low Cost INS/GPS for Land Applications*. Dept. of Geomatics Eng., the University of Calgary, Calgary, Canada.

Stephen, J. (2000). *Development of a Multi-Sensor GNSS Based Vehicle Navigation System*. Dept. of Geomatics Eng., the University of Calgary, Calgary, Canada.

Titterton, D.H. and Weston, J.L. (1997). *Strapdown Inertial Navigation Technology*. Peter Peregrinus Ltd, UK.

Tung, S. (2000). Position Paper: An Overview of MEMS Inertial Sensors, University of Arkansas, Fayetteville, AR.